UNIVERSITÀ DEGLI STUDI DI PADOVA

CORSO DI LAUREA MAGISTRALE IN INGEGNERIA ELETTRICA

TESI DI LAUREA MAGISTRALE

Performance limits of UK low voltage networks and potential for reactive power compensation

RELATORE: CH.MO PROF. ROBERTO TURRI

DIPARTIMENTO DI INGEGNERIA INDUSTRIALE

CORRELATORE: CH.MO PROF. HUW GRIFFITHS

SCHOOL OF ENGINEERING - CARDIFF UNIVERSITY

LAUREANDO:NICOLA DALLA RIZZA

ANNO ACCADEMICO 2012-2013

Riassunto della tesi

In questa tesi sono stati analizzati dati reali relativi a cinque reti elettriche radiali di bassa tensione (BT), urbane e rurali, al fine di comprendere gli andamenti di V, I, P, Q e fattore di potenza. Attraverso le analisi statistiche delle distribuzioni di tensione e corrente, è stato valutato il comportamento delle reti con lo scopo di verificare se i limiti tecnici di legge fossero violati o meno.
In questo progetto è stato utilizzato un nuovo approccio per la modellazione delle reti BT equilibrate/squilibrate sfruttando OpenDSS, un software di simulazione progettato per essere largamente espandibile al fine di incontrare le possibili future esigenze quali Smart Grids.
I dati di rete sono stati forniti da Western Power Distribution (WPD), che è il gestore della rete di distribuzione (DNO) nel sud del Galles (UK). Inizialmente sono state modellate quattro reti BT alle quali sono stati connessi dei carichi trifase equilibrati, mentre la quinta rete, Angus Street, la più estesa e squilibrata, è stata accuratamente modellata e simulata considerando solamente carichi monofase squilibrati.
Tutte le simulazioni sono state effettuate considerando differenti condizioni di funzionamento quali: variazione del fattore di potenza (decrescente), presenza di generazione distribuita e compensazione della potenza reattiva alla sbarra di alimentazione dei feeder. Queste ipotetiche condizioni di lavoro delle reti BT sono stati concordati con WPD al termine di alcuni meeting tenuti presso la Cardiff University ed inoltre valutando i dati tecnici forniti dall'ente stesso.

È stato valutato inoltre un preliminare studio sulla compensazione della potenza reattiva in Angus Street al fine di attenuare il forte squilibrio delle fasi e per comprendere i possibili vantaggi in termini di mitigazione dei profili di tensioni e corrente. Diverse tecniche e dispositivi possono essere utilizzati nella compensazione reattiva delle reti BT tuttavia è stato scelto di analizzare solamente la compensazione reattiva centralizzata, inserendo un unico banco di condensatori al secondario del trasformatore 11/0.415 kV. Al fine di individuare la migliore collocazione dei dispositivi compensatori, un importante parametro elettrico, definito dal rapporto X/R di ogni cavo o linea aerea della rete e dei singoli trasformatori, è stato preso in considerazione; a tal scopo è stato sviluppato un database dei principali parametri elettrici dei cavi e delle linee aeree utilizzate nelle reti radiali BT sotto supervisione di Western Power Distribution nel Galles.

Con l'avvento delle Smart Grids, i flussi di potenza stanno gradualmente cambiando, questo aspetto soprattutto nelle reti BT desta particolare interesse in quanto le necessità degli utenti di reti si stanno evolvendo. Le reti future prevedono la generazione integrata soprattutto da parte delle forti rinnovabili, suscita quindi particolare interesse la valutazione delle relative variazioni di: tensione, corrente, THD , dello sbilanciamento tra le fasi ed ulteriori potenziali cambiamenti.
Lo studio di tali possibili scenari in reti BT partono dal presupposto di una conoscenza tecnica dei parametri stessi delle reti come ad esempio le curve di carico degli utenti connessi ed i limiti di legge della fornitura di energia elettrica da rispettare. In questo lavoro di tesi è stato valutato l'impatto della generazione integrata, con relativa bassa penetrazione di sistemi fotovoltaici monofase, considerando la configurazione di rete durante il normale funzionamento in un determinato giorno dell'anno, scelta definita dall'accurata analisi dei dati raccolti dai contatori a valle dei trasformatori di rete. Oltre a ciò, è stato studiato un ulteriore caso, sempre riguardante l'impatto della generazione integrata ma durante un corrispettivo funzionamento estremo, in cui la domanda di energia degli utenti BT è stata ipotizzata bassa mentre la generazione da fonte rinnovabile, nel nostro caso da soli sistemi fotovoltaici, raggiunge il picco di generazione. Questi tipi di simulazione sono legati al concetto di Hosting Capacity ovvero la capacità della rete di accogliere flussi di potenza, derivanti da generazione distribuita, senza apportare alcuna modifica sostanziale della rete in esame. L'Hosting Capacity è ad oggi un aspetto molto importante che va preso in considerazione per valutare i cost-effective e le prestazioni di rete relative alla crescente generazione integrata da fonti rinnovabili.

Un' analisi di questo tipo può essere valutata tramite l'uso software di simulazione, quali ad esempio OpenDSS, al fine di esaminare: limiti di corrente, variazioni della tensione di alimentazione (SVV) di ogni bus , variazioni rapide di tensione (RVC) relativi alle improvvise variazioni dei flussi di potenza da generazioni distribuita, analisi di flussi armonici , flussi di potenza ed effetti della compensazione della potenza reattiva.

Per compiere studi di reti BT occorre scegliere un software di simulazione che possa compiere un'analisi dei sistemi di distribuzione. Questa scelta può dipendere da vari fattori, i principali potrebbero essere: il tipo di sistema di alimentazione (AT, MT o BT), tipi di conduttori utilizzati (cavi o di linee aeree), la tipologia di studio desiderato (flusso di potenza , flussi armonici, studi in regime di guasto ecc.). In questo progetto la scelta è caduta su OpenDSS un programma open source sviluppato da EPRI. Questo software sta rapidamente prendendo piede in ambiti accademici nello studio di reti di distribuzione. Una particolarità di OpenDSS è legata alla possibilità di modellare sistemi monofase e trifase squilibrati con una certa facilità, caratteristica non molto comune negli altri più famosi software commerciali quali ad esempio Neplan.

Giungendo alle conclusioni di questo lavoro di tesi si evince che nelle reti elettriche BT urbane i flussi di potenza sono abbastanza prevedibili durante i giorni feriali mentre per quanto riguarda le reti rurali gli stessi andamenti sono molto più variabili a causa dei numerosi carichi domestici connessi alle reti. Attraverso le analisi statistiche dei dati raccolti dai contatori di rete è stato valutata una distribuzione di tensione di tipo gaussiana mentre per le correnti si è evidenziata una distribuzione differente in ambito rurale ed urbano. Infatti, in sottostazioni rurali vi è una distribuzione con andamento approssimativo di Poisson mentre nelle reti urbane una distribuzione bi-modale o tri-modale. Tuttavia, i limiti di legge sono stati sempre rispettati.
Significative variazioni di fattore di potenza (FP) sono state osservate durante tutto il periodo di carico giornaliero ed i relativi andamenti risultavano diversi in ogni sottostazione analizzata. In particolare, nelle reti urbane si è constatato che il fattore di potenza può variare in modo inversamente proporzionale con il carico durante tutto l'arco del giorno, tale variazione però è più accentuata in reti rurali.
Per quanto concerne i profili di tensione delle reti BT analizzate, la caduta di tensione del trasformatore di alimentazione è influenzata maggiormente dalla variazione della FP rispetto alla caduta di tensione attraverso i feeder, ciò grazie al maggior valore di ogni singolo rapporto X/R delle linee.
Lo studio della compensazione della potenza reattiva realizzata sulla rete Angus Street ha dimostrato come il compensatore shunt collegato al secondario del trasformatore di alimentazione può essere utile per limitare la caduta di tensione ed i valori di corrente erogati dal trasformatore stesso. Al contrario , se i dispositivi di compensazione fossero applicati a valle del trasformatore, i contributi della compensazione della potenza reattiva non è così efficace nel ridurre la caduta di tensione di alimentazione , ma possono contribuire a ridurre in parte le correnti circolanti nelle linee in cavo al fine di controllare le relative soglie limite di ampacity.

L'analisi dei risultati delle simulazione riguardanti la generazione distribuita da fonti rinnovabili in Angus Street ha indicato che una bassa penetrazione di sistemi fotovoltaici monofase (96.5 kW totali) connessi alla rete, in determinati punti chiave, sono in grado di mitigare le cadute di tensione e le corrente di fase dei conduttori. Mentre con un'alta penetrazione di sistemi rinnovabili (300 kW totali) vi è un sostanziale miglioramento generale dei profili di tensione e corrente; laddove però i rami di distribuzione della rete hanno una bassa domanda di energia da soddisfare, i relativi flussi di potenza sono tali da creare un sostanziale peggioramento dello squilibrio tra fasi con conseguenti ripercussioni di sovraccarico di corrente nei cavi, dei profili di tensione e del THD di rete.

In questa tesi si è voluto quantizzare e definire le performance di alcune reti BT Gallesi. Per questo motivo alcune tematiche di tale lavoro potrebbero risultare interessanti per un ulteriore sviluppo futuro. Un primo ulteriore studio potrebbe essere quello riguardante una estesa analisi di altre reti WPD squilibrate, sempre con l'ausilio di OpenDSS, dalle quali poi sviluppare: ulteriori quantificazioni di Hosting Capacity, indagini nei vantaggi della compensazione della potenza reattiva in BT confrontando diverse tecniche, esaminare i relativi effetti di compensazione reattiva lato bassa (415 V) e media tensione (11kV). In fine un altro aspetto molto interessante potrebbe essere quello di valutare l'impatto dell'inverter-interfaced DG units per la regolazione della tensione locale di rete ed inoltre il loro relativo impatto transitorio sulle reti WPD di bassa tensione.

A coloro che hanno creduto in me…

Table of contents

Abstract

In this thesis a deep analyses on real data of five low voltage (LV) networks has been carried out in order to understand the trends of V, I, P, Q and calculated power factor (PF). Through statistical analyses of voltage and current distributions, it has been assessed the behaviours of the networks and also the statutory limits were checked.

A new approach to modelling the balanced/unbalanced LV networks was carried out using OpenDSS, a simulation software designed to be expandable to meet future needs (smart grids).

The networks data have been provided by Western Power Distribution (WPD), which is the Distribution Network Operator (DNO) for the Wales (UK). Four LV networks were modelled with balance three-phase loads whereas for the most extensive and most unbalance one, Angus Street, has been modelled such a properly unbalance network, in this case accurate simulations in different operating scenarios have been assessed (PF decreasing, embedded generation and reactive power compensation).

A study on reactive power compensation has been developed in order to mitigate the strong unbalance on Angus Street network and to better understand the possible voltage advantages for the network. The X/R ratio of each cable and lines of the networks was calculated to finding the worthwhile collocation of the reactive power compensator devices. To accomplish the purposes of the project, a robust data base of underground cables and overhead lines has been developed, in which are present the manufacturer and the calculated parameters.

In the last section of the thesis, an hosting capacity approach, which was referred to Angus Street network, has been shown in order to assess the network performances with different types of renewable penetration.

Introduction

In the modern low-voltage (LV) power distribution systems the power quality is one of the most important parameter for Distribution Network Operators (DNOs). Power quality is directly linked with the evolutions of the new loads types, active and passive. In fact, the growing quantity of embedded generation and electronic devices tied to the low voltage networks have consequences on the electricity supply. Nowadays with the advent of the smart grids, accurate studies, especially in low voltage networks, should be carry out in order to reduce possible variations in voltage, current, THD, phase unbalance and other potential drawbacks. With the aid of energy meters located in strategic network buses, recorded data may be used to find out the typical load shapes of the feeders network, and also to make assumptions on the customer loads. Once known the technical parameters, the main network characteristics and the statutory limits, a power system simulator software should be used to exploring the network behaviours in different operating scenarios. This type of studies may examine thermal limits, supply voltage variations (SVV) of each bus, rapid voltage changes (RVC) related to of sudden variations of distributed generations (DGs) power output, harmonic flow analyses, power flow and effects of reactive power compensations.

By these analyses there is also the possibility to carry out some studies on the network hosting capacity which is, nowadays, a very important aspect to take into account because of the growing penetration of the embedded generation by renewable sources.

The software choice may depend on different factors, the main ones might be the type of supply system (high or low voltage), types of conductors used (cables or overhead lines) the type of study desired (power flow, harmonic flows, fault studies and more). In this project the choice fell on OpenDSS an open source program developed by EPRI.

The OpenDSS software is a simulation tool intended primarily for the analysis of electric utility power distribution systems. This software, that is swiftly emerging on the academic electrical fields, can performs sinusoidal steady-state analyses and is particularly useful for LV systems. OpenDSS has the facility to model unbalanced three-phases systems including unbalanced loads, feature not common in the other commercial simulate software products. Furthermore, OpenDSS is designed to be expandable and can be modified to meet future needs (smart grids). The program is constantly under updating by EPRI's programmers. A strength of this software is the EPRI' support, which is provided on a dedicated website where are present explanations, suggestions on the features of OpenDSS and a online help.

In this project has been involved Western Power Distribution (WPD) the DNO of the Wales (UK). WPD has provided several measured data on five urban and rural LV networks that were exploited in order to assess their performances by OpenDSS simulations on: normal operating conditions, with embedded generation and on reactive power compensator devices tied to the network.

Chapter 1

Analysis of electrical data recordings at the supply point of low voltage urban and rural networks

1.1 Introduction

Western Power Distribution (WPD) has installed electrical data recording equipment at several low voltage (LV) substations. This chapter presents an analysis of the measured values of voltages, currents and powers of selected networks in order to describe magnitudes and variation of the measured quantities in relation to their defined limits (voltage and current). Particular focus is given to the network power factor which is calculated from the recorded values. The analysis of these data will be used to inform the selection of assumed load conditions for the detailed computer simulations of the same networks presented in chapter 3 and 4.

1.2 Description of recorded electrical data

Data from five LV networks have been provided by WPD. The networks include examples of both urban and rural locations. The data sets were obtained from energy meters placed at the feeding point of the networks. The data were recorded every 10 minutes over a period of approximately six months starting from April/May 2012 until September/October 2012. The details of the recorded data are shown in Table 1. Figure 1.1 shows the typical arrangement at 11kV/415V UK substations [1], where the metering position can be seen.

Table 1: Electrical data recorded at metering point.

Data symbols	Description	Units of measurement
V_1, V_2, V_3	RMS values of phase to neutral voltages	V
I_1, I_2, I_3	RMS values of phase currents	A
$THD(V)_1$, $THD(V)_2$, $THD(V)_3$	Total harmonic voltage distortion of each phase to neutral voltage	–
P_i	Real power imported (entering the LV network)	kW
P_o	Real power exported (imported into HV network)	kW
Q_i	Reactive power imported (entering the LV network)	kVAr
Q_o	Reactive power exported (imported into HV network)	kVAr
P	RMS net real power $P = P_i - P_o$	kW
Q	RMS net reactive power $Q = Q_i - Q_o$	kVAr

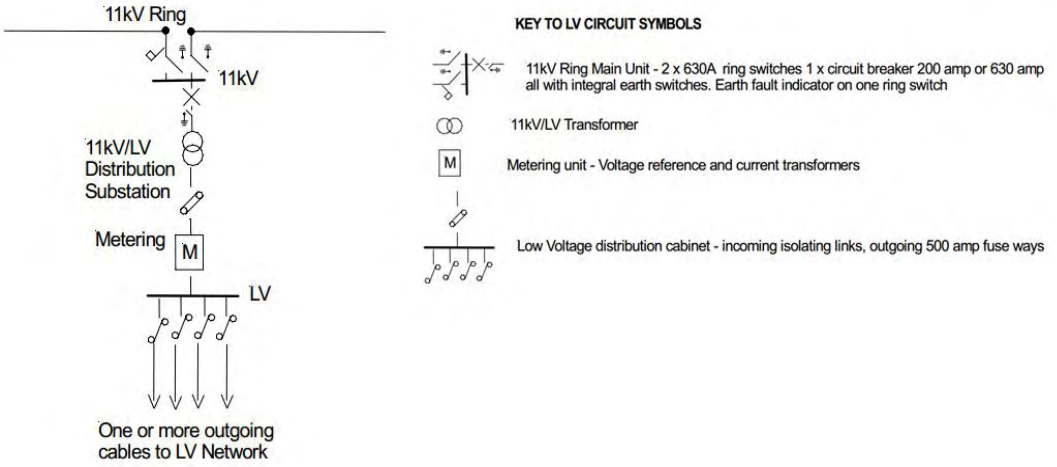

Figure 1.1 Typical arrangement at 11kV/415V UK substation [1]

1.3 Data analysis methodology

Due to the large quantity of data provided, the analysis begins with a presentation of selected data to reveal:

I. Typical daily trend of each phase-neutral voltage at the substation
II. Typical daily trend of each phase current at the substation
III. Typical daily trends real and reactive total three phase power at the substation
IV. Typical daily trend of apparent total three phase power at the substation
V. Typical daily power factor trend at the substation
VI. Long-term of real power trend at the substation

1.4 Data analysis of selected low voltage networks

The five networks provided by WPD which are analysed in this project are:

1. Stuttgarter Strasse (urban), Cardiff
2. Nettlefold Road (urban), Cardiff
3. Angus Street, (urban), Cardiff
4. Rhos Wenallt Abernant (rural), Aberdare
5. Fforchneol Farm Godreaman (rural), Aberdare

1.4.1 Daily trends of electrical quantities at Stuttgarter Strasse network (Urban)

Figure 1.2 shows the recorded voltages (line-neutral) of the three phases at the feeding point of Stuttgarter Strasse network. The 25th July 2012 has been chosen as the date of peak load demand of the provided data recorded. As can be seen from the figure there is considerable fluctuation in voltage over the day and also all of the phases follow almost the same trends. For this particular day the voltages remain within the range 105.2% − 108.0% of nominal voltage and this is well within statutory limits (-6%/+10% of 230V) [2]. There is a slight unbalance between the phase voltages but the difference between one phase and another does not exceeded about 1V.

Figure 1.3 shows the recorded currents of the three phases at the feeding point of Stuttgarter Strasse network. This graph shows the typical daily load current shape for the network. From the figure, it can be seen that there is a sudden pickup in phase current in the early morning around

4.00, followed by a gradual increased until the peak is reached at 15.00. After the peak, the current reduces gradually and at 20.00 falls off substantially to a plateau value until 4.00 the next morning. Concering differences between phase currents, the data reveals that there is significance imbalance. During this day the maximum difference in current magnitude between L_1 and L_3 is 41 A while between L_2 and L_3 it is 64 A. The load shape seen in figure 1.3 is very typical of any weekday at Stuttgarter Strasse network.

Figure 1.4 shows the powers trend of the total three phases powers at the feeding point of Stuttgarter Strasse network. The trend of the real power imported (P_i) follows that of the current while the real power exported (P_o) is always zero (as expected due to the absence of embedded generation). The reactive power imported (Q_i) has fluctuations with same frequency as P_i from 4.00 till 20.30 while Q_o values are, in the same period, equal to zero. During the remainder of the day (20.00 to 4.00), the Q_o values are slightly positive while Q_i is zero. The maximum value of P_i is 218.2 kW for Q_i is 83.8 kVAr, and for Q_o is 7.4 kVAr.

Figure 1.5 shows a comparison of calculated apparent power at Stuttgarter Strasse network using two different methods which are:

a) Method that consider the net real and reactive powers of recorded network data provided:

$$\left|S^{'}\right| = \sqrt{|P^2| + |Q^2|} \quad (1.1)$$

Where:

$$|P| = |P_i| - |P_o| \ \text{[kW]}$$

$$|Q| = |Q_i| - |Q_o| \ \text{[kVA]}$$

b) Method that consider the line-ground voltages and phase currents modules of recorded network data provided:

$$\left|S^{''}\right| = (|V_1| \cdot |I_1| + |V_2| \cdot |I_2| + |V_3| \cdot |I_3|)/1000 \quad (1.2)$$

Where:

V_1, V_2, V_3 are the line-ground voltages in module [V]
I_1, I_2, I_3 are the currents of each phase in module [A]

In this project only one method has been chosen. In order to make this choice, (1.1) and (1.2) were compared to find out some possible relevant differences in the result values.
For this reason has been calculated the apparent powers percentage difference with the following formula:

$$Diff\% = \frac{S_i'' - S_i'}{S_i''} \cdot 100 \quad (1.3)$$

Where:

$S_i^{'}$= Apparent power calculated using a) method
$S_i^{''}$= Apparent power calculated using b) method
i = is the calculated apparent power every 10 min (according to recorded data provided)

N.B.: Except some cases, $S_i^{'}$ values could be lower than $S_i^{''}$

In order to choose the best calculation method it has been also calculated the average apparent powers percentage difference value ($\overline{Diff\%}$.) of each network analysed. These values are always lower than 4% therefore it means that the two methods have just slightly differences in the results. However only the first method is valid because the second one produces not reasonable power factor calculations, in fact cosϕ'' values sometimes are greater than 1. This is due to S'' that sometimes may decrease to a lower value than the net real power (P). According to electrical engineering laws the PF>1 cannot exists in a electrical systems, thus to avoid every kind of problems on the calculations of PF the second method will not considered in the network analyses.
Only in Stuttgarter Strasse network analysis a comparison of the apparent power calculated using the two approaches depicted above have been shown.

Figure 1.6 shows the typical tendency of the power factor (PF) during a typical day at Stuttgarter Strasse network. There are two distinct periods. The first, during the night time from 20.00 to 4.00, where the PF is close to unity and this corresponds to the period of the lower demand. However during the time interval from 4.00 till 20.00 (period of most energy demand) the PF significantly decreases and fluctuates according to the changes in real power. The PF minimum value is 0.916. As real power increases, PF is seen to decrease.

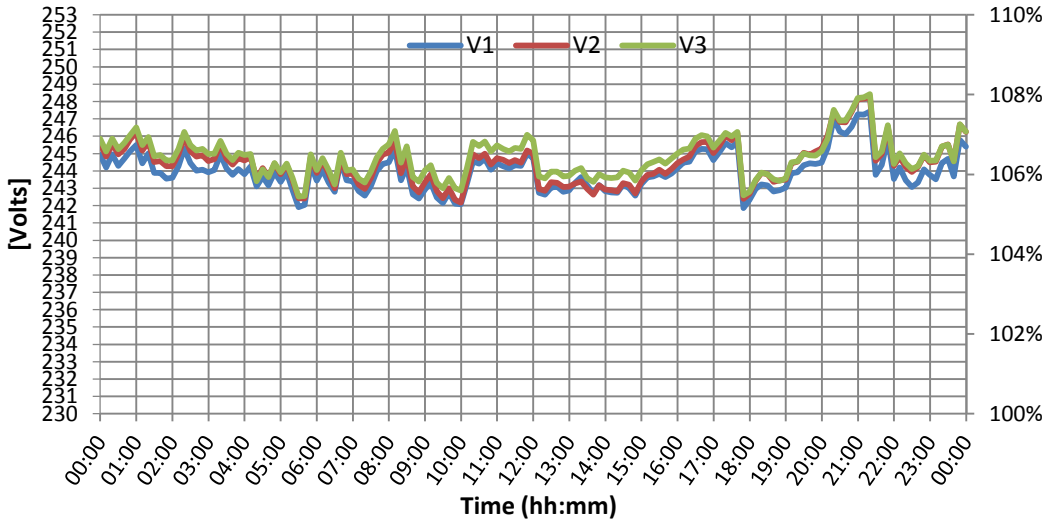

Figure 1.2 Daily variation of measured phase voltages values (Stuttgarter Strasse - urban network - 25th July 2012)

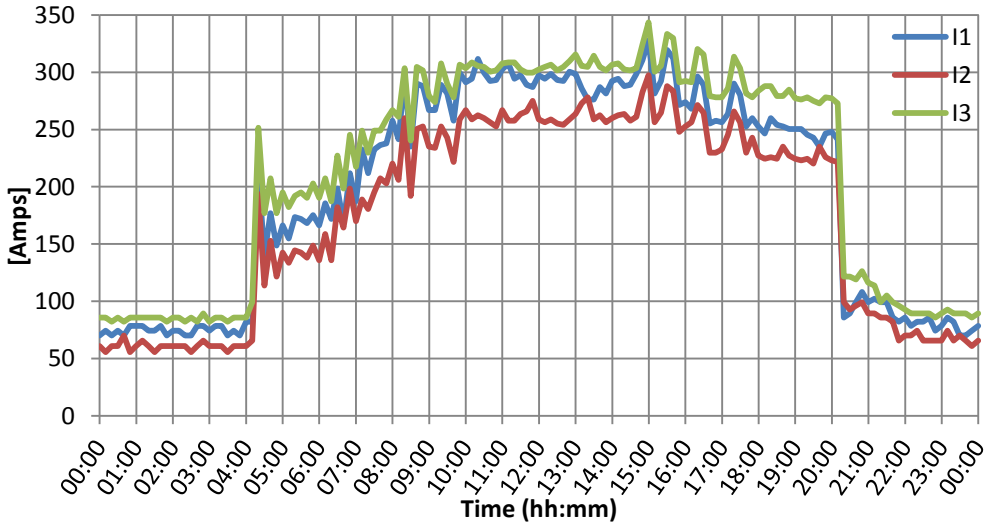

Figure 1.3 Typical daily variations of measured phase currents values (Stuttgarter Strasse - urban network - 25th July 2012)

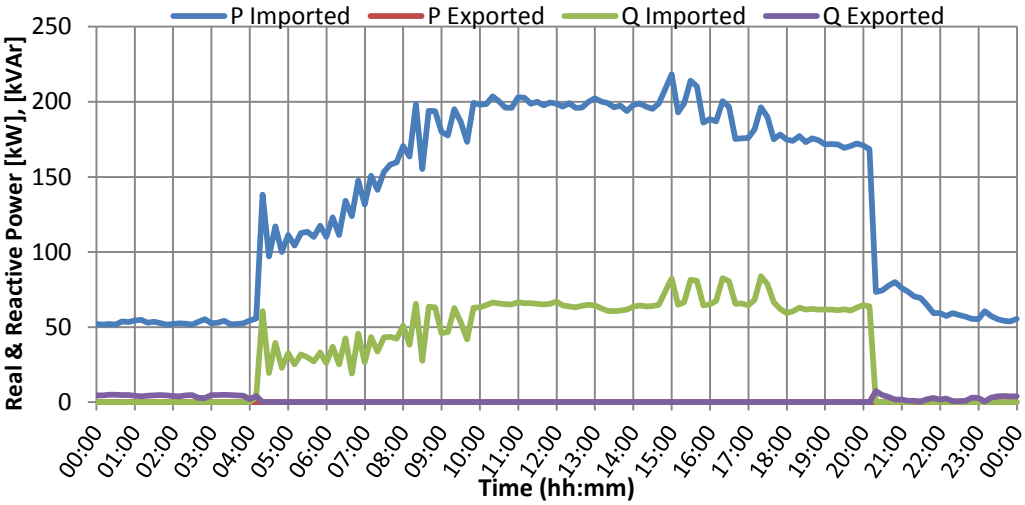

Figure 1.4 Typical daily variation of measured total real power imported/exported and reactive power import/export (Stuttgarter Strasse - urban network - 25th July 2012)

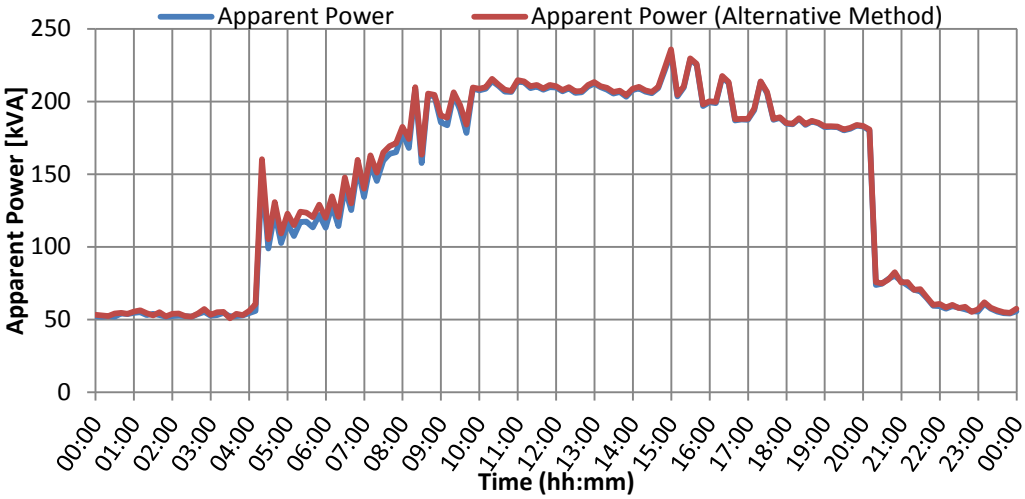

Figure 1.5 Typical daily variations of the calculated apparent power by two different methods (Stuttgarter Strasse - urban network - 25th July 2012)

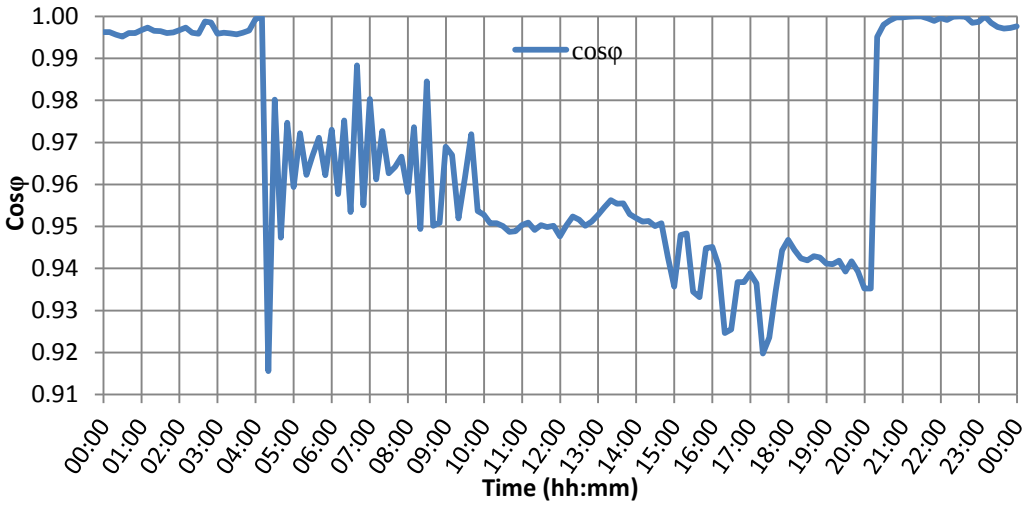

Figure 1.6 Typical daily variation of calculated power factor (Stuttgarter Strasse - urban network - 25th July 2012)

1.4.2 Daily trends of electrical quantities at Nettlefold Road network (Urban)

Figure 1.7 shows the recorded voltages (line-neutral) of the three phases at the feeding point of Nettlefold Road network. The 30th April 2012 has been chosen as the date of peak load demand of the provided data recorded. As can be seen from the figure there is considerable fluctuation in voltage over the day and also all the phases follow almost the same trends.
For this particular day the voltages remain within the range 102.8% − 108.3% of nominal voltage and this is well within statutory limits (-6%/+10% of 230V) [2].
There is a slight unbalance between the phase voltages indeed the difference between one phase and another does not exceed ≈1V.
More precisely the V_1 and V_2 values are more close to each other ($V_1 \approx V_2$) then V_3 values during the peak load demand, which starting from 5.30 till 18.00.
A difference between the urban networks analysed so far is the marked voltages decreasing tendencies of Nettlefold Road network during the peak load demand.

Figure 1.8 shows the recorded currents of the three phases at the feeding point of Nettlefold Road network. This graph shows the typical daily current shape of the network. From the figure it can be seen that there is a sudden pickup in phase current in the early morning around 6.00, followed by a gradual increasing until the peak is reached at 11.10.
After the peak, the current reduces gradually and at 19.00 falls off substantially to a plateau value until 6.00 the next morning.
Regarding differences between phase current, the data reveals that there is a significance unbalance and also that the second phase is more loaded than the other two.
During this typical day the maximum difference in current between L_1 and L_2 is 122.18 A, L_2 and L_3 is 120.44 Amps and between L_3 and L_1 is 76.37 A . The load shape seen in figure 1.8 is very typical of any weekday at Nettlefold Road. The maximum current value of L_2 during the peak is 526.4 A and the minimum value is about 93 A.

Figure 1.9 shows the powers trend of the total three phases at the feeding point of Nettlefold Road. The trend of the real power imported (P_i) follows that of the current while the real power exported (P_o) is always zero (as expected due to the absence of embedded generation). The reactive power imported (Q_i) has fluctuations with same frequency as P_i from 5.30 till 17.30 while Q_o values are, in the same period, equal to zero.
During the remainder of the day (17.30 to 5.30 of the day after), the Q_o values are slightly positive while Q_i is zero. The maximum value of P_i is 326.9 kW for Q_i is 75.4 kVAr and for Q_o is 20.83 kVAr.

Figure 1.10 shows the typical tendency of the power factor (PF) during a typical day at Nettlefold Road network. The PF trend has different periods, two of them during the early morning from 4.00 till 6.00 and on the late afternoon at 16.00 till 18.00 with a PF close to unity which these intervals correspond to the period before and after the highest demand respectively. While during the period of most energy request, from 5.30 till 17.30, the PF significantly decreases and fluctuates according to the changes in real power.
As real power increases, PF is seen to decrease expect during the night period from 00.00 to 3.00 where PF decreases even if the power demand is low. The PF minimum value is 0.962 whereas the maximum is very close to unity.

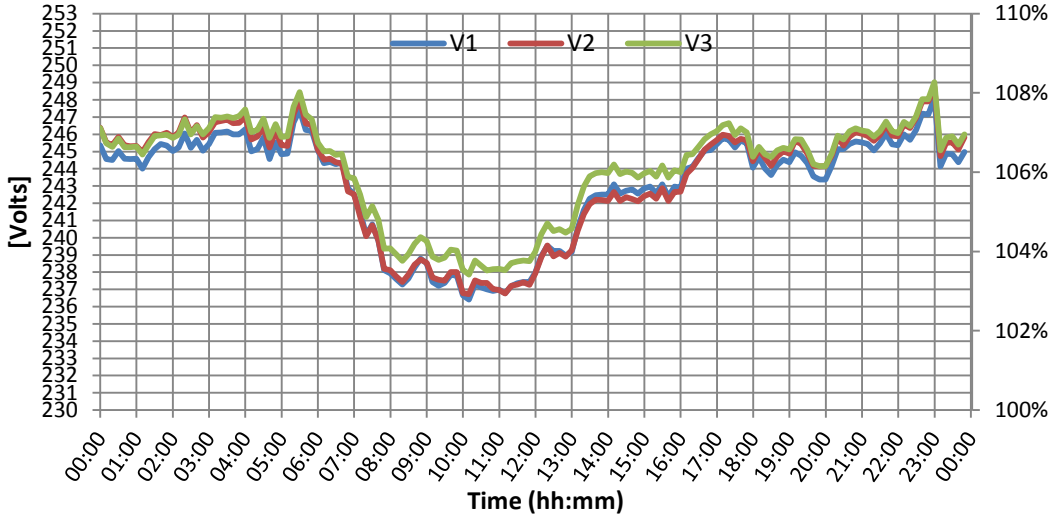

Figure 1.7 Example of daily variation of measured phase voltages values (Nettlefold Road - urban network - 30th April 2012)

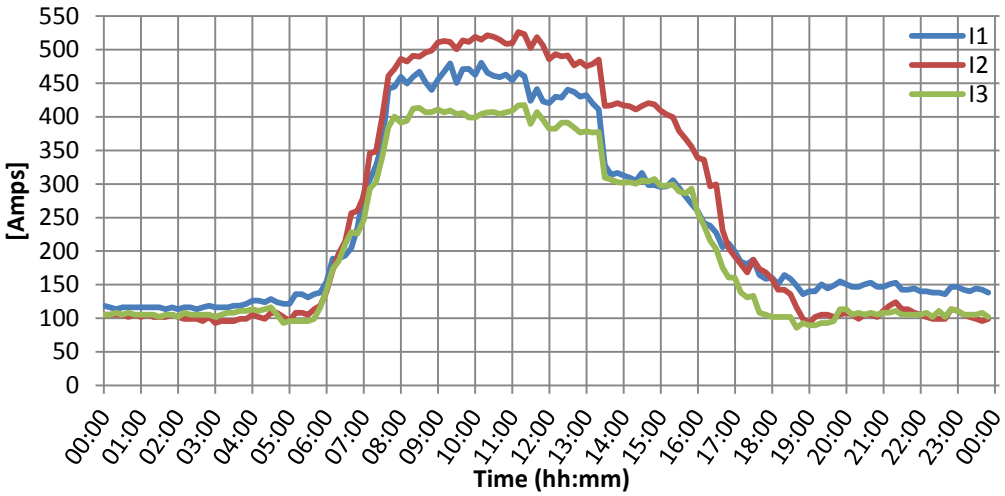

Figure 1.8 Typical daily variations of measured phase currents values (Nettlefold Road - urban network - 30th April 2012).

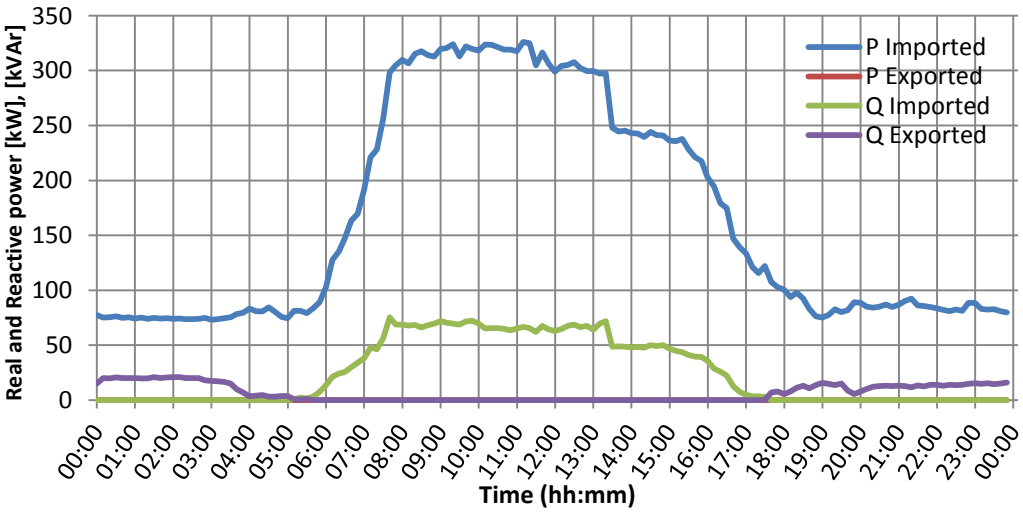

Figure 1.9 Typical daily variation of measured phase values of real power imported/exported and reactive power import/export (Nettlefold Road - urban network - 30th April 2012).

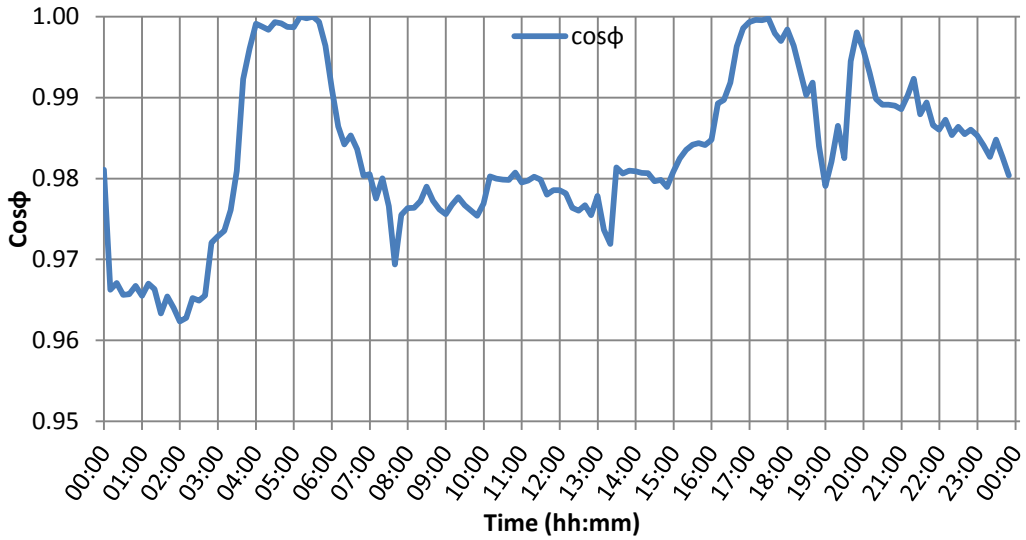

Figure 1.10 Example of daily variation of calculated power factor (Nettlefold Road - urban network - 30th April 2012).

1.4.3 Daily trends of electrical quantities at Angus Street network(Urban)

Figure 1.11 shows the recorded voltages (line-neutral) of the three phases at the feeding point of Angus Street network. The 25th April 2012 has been chosen as the date of peak load demand of the provided data recorded. As can be seen from the figure there is considerable fluctuation in voltage over the day and also all of the phases follow almost the same trends.
For this particular day the voltages remain within the range 103.6% – 107.0% of nominal voltage and this is well within statutory limits (-6%/+10% of 230V) [2]. There is a slight unbalance between the phase voltages, the maximum voltage difference between the phases: L_1 - L_2 is 1.9 V, L_2 - L_3 is 1.2 V and L_1 - L3 is 2.7 V.

Figure 1.12 shows the recorded currents of the three phases at the feeding point of Angus Street network. This graph shows the typical daily load current shape for the network.
As the current trends of the previous two urban network, from the figure it can be seen that there is a sudden pick up in phase currents in the early morning around 6.00 followed by its gradual increasing until the peak is reached at 13.50.
After the peak, the current reduces gradually except in the interval from 17.30 till 20.30 in which the phase current tendencies are quite constant with an average three phase value of 487 A. Afterwards the current falls off substantially to a plateau value until 6.00 the next morning. Concerning the differences between phase currents, the data reveals that there is an important imbalance in fact the graph reveals that the third phase is most loaded in comparison with the other two. During this typical day the maximum difference in current magnitude between the phases: L_1 - L_2 is 166 A, L_3 - L_2 is 255 A and L_3 - L_1 is 179 A. The current shape seen in figure 1.13 is very typical of any weekday at Angus Street.

Figure 1.13 shows the total three phases powers trend at the feeding point of Angus Street network. The trend of the real power imported (P_i) follows that of the current while the real power exported (P_o) is always zero (as expected due to the absence of embedded generation).
The reactive power imported (Q_i) has fluctuations with very similar frequency as P_i from 6.00 till 23.00 while Q_o is always equal to zero. The maximum value of P_i is 630.24 kW and for Q_i is 108.67 kVAr.

Figure 1.14 shows the tendency of the power factor (PF) during a typical day at Angus Street network. The PF trend has fluctuations according to the changes in real power. These PF variations

are present all over the day inside a range of 0.98 – 0.99, but especially during the late evening, from 21.00 till 00.00, there is a sudden pickup in PF. The maximum PF value of the day is about 0.993 at 23.00 while the minimum PF value is 0.98.

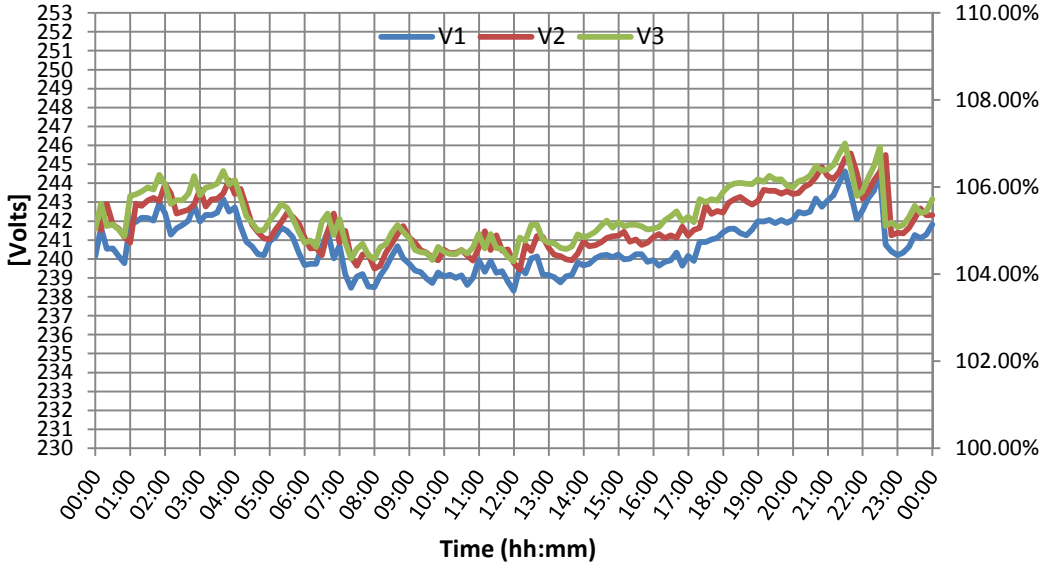

Figure 1.11 Example of daily variation of measured phase voltages values (Angus Street - urban network - 25th April 2012)

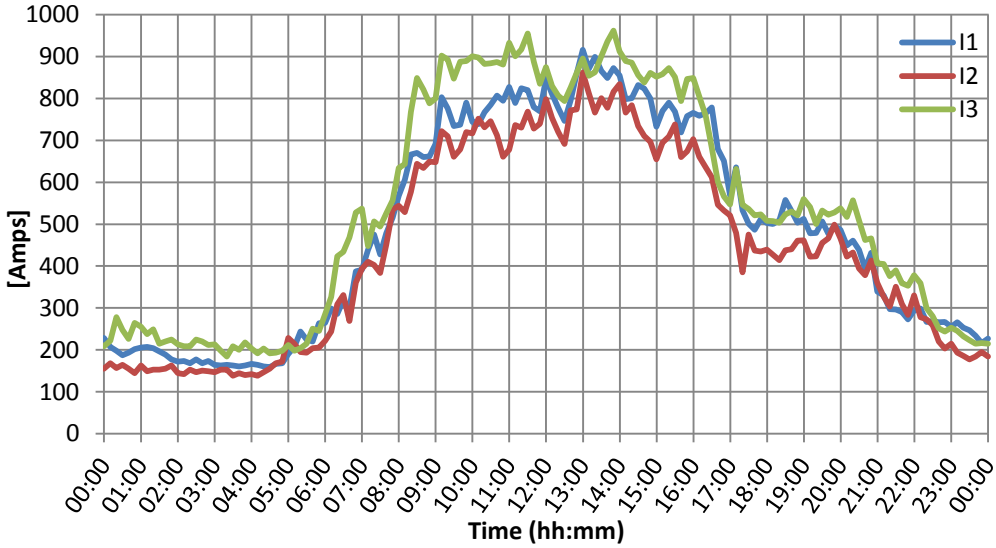

Figure 1.12 Daily variation of measured phase currents values (Angus Street - urban network - 25th April 2012)

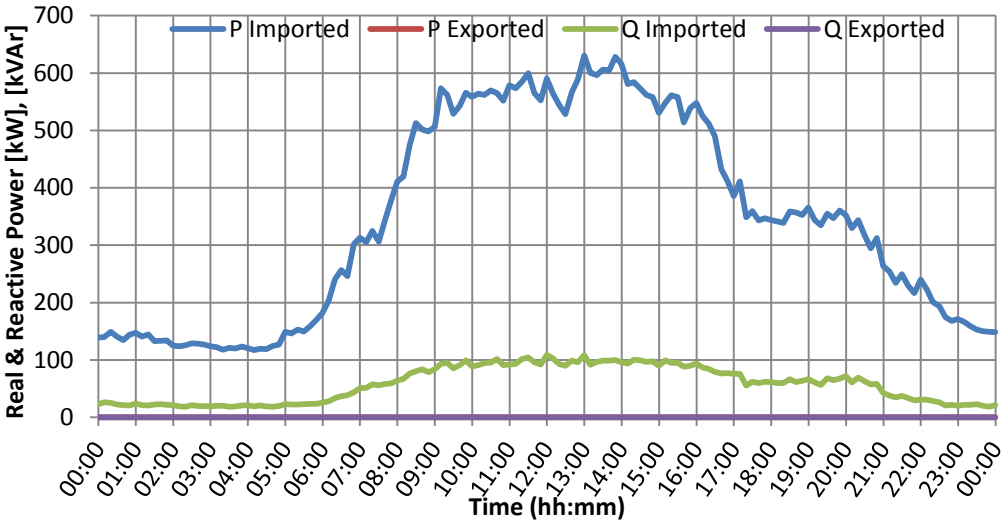

Figure 1.13 Typical daily variation of measured phase values of real power imported/exported and reactive power import/export (Angus Street - urban network - 25th April 2012)

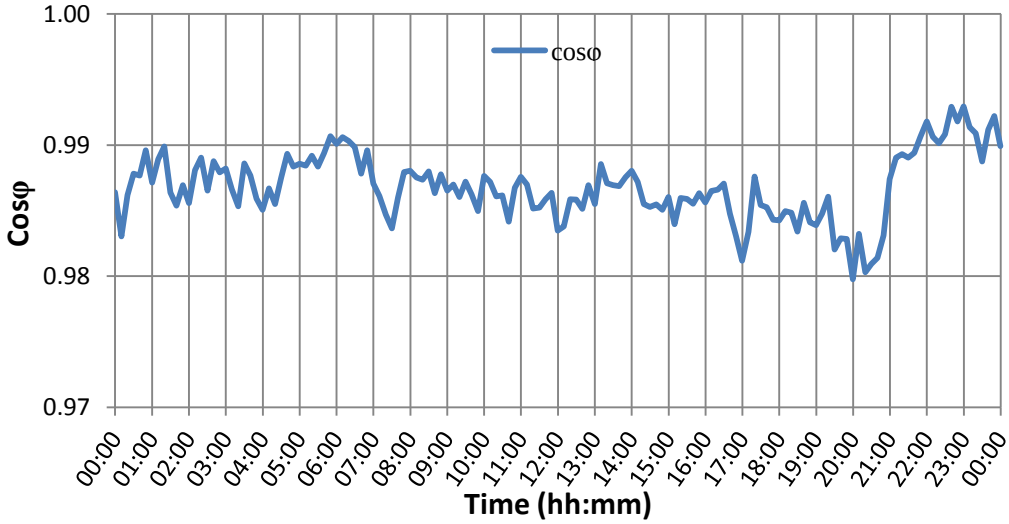

Figure 1.14 Example of daily variation of calculated power factor (Angus Street - urban network - 25th April 2012)

1.4.4 Daily trends of electrical quantities at Rhos Wenallt Abernant network (Rural)

Figure 1.15 shows the recorded voltage (line-neutral) of the three phases at the feeding point of Rhos Wenallt Abernant network. The 14th October 2012 has been chosen as the date of peak load demand of the provided data recorded. As can be seen from the figure there is considerable fluctuation in voltage over the day and also all of the phases follow almost the same trends. For this particular day the voltages remain within the range 104.5% − 107.4% of nominal voltage and this is well within statutory limits (-6%/+10% of 230V) [2]. There is a slight unbalance between the phase voltages, the difference between one phase and another does not exceeded ≈1V, except during lunch time at 13.10 where is reached the maximum voltage difference of about 2.2V between phase V_2-V_3.

Figure 1.16 shows the recorded currents of the three phases at the feeding point of Rhos Wenallt Abernant network. The data reveals that there is a very important imbalance indeed it can be seen from the figure that the second phase (L_2) is more loaded than the other two during the interval 7.30

till 00.00 whereas from 00.00 to 7.30 the current values of L_1 and L_3 are bigger than L_2. During this day the maximum difference in current magnitude between L_1 and L_2 is 53 A, L_2 and L_3 is 65 A and between L_1 and L_3 is 52 A.

Figure 1.17 shows the total three phase power trend at the feeding point of Rhos Wenallt Abernant network. The trend of the real power imported (P_i) follows that the current while the real power exported (P_o) is always zero (as expected due to the absence of embedded generation). The reactive power imported (Q_i) has fluctuations with same frequency as P_i while the reactive power exported (Q_o) is always zero. The maximum value of P_i is 37.42 kW while for Q_i is 8.16 kVAr, these power values are very lower in comparison with the other urban networks analysed. This is due to different type of loads that are connected in the networks, as matter of fact in rural network are present only houses and little farms or hotel. The load shape seen in figure 1.17 is not typical of any weekday because in general on rural networks the power demand of each day is very unpredictable.

Figure 1.18 shows a daily tendency of the power factor (PF) at Rhos Wenallt Abernant network. The PF trend has fluctuations aver the day according to the changes in real power. From the figure it can be seen that from 00.00 till 3.00 the PF trend tend to increase until the maximum PF value but afterwards from 3.00 until 23.30 this tendency decrease with several fluctuations. The maximum PF value of the day is about 0.997 at 3.00 while the minimum PF value is 0.944 at 13.30.

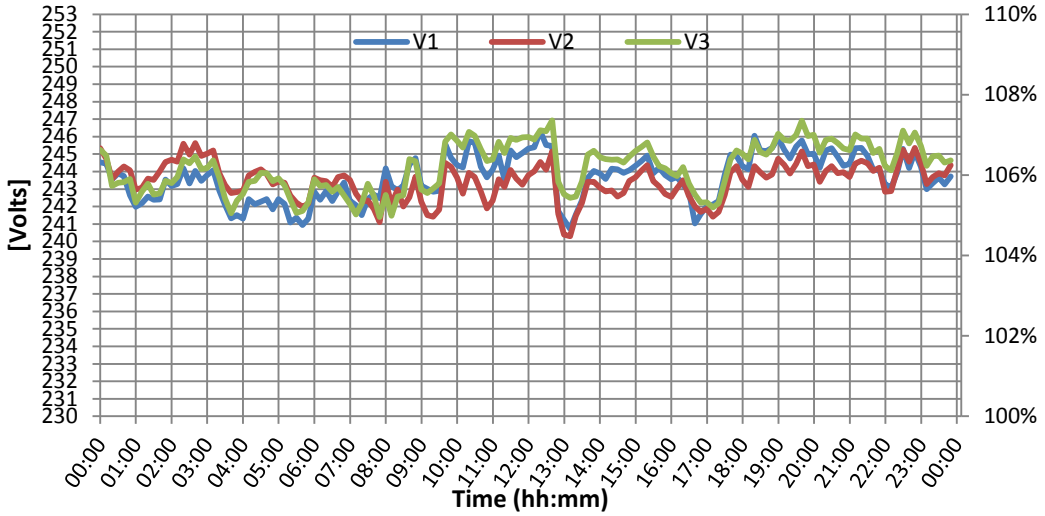

Figure 1.15 Example of daily variation of measured phase voltages values (Rhos Wenallt Abernant Aberdare - rural network - 14th October 2012)

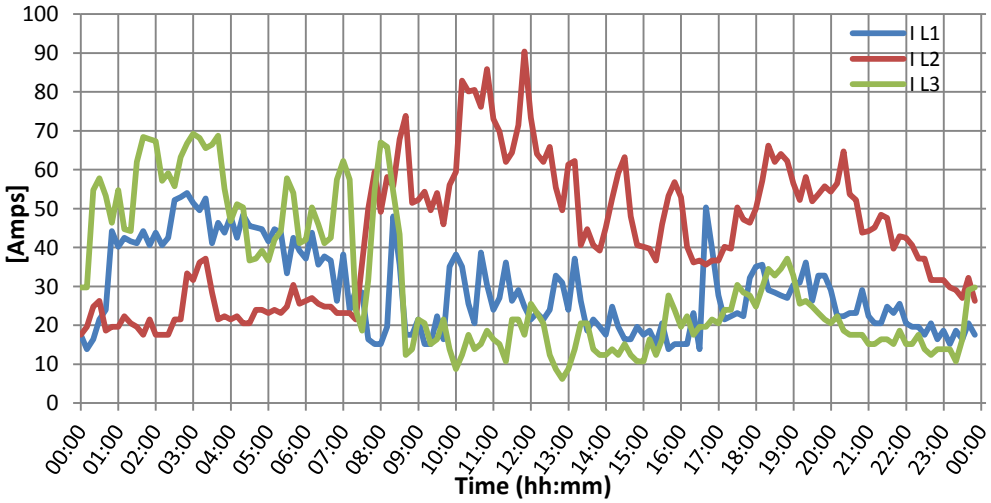

Figure 1.16 Example of daily variation of measured phase currents values (Rhos Wenallt Abernant Aberdare - rural network - 14th October 2012)

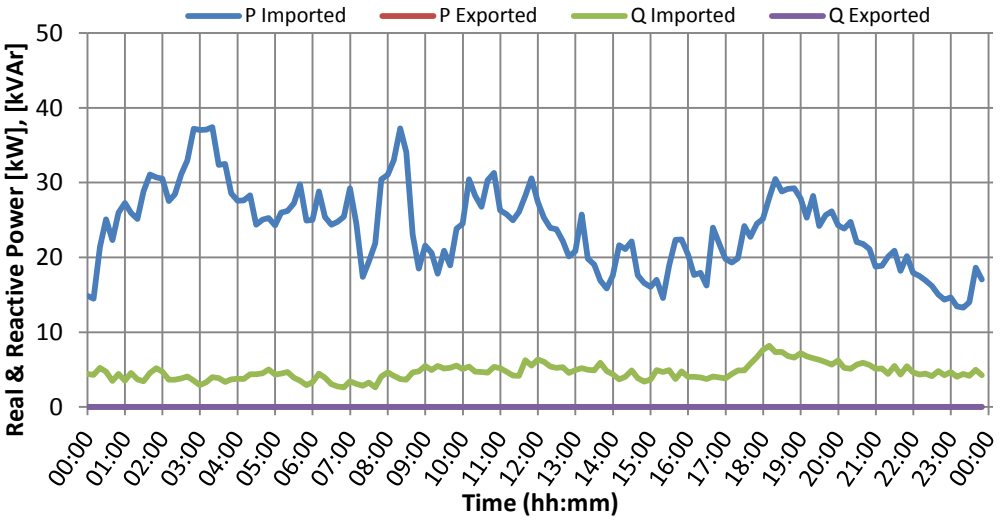

Figure 1.17 Example of daily variation of measured phase values of real power imported/exported and reactive power import/export (Rhos Wenallt Abernant Aberdare - rural network - 14th October 2012)

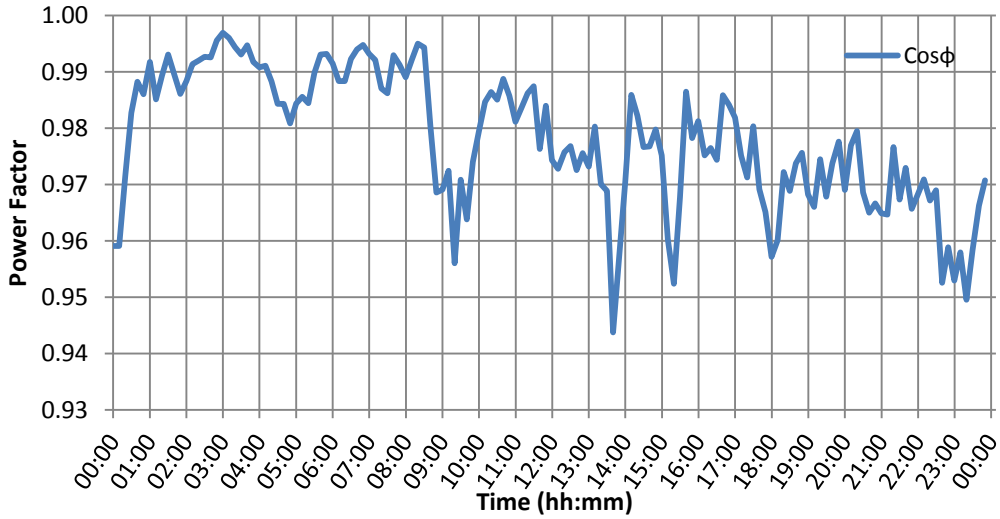

Figure 1.18 Example of daily variation of calculated power factor (Rhos Wenallt Abernant Aberdare - rural network - 14th October 2012)

1.4.5 Daily trends of electrical quantities at Fforchneol Farm Godreaman network (Rural)

Figure 1.19 shows the recorded voltages (line-neutral) of the three phases at the feeding point of Fforchneol Farm Godreaman network. As can be seen from the figure there is considerable fluctuation in voltage over the day and also all of the phases follow almost the same trends. For this particular day the voltages remain within the range 104.7% – 108.5% of nominal voltage and this is well within statutory limits (-6%/+10% of 230V) [2]. There is a slight unbalance between the phase voltages, the maximum difference between the phases: L_1 - L_2 is 3.8 V, L_2 - L_3 is 3.6 V and L_1 - L_3 is 2.1V.

Figure 1.20 shows the recorded currents of the three phases at the feeding point of Fforchneol Farm Godreaman Aberdare network. This graph shows the daily current tendencies of the network, it can be seen that there is a pickup in phase current at 5.30 until 19.00, afterwards the current reduces and at 22.00 falls off to a plateau value until 5.30 of the following morning.

The graph reveals that L_1 and L_3 are the most loaded phases on the network. Considering the differences between phase currents, the data reveals that there is significant imbalance.
During the day analysed, the maximum difference in current magnitude between L_1 and L_2 is 61 A, L_1 and L_3 is 41 A and between L_2 and L_3 is 37 A whereas the maximum current values of the single phases are: for L_1 98.2 A at 11.40, for L_2 77.4 A at 13.00 and for L_3 103 A at 14.20. As for Rhos Wenallt Abernant network, the currents trends seen in figure 1.20 are not typical of any weekday.

Figure 1.21 shows the total three phase power trend at the feeding point of Fforchneol Farm Godreaman network. The trend of the real power imported (P_i) follows that of the current while the real power exported (P_o) is always zero (as expected due to the absence of embedded generation). The reactive power imported (Q_i) has fluctuations with same frequency as P_i while the reactive power exported (Q_o) is always zero.
The maximum value of P_i is 51.3 kW while for Q_i is 5.76 kVAr. Should be noted that in these two rural networks analysed Q_o is always zero, this is due to the absence of reactive power compensator devices at the substations.

Figure 1.22 shows the power factor (PF) tendency on 29th April 2012 at Fforchneol Farm Godreaman Aberdare network. The PF trend has fluctuations over the day according to the changes in real power. From the figure it can be seen that from 21.50 until 11.30 of next day, the PF is very variable inside the range 0.978 – 0.998, which are respectively the minimum and maximum PF values over the day. While from 11.40 till 21.40, during the peak load demand, there is a significant PF improvement, indeed the PF is quite constant with an average value of 0.995.

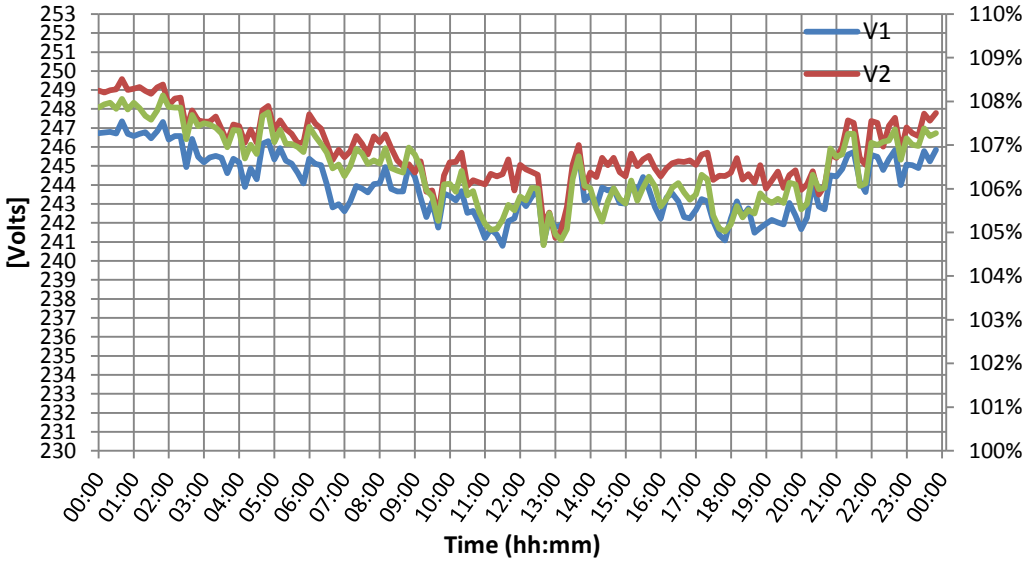

Figure 1.19 Example of daily variation of measured phase voltages values (Fforchneol Farm Godreaman Aberdare - rural network - 29th April 2012).

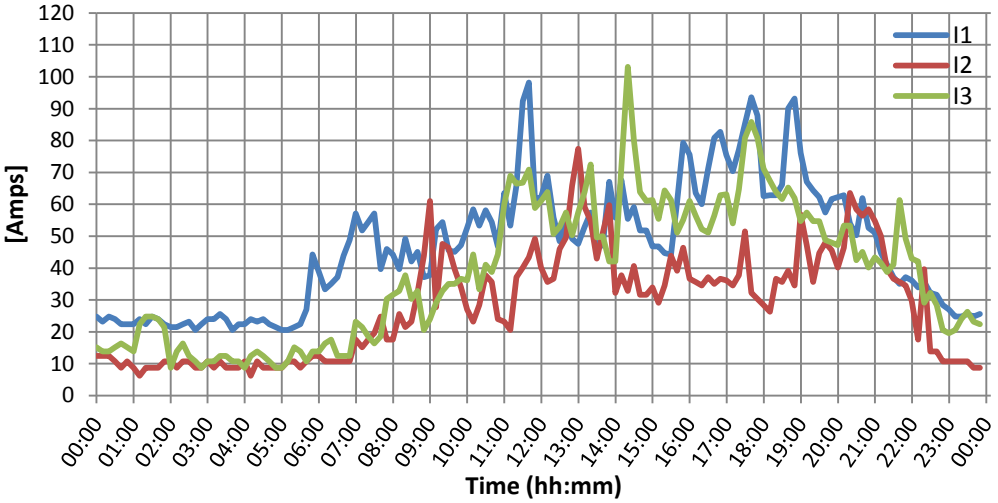

Figure 1.20 Example of daily variation of measured phase currents values (Fforchneol Farm Godreaman Aberdare - rural network - 29th April 2012)

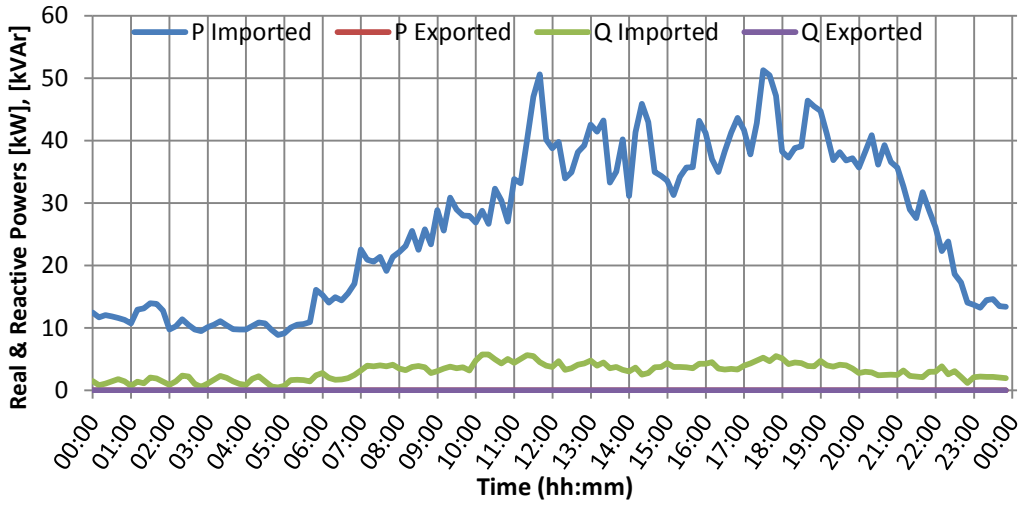

Figure 1.21 Example of daily variation of measured phase values of real power imported/exported and reactive power import/export (Fforchneol Farm Godreaman - rural

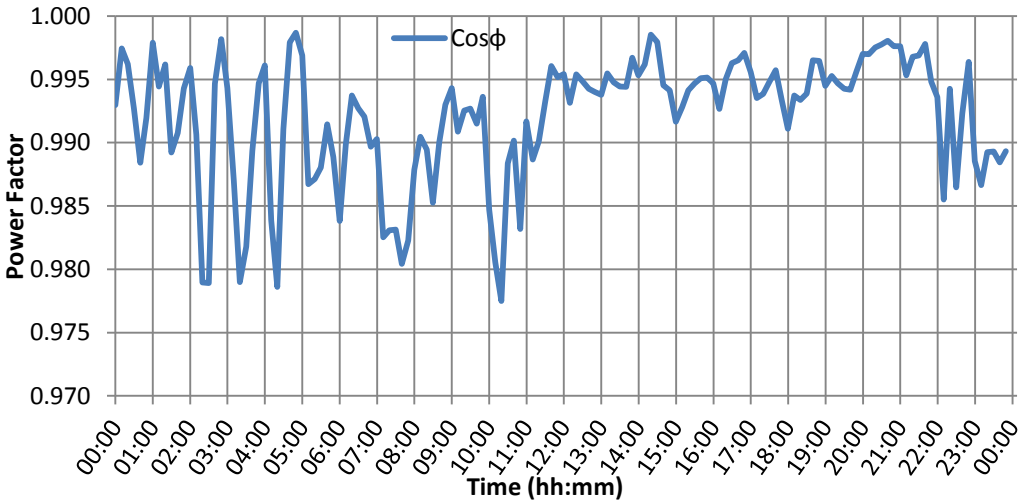

Figure 1.22 Example of daily variation of calculated power factor (Fforchneol Farm Godreaman Aberdare - rural network - 29th April 2012)

1.5.1 Long-term trends of real power at Stuttgarter Strasse network (Urban)

Figure 1.23 shows the power trends of the three phases at the feeding point of the Stuttgarter Strasse network. In this types of graphs have been plotted the minimum, the average and the maximum real power imported (P_i) over each day of the recorded data provided by WPD. This power tendency has a weekly cycle over the time period, indeed during every week-end P_i demand falls off of considerable values if compared to the weekdays magnitude. The maximum P_i value of the recorded data is 219.1 kW on 26th July 2012.

Should be noted that in this graph, as for the other networks, is not present the real power exported P_o due to the absence of embedded generation. Furthermore, a common characteristic present in all of the networks analysed is the trend of minimum real power between the weekdays and the week-ends, in fact the relative both power values are always very close to each other, while the overage and the maximum real power values are more variable.

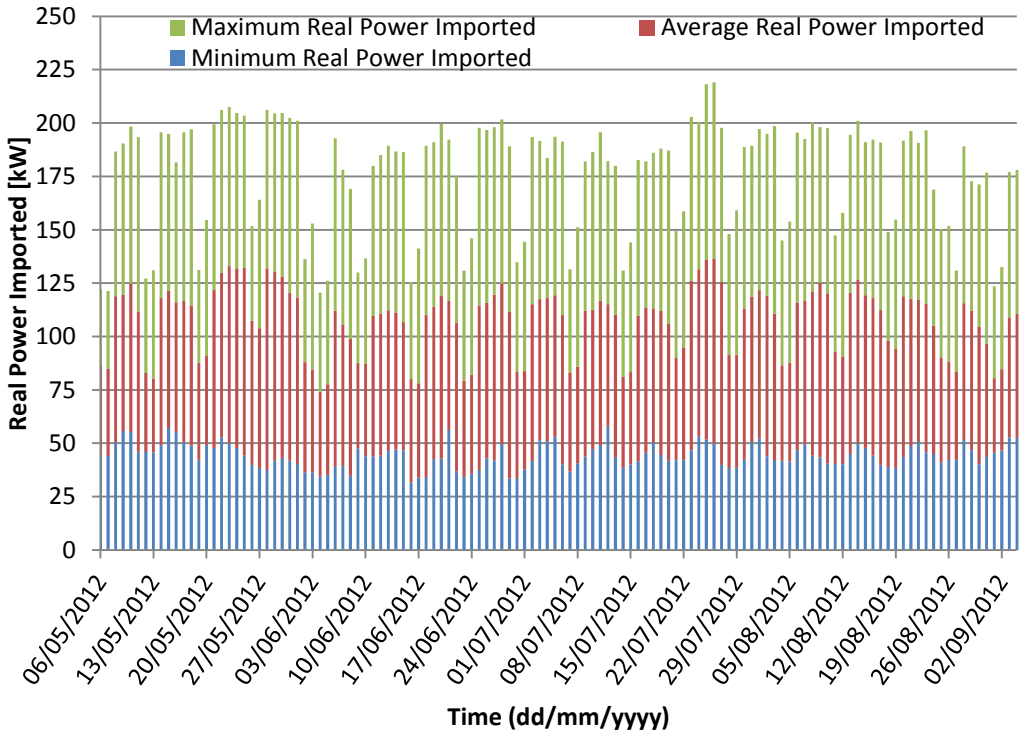

Figure 1.23 Long-term variation of minimum, average and maximum real power imported (Stuttgarter Strasse - urban network - 6th May till 4th September 2012)

1.5.2 Long-term trends of real power at Nettlefold Road network (Urban)

Figure 1.24 shows the power trends of the three phases at the feeding point of the Nettlefold Road network. As the previous graph (Figure 1.23) the power tendency has a weekly cycle over the time period provided, indeed also in this urban network there is a significant difference P_i demand between the week-ends and the weekdays. The maximum P_i value on the recorded data is 325.92 kW on 30th April 2012.

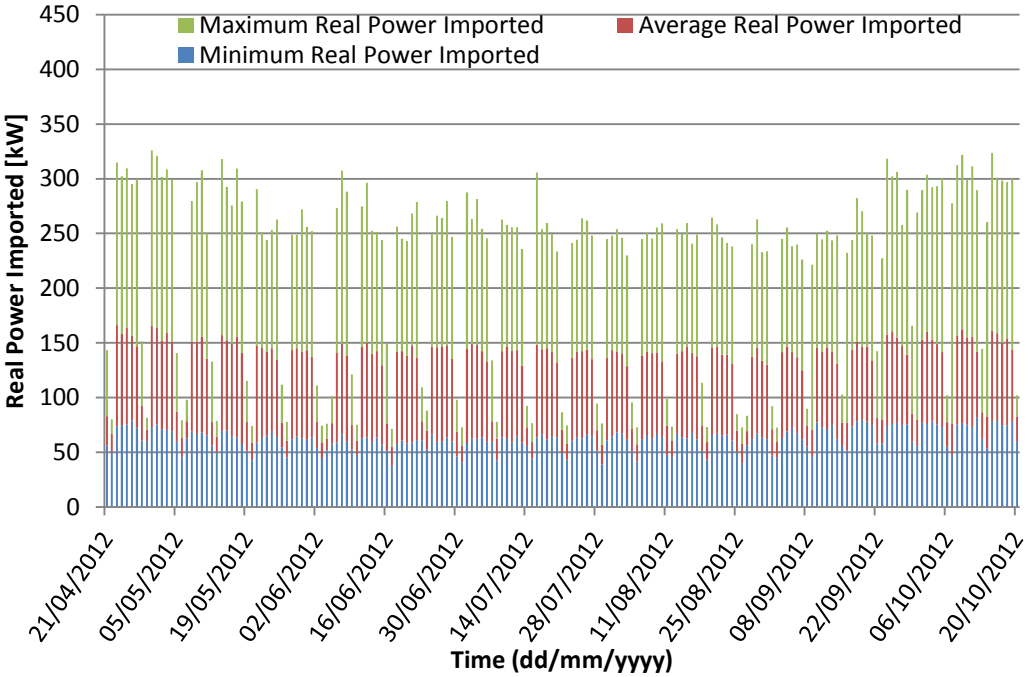

Figure 1.24 Long term variations of minimum, average and maximum real power imported (Nettlefold Road - urban network - 21th April till 20th October 2012)

1.5.3 Long-term trends of real power at Angus Street network (Urban)

Figure 1.25 shows the power trends of the three phases at the feeding point of the Angus Street network. In this network has some differences if compared with the other two urban networks, in fact only every Sunday the P_i demand falls off to lower values than weekdays. The maximum P_i demand value of the recorded data is 630.24 kW on 25th April 2012 which is the higher power demand reached in all of the networks analysed.

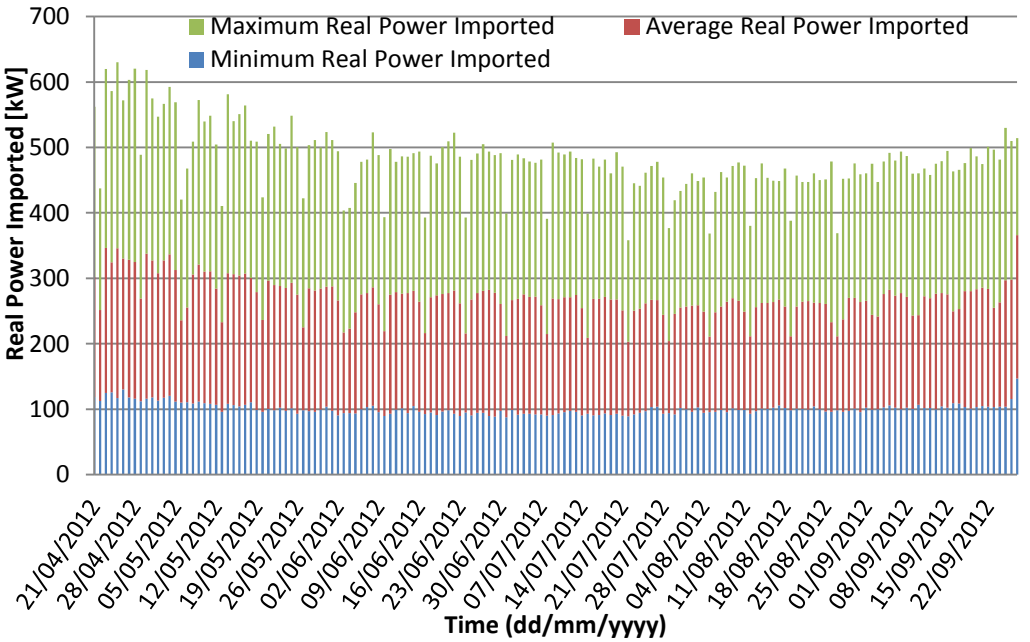

Figure 1.25 Long term variations of minimum, average and maximum real power imported (Angus Street - urban network - 21th April till 26th September 2012)

1.5.6 Long-term trends of real power at Rhos Wenallt Abernant network (Rural)

Figure 1.26 shows the power trends of the three phases at the feeding point of the Rhos Wenallt Abernant network. The power tendency has not a weekly or monthly cycle over the time period indeed the P_i demand is very unpredictable due to domestic customers (residential areas) connected on the network.
The maximum P_i value of the recorded data is 39.38 kW on 19th October 2012. This rural substation has the lowest power demand of the all networks analysed.

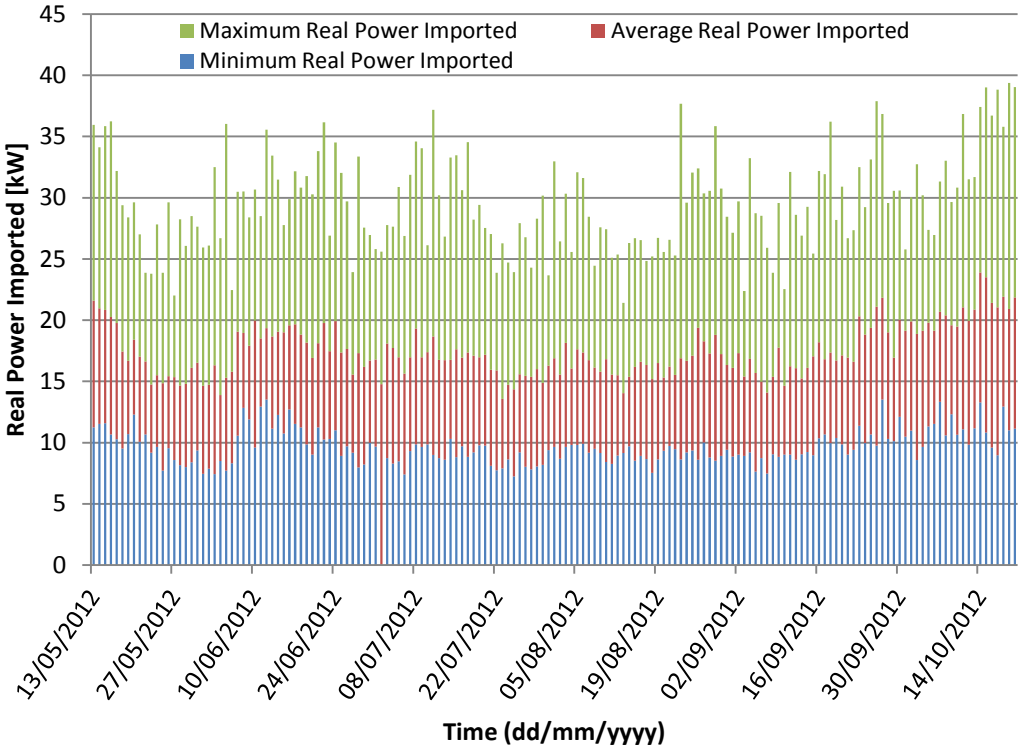

Figure 1.26 Long term variations of minimum, average and maximum real power imported (Rhos Wenallt Abernant Aberdare - Rural network - 13th May till 20th October 2012).

1.5.7 Long-term trends of real power at Fforchneol Farm Godreaman network (Rural)

Figure 1.27 shows the power trends of the three phases at the feeding point of the Fforchneol Farm Godreaman network. In this network, as the previous rural one, the power tendency has not a weekly or monthly cycle over the time period indeed the power demand is very unpredictable due to the domestic customers connected on the network.
The maximum P_i value on the recorded data is 39.38 kW on 25th April 2012. In both rural networks analysed the peak power demand is very low in comparison with the other urban networks, this is main due to the load types tied to the network in fact are present only houses or little pub/hotel.

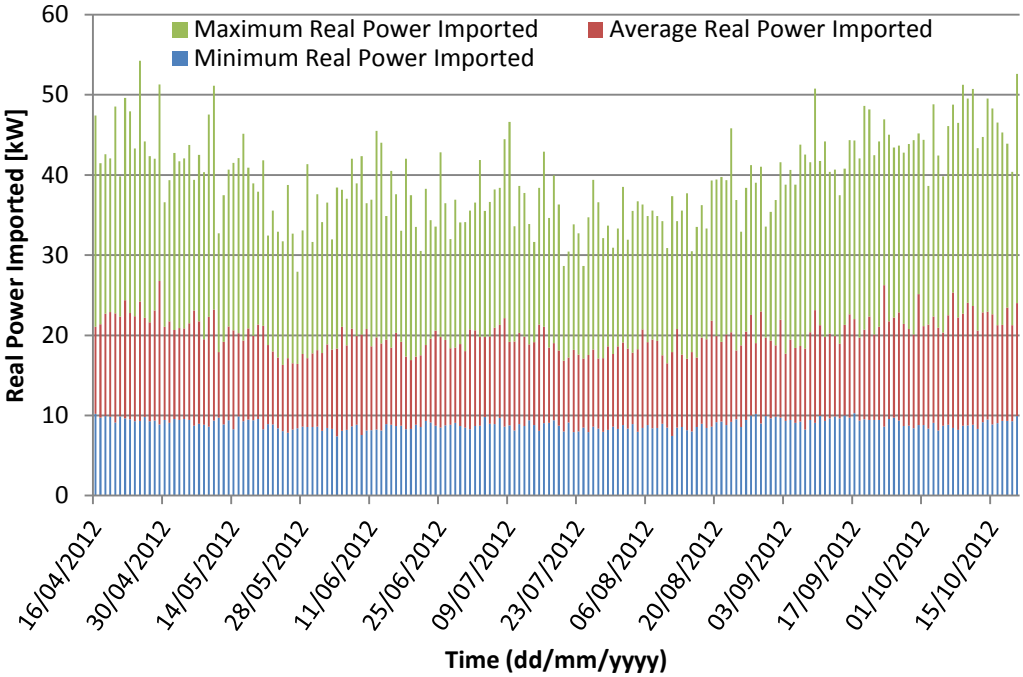

Figure 1.27 Long term variations of minimum, average and maximum real power imported (Fforchneol Farm Godreaman Aberdare - rural network - 16th April till 20th October 2012)

1.6 Statistical analysis

In this section a statistical analysis on five LV network is presented. These analyses show the voltage and current distributions of some recorded data provided for each network. As can be seen from the next figures depicted, the recorded voltage and current values of each network follow in general a Gaussian, a bi-modal, tri-model or an approximate Poisson distribution. According with some studies on the system loads distributions [3], to represent for a instance a bi-modal or a tri-model distribution may be use the probabilistic approach of the Gaussian Mixture Model (GMM).
The GMM has the advantageous that distinct types of distributions can be completely described by two parameters: mean and variance, in fact GMM is a convex combination of several normal distribution with respective means and variances [3].

Figure 1.28 shows the statistical voltage distribution of the three phases at the feeding point of the Stuttgarter Strasse (urban) network. From the figure can be seen that the voltage values are following a Gaussian distribution. The mean values of the phase voltages vary slightly between each other: $V_{mean\ ph1}$= 244.55 V, $V_{mean\ ph2}$= 245.34 V and $V_{mean\ ph3}$= 245.57 V. The graph shows also the 1% and 99% distribution limits which are 240.11 V and 250.4 V respectively, these values lie comfortably within the statutory limits which are never violated.

Figure 1.29 shows the statistical current distribution of the three phases at the feeding point of the Stuttgarter Strasse (urban) network. As shown in the figure there is a bi-model current distribution. In the phase currents interval is present an high relative frequency of values in the lower end and a relevant frequency in the upper end. Furthermore as can been seen in the graph current distributions are not violating the transformer nominal rating (696 A).

Figure 1.30 shows the statistical voltage distribution of the three phases at the feeding point of the Nettlefold Road (urban) network. As the previous network analysed, at the main supply point the voltage values are following a Gaussian distribution. The mean values of the phase voltages vary slightly between each other: $V_{mean\ ph1}$= 245.28 V, $V_{mean\ ph2}$= 245.44 V and $V_{mean\ ph3}$= 246 V. The 1% and

99% distribution limits values are 231.71 V and 251.8 V respectively therefore the current frequency interval is wider than that of Stuttgarter Strasse network.

Figure 1.31 shows the statistical current distribution of the three phases at the feeding point of the Nettlefold Road (urban) network. The current distributions at the main busbar have an higher relative frequency in the lower end and relevant phase currents frequencies in the upper end. Therefore the current pattern is following a bi-modal distribution. Considering the GMM approach the current distribution is a convex combination of three main normal distribution. Additionally it ensure from the graph that current distributions are not violating the transformer nominal rating (1113 A).

Figure 1.32 shows the statistical voltage distribution of the three phases at the feeding point of the Angus Street (urban) network. Also in this figure can be seen that the recorded voltage values are following a Gaussian distribution. The mean values of the phase voltages are not much different between each other: $V_{mean\ ph1}$= 241.13 V, $V_{mean\ ph2}$= 241.96 V and $V_{mean\ ph3}$= 242.47 V. The 1% and 99% distribution limits values are 236.11 V and 246.4 V respectively. Even if this network is the most unbalance one if compared with the other studied, the recording data shows that there are no voltage violations of the statutory limits.

Figure 1.33 shows the statistical current distribution of the three phases at the feeding point of the Angus Street (urban) network. At the main busbar of Angus Street network the current distributions have higher frequency in the lower end and also relevant frequencies in the middle and upper end. Therefore the phase current values are following a tri-modal distribution. Furthermore the graph shows no violations of the transformer nominal rating (1391 A).

Figure 1.34 shows the statistical voltage distribution of the three phases at the feeding point of the Rhos Wenallt Abernant (rural) network. Even at this network the voltage values are following a Gaussian distribution and the mean values of the phase voltages vary slightly between each other: $V_{mean\ ph1}$= 243.85 V, $V_{mean\ ph2}$= 243.83 V and $V_{mean\ ph3}$= 244.8 V. In the figure are highlighted the 1% and 99% distribution limits which are 238.61 V and 249.39 V respectively. The recording data shows that there are no voltage violations of the statutory limits.

Figure 1.35 shows the statistical current distribution of the three phases at the feeding point of the Rhos Wenallt Abernant (rural) network. In this case the current values are following an approximate Poisson distribution with an high relative frequency in the lower end on the current interval. For the two rural networks are highlighted the transformer nominal rating (139 A) because some current values with low relative frequency are not so far from the thermal limit.

Figure 1.36 shows the statistical voltage distribution of the three phases at the feeding point of the Fforchneol Farm Godreaman (rural) network. The recorded voltage values at the main busbar of this rural network are following a Gaussian distribution. As shown in the other figures, the mean values of the phase voltages vary slightly between each other: $V_{mean\ ph1}$= 245.81 V, $V_{mean\ ph2}$= 247.23 V and $V_{mean\ ph3}$= 246.87 V. The 1% and 99% distribution limits values are 233.69 V and 252.31 V respectively. The recording data shows that there are no voltage violations of the statutory limits.

Figure 1.37 shows the statistical current distribution of the three phases at the feeding point of the Fforchneol Farm Godreaman (rural) network. Should be noted that even in this case the current values follow an approximate Poisson distribution. Furthermore the transformer nominal rating (139 A) is still far from the typical currents values, that it means no current violations in the operating conditions of the network.

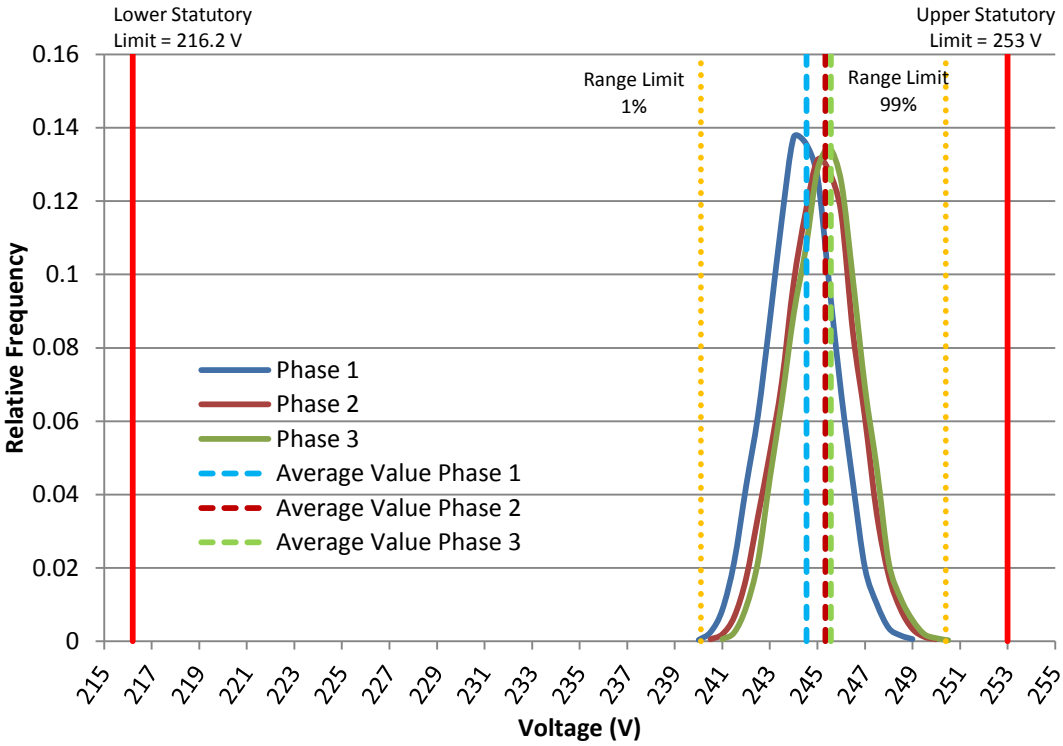

Figure 1.28 Statistical voltage distribution of the recorded data at the feeding point of Stuttgarter Strasse network

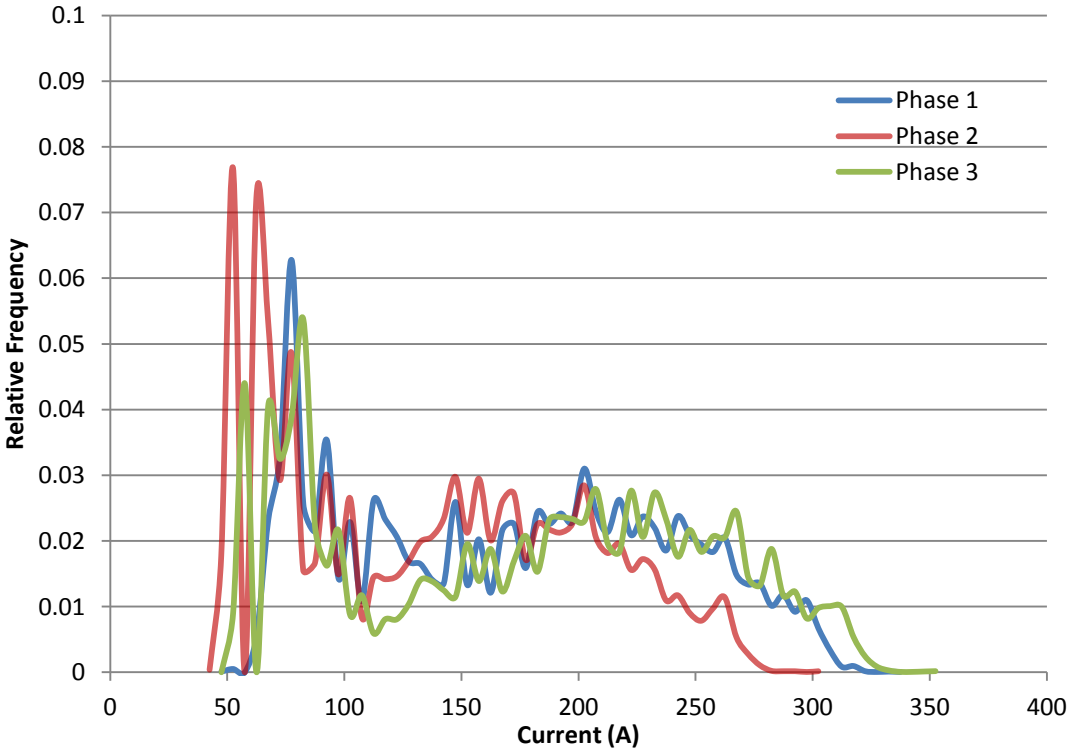

Figure 1.29 Statistical current distribution of the recorded data at the feeding point of Stuttgarter Strasse network

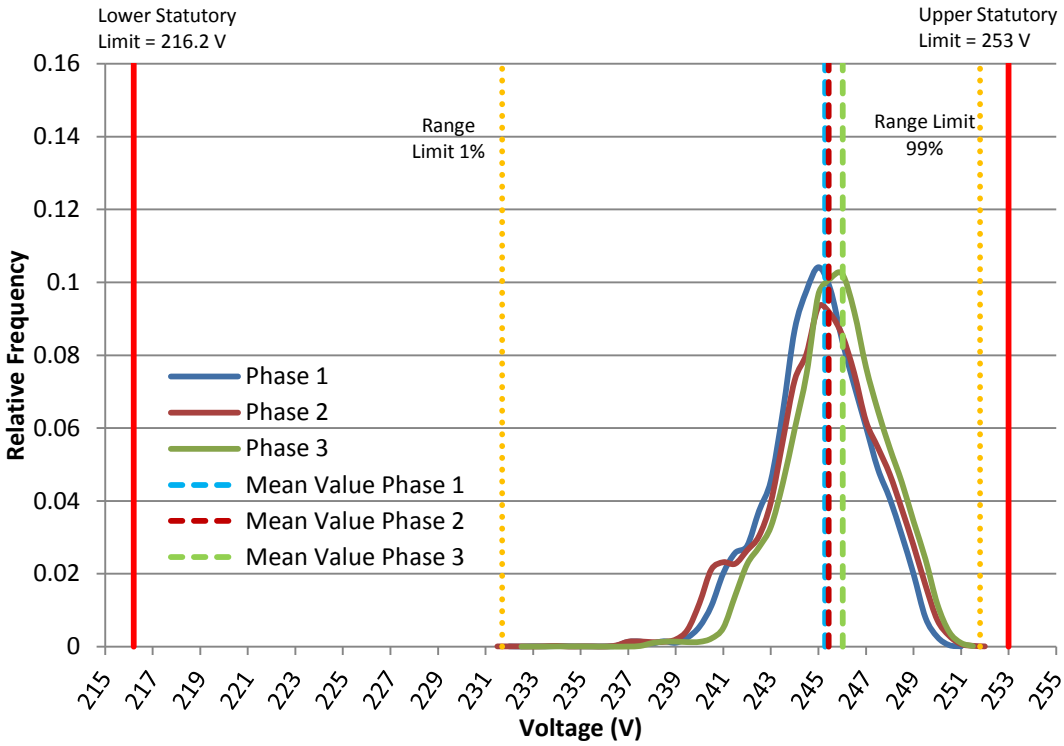

Figure 1.30 Statistical voltage distribution of the recorded data at the feeding point of Nettlefold Road network

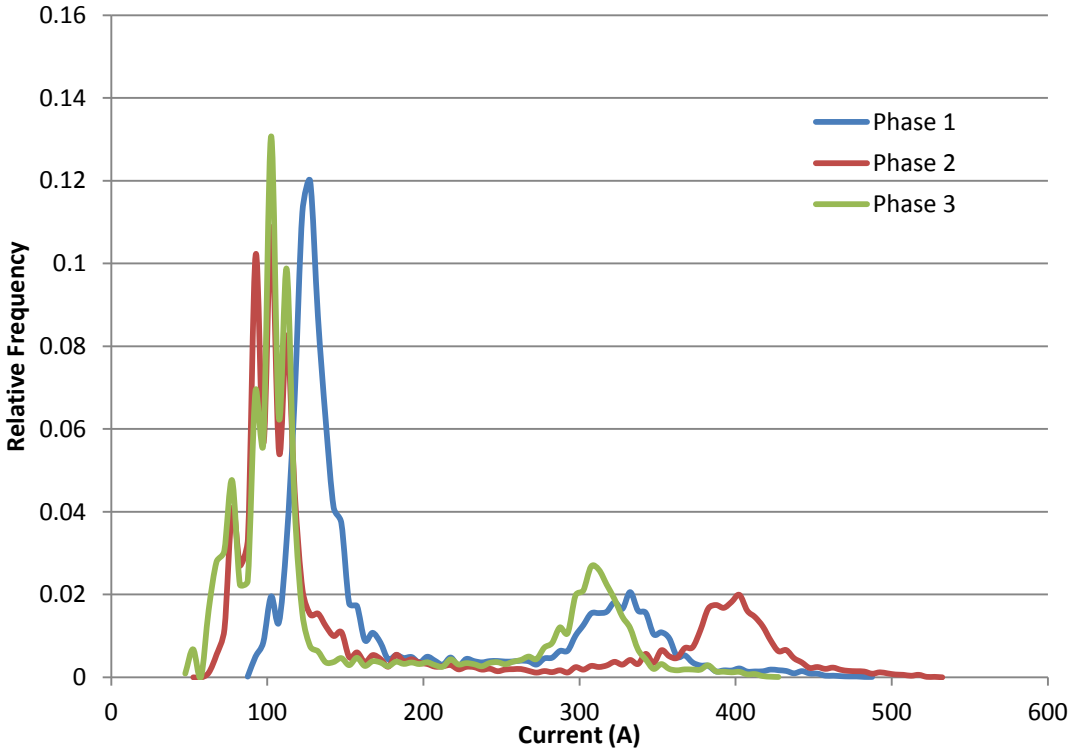

Figure 1.31 Statistical current distribution of the recorded data at the feeding point of the Nettlefold Road network

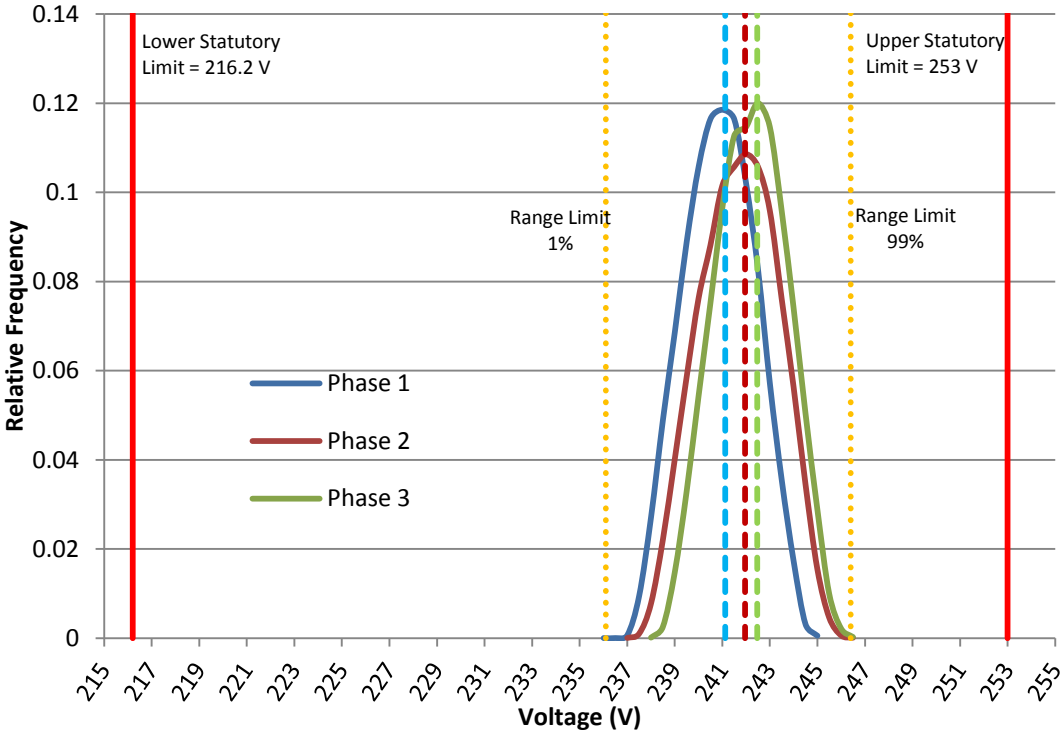

Figure 1.32 Statistical voltage distribution of the recorded data at the feeding point of the Angus Street network

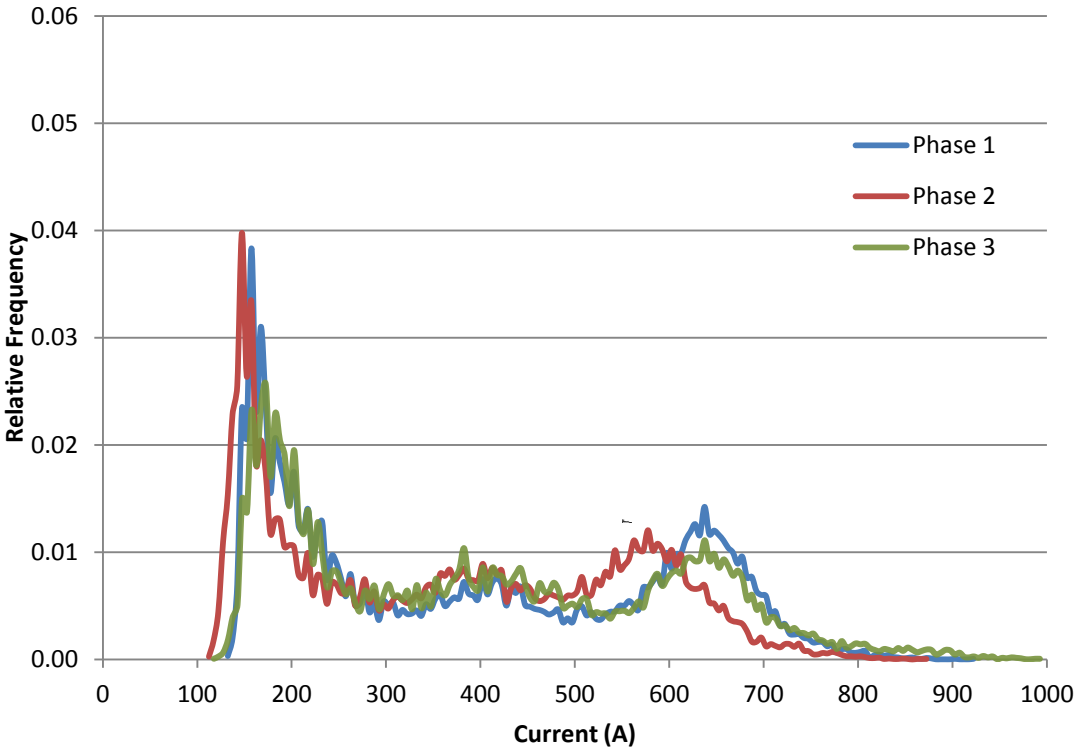

Figure 1.33 Statistical current distribution of the recorded data at the feeding point of the Angus Street network

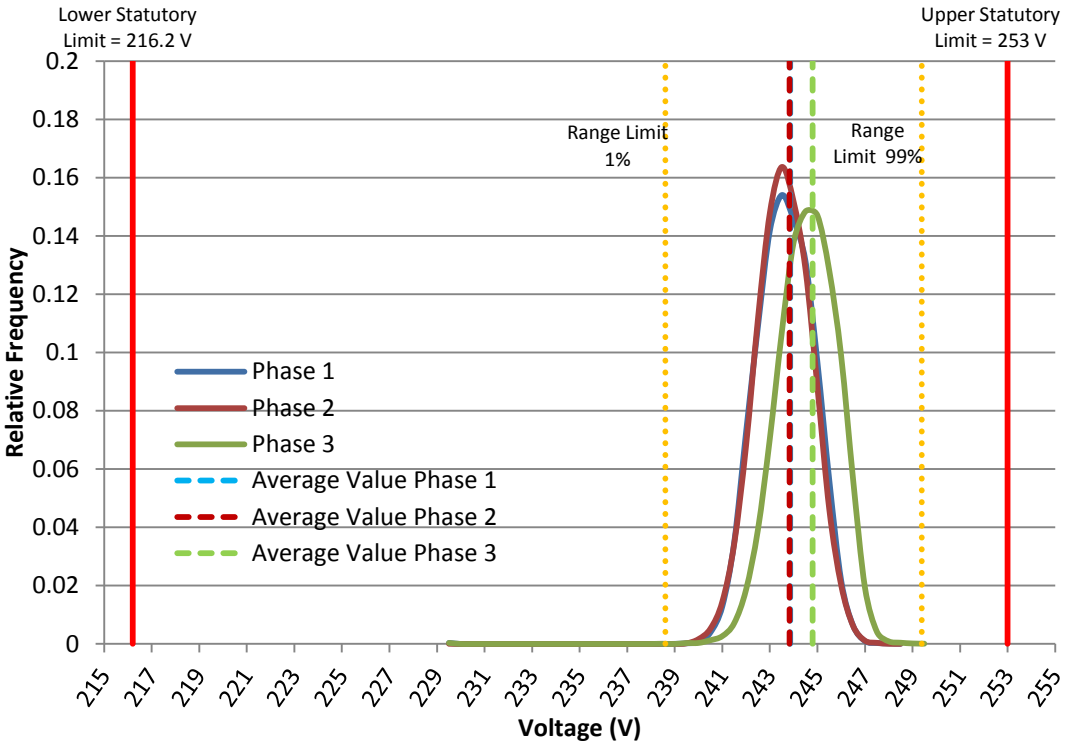

Figure 1.34 Statistical voltage distribution of the recorded data at the feeding point of the Rhos Wenallt Abernant network

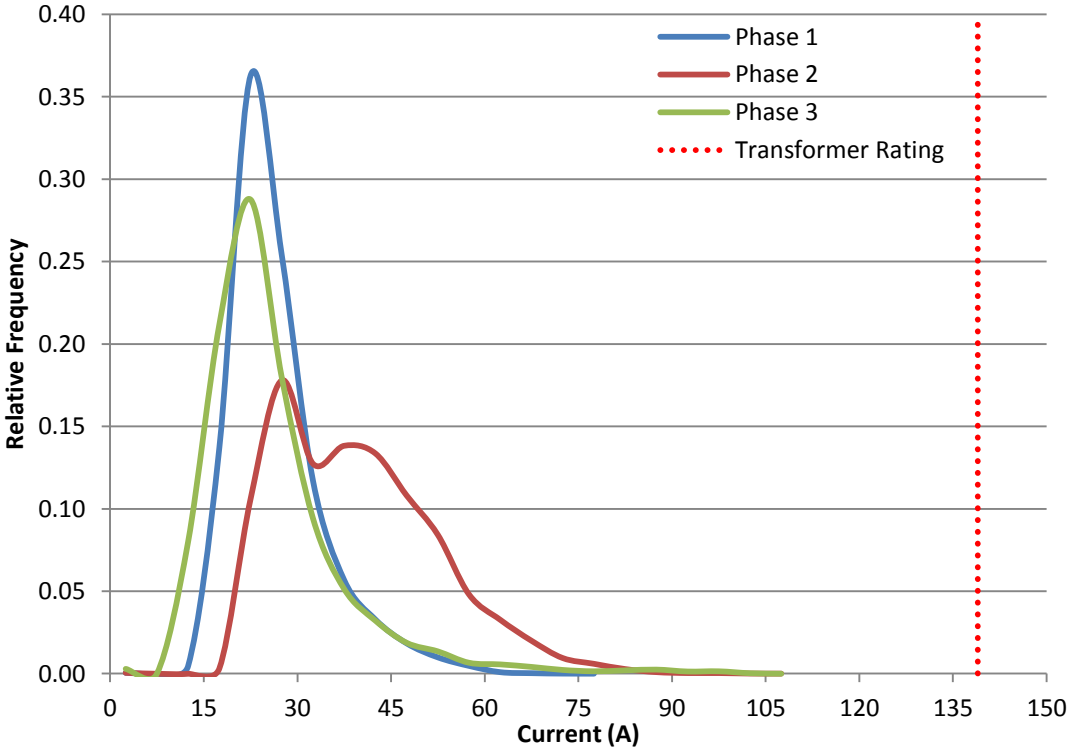

Figure 1.35 Statistical current distribution of the recorded data at the feeding point of the Rhos Wenallt Abernant network

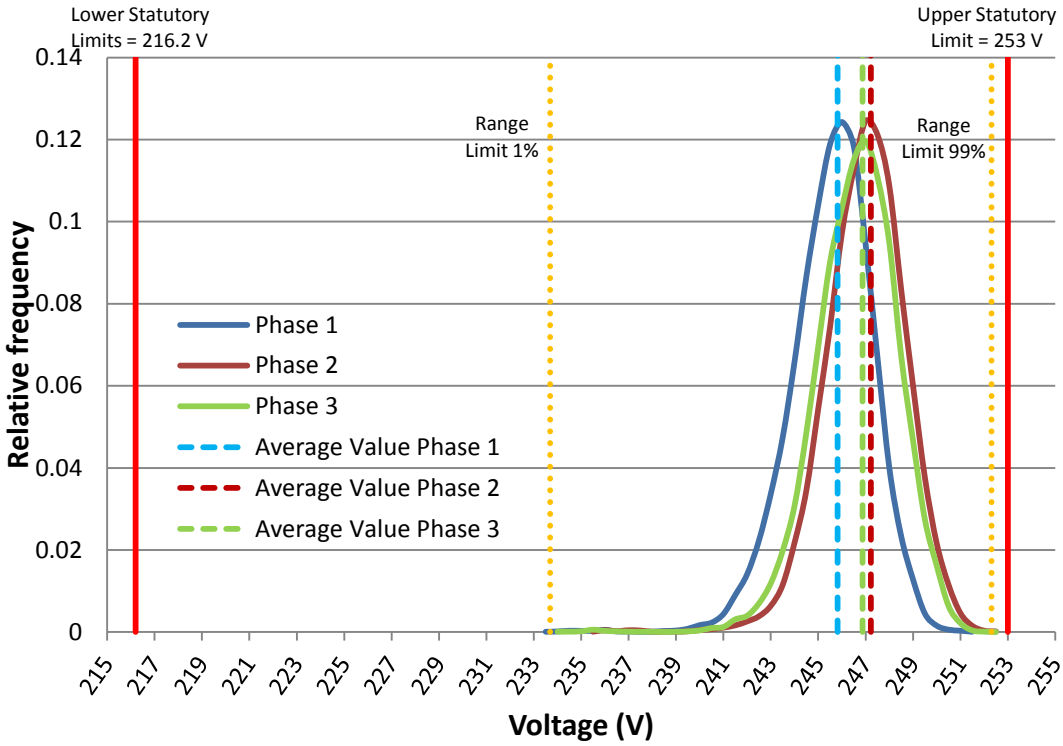

Figure 1.36 Statistical voltage distribution of the recorded data at the feeding point of the Fforchneol Farm Godreaman network

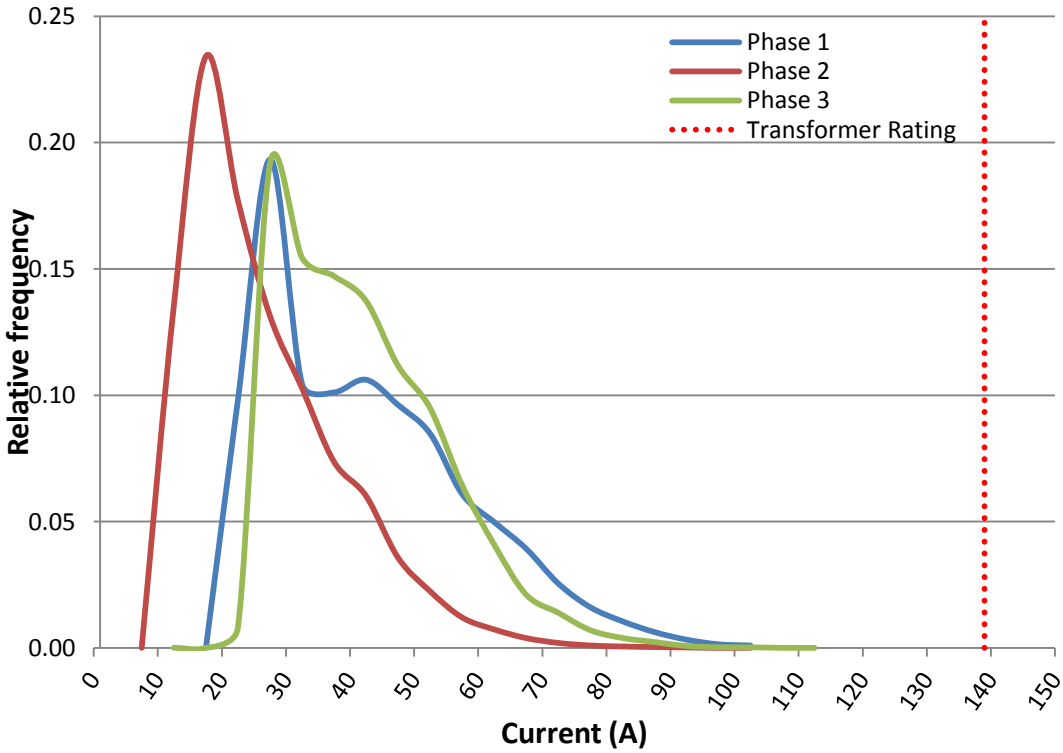

Figure 1.37 Statistical current distribution of the recorded data at the feeding point of the Fforchneol Farm Godreaman network

Chapter 2

Networks description

2.1 Networks provided by Western Power Distribution

In this chapter are described the five networks provided by Western Power Distribution (WPD) and also are illustrated the low voltage (LV) cables and overhead lines characteristics of the networks analysed.
The networks analysed in this thesis are located in Cardiff and in its northern countryside. These networks are under supervision of WPD which has provided us some technical data regarding cables, bus coordinates, voltage, current, power flow and maps. Next figures, from 2.1 to 2.10, show the maps and the line diagrams of all the networks studied. For more technical information about the WPD networks and about the relative underground cables/overhead lines database see appendix A and B.

- Stuttgarter Strasse, Cardiff:

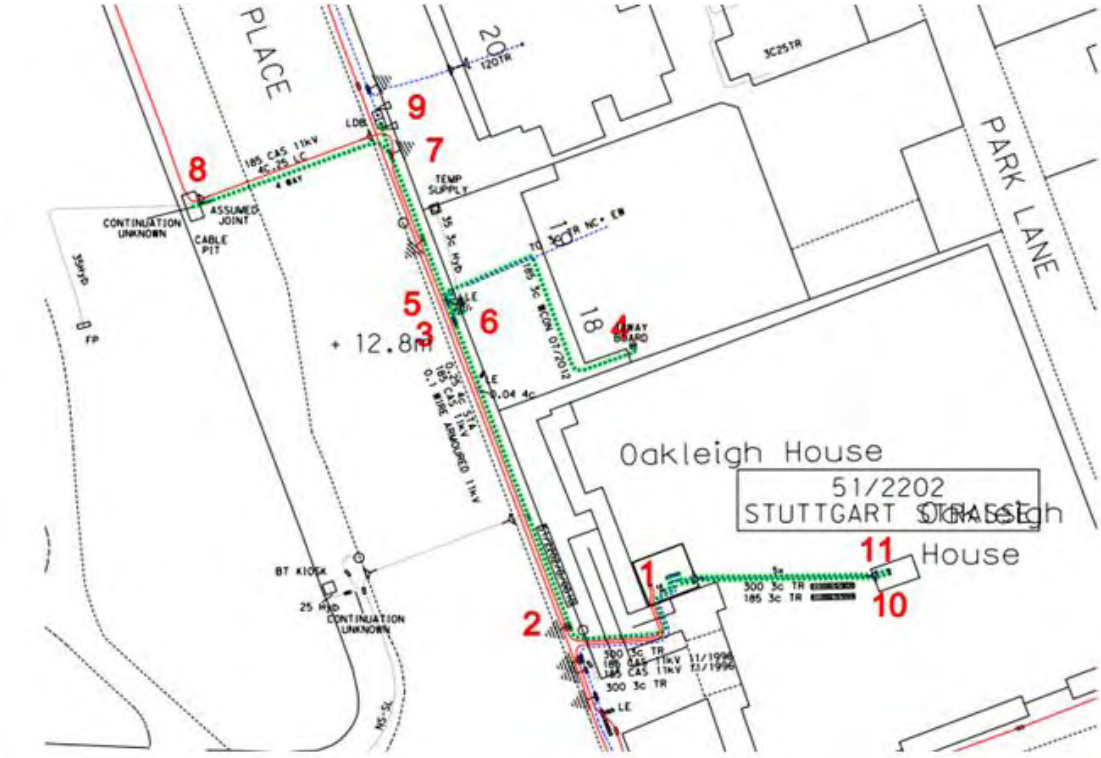

Figure 2.1 Map of Stuttgarter Strasse network.

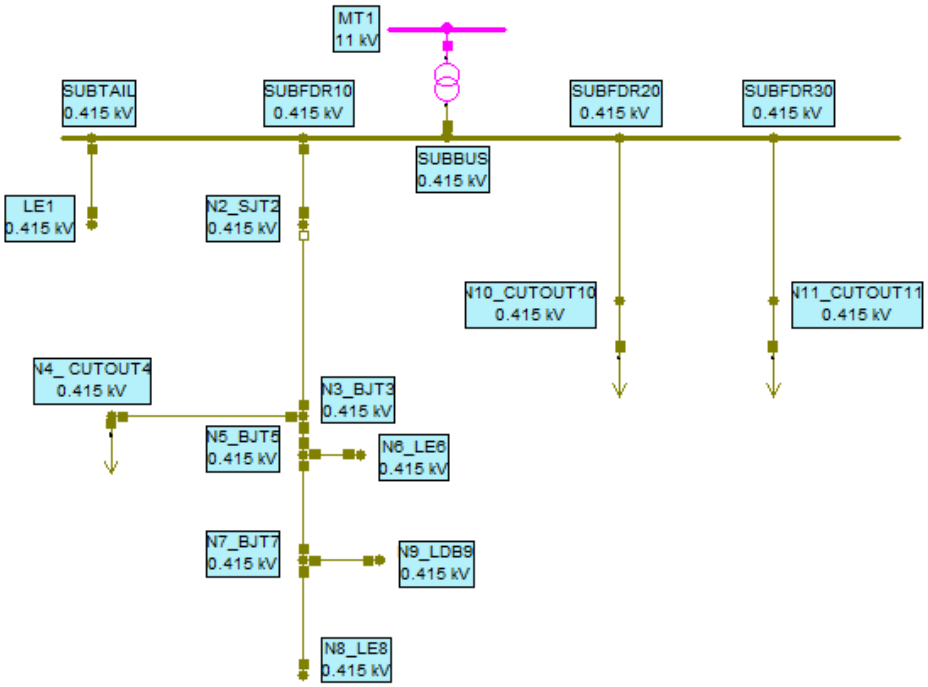

Figure 2.2 Line diagram of Stuttgarter Strasse network

❖ Nettlefold Road, Cardiff:

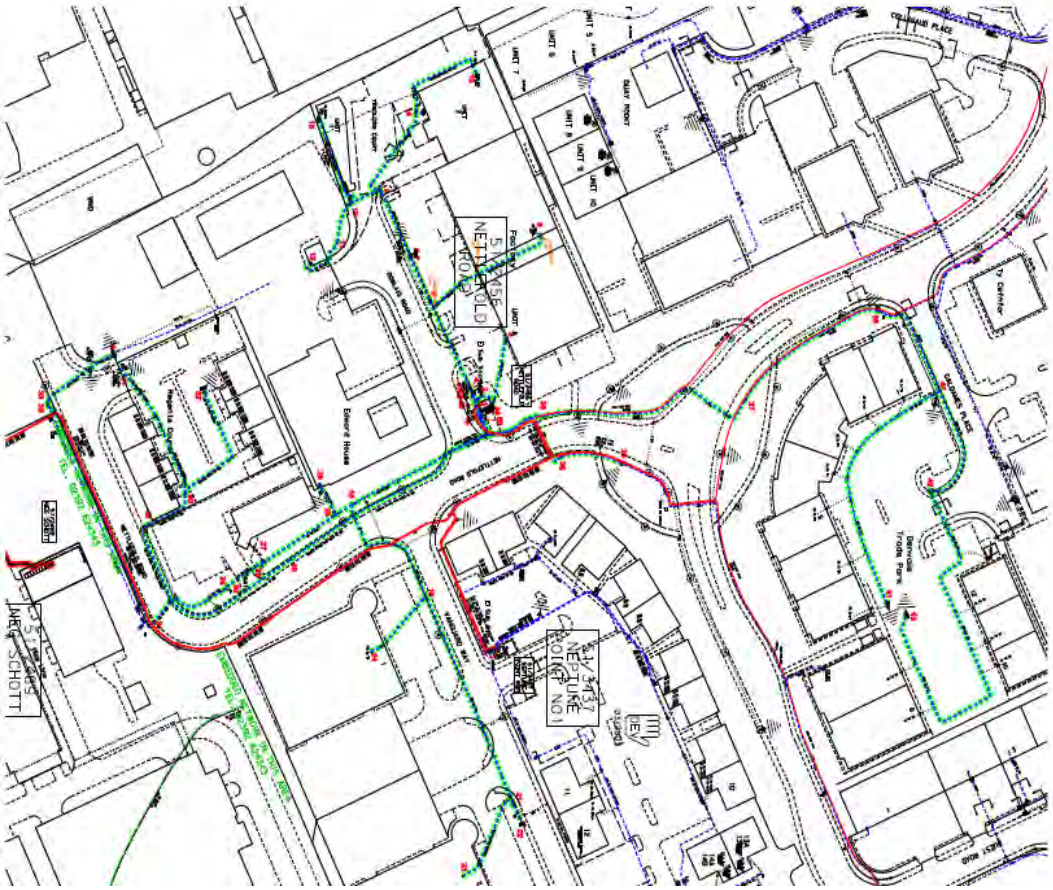

Figure 2.3 Map of Nettlefold Road network

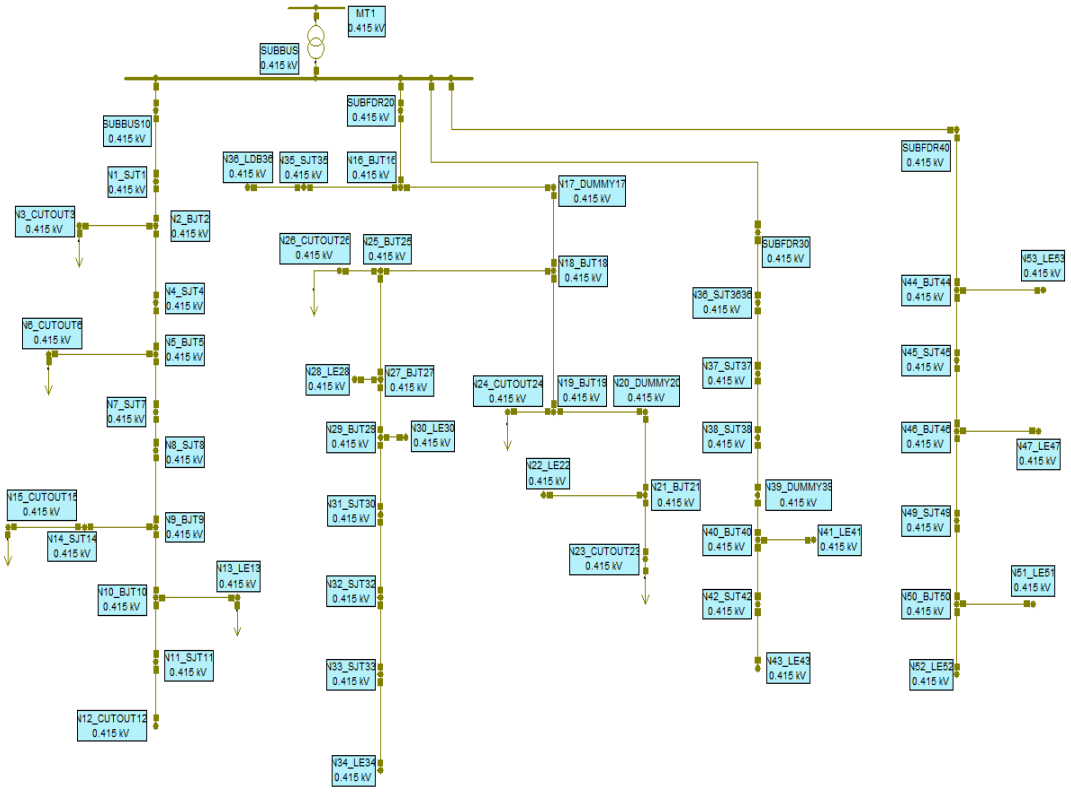

Figure2.4 Line diagram of Nettlefold Road network

- Angus Street, Cardiff:

Figure 2.5 Map of Angus Street network

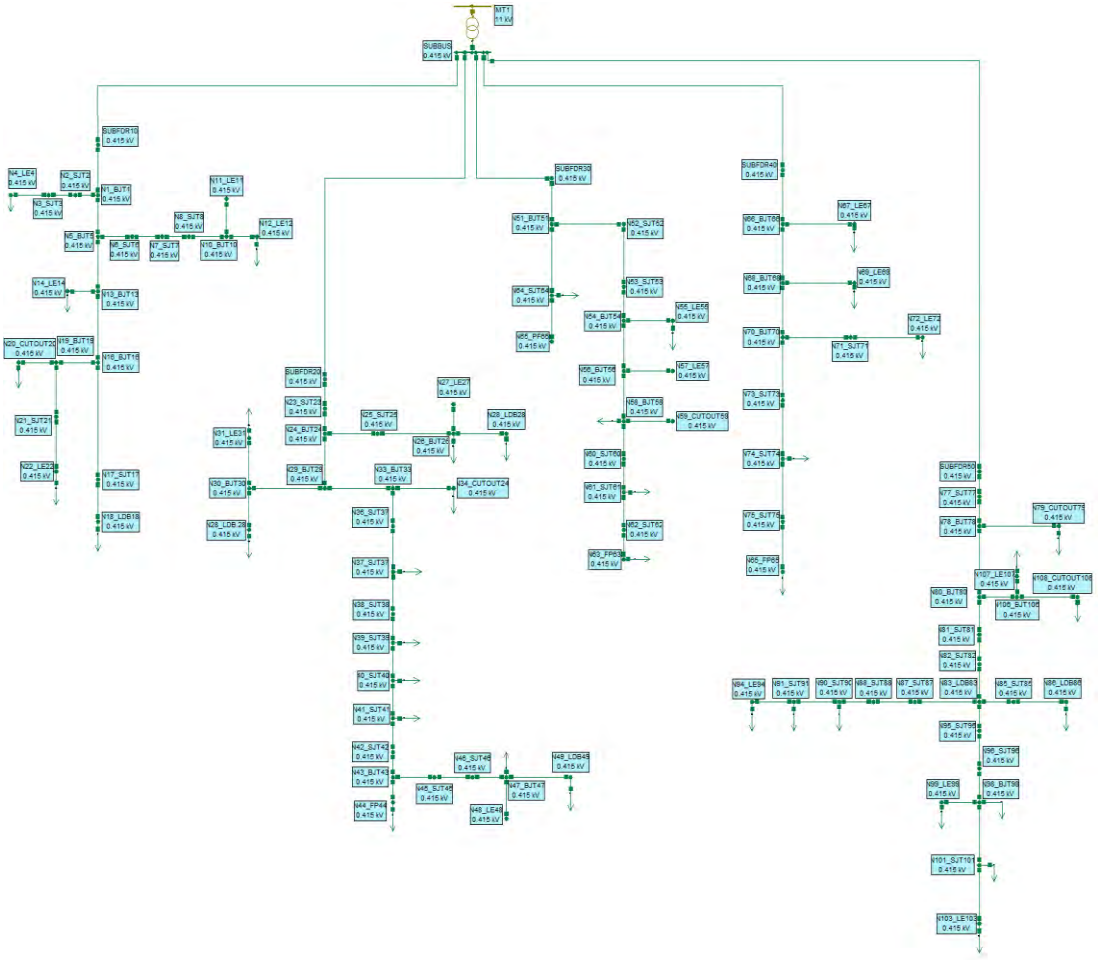

Figure 2.6 Line diagram of Angus Street network

- Rhos Wenallt, Abernant Aberdare:

Figure 2.7 Map of Rhos Wenallt network.

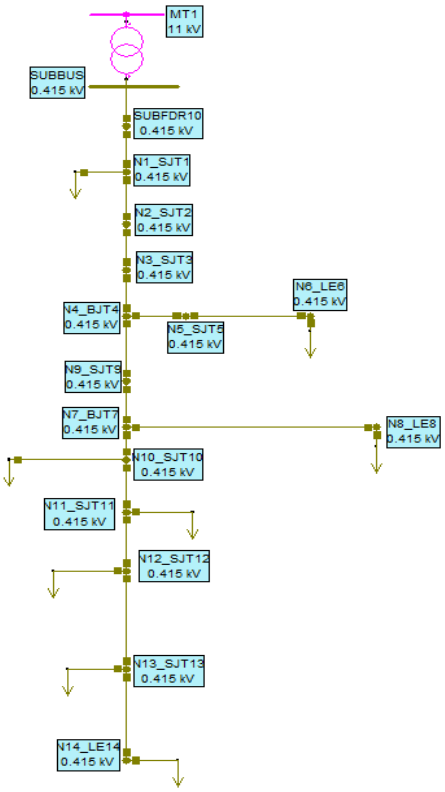

Figure 2.8 Line diagram of Rhos Wenallt network

❖ Fforchneol Farm Godreaman, Aberdare:

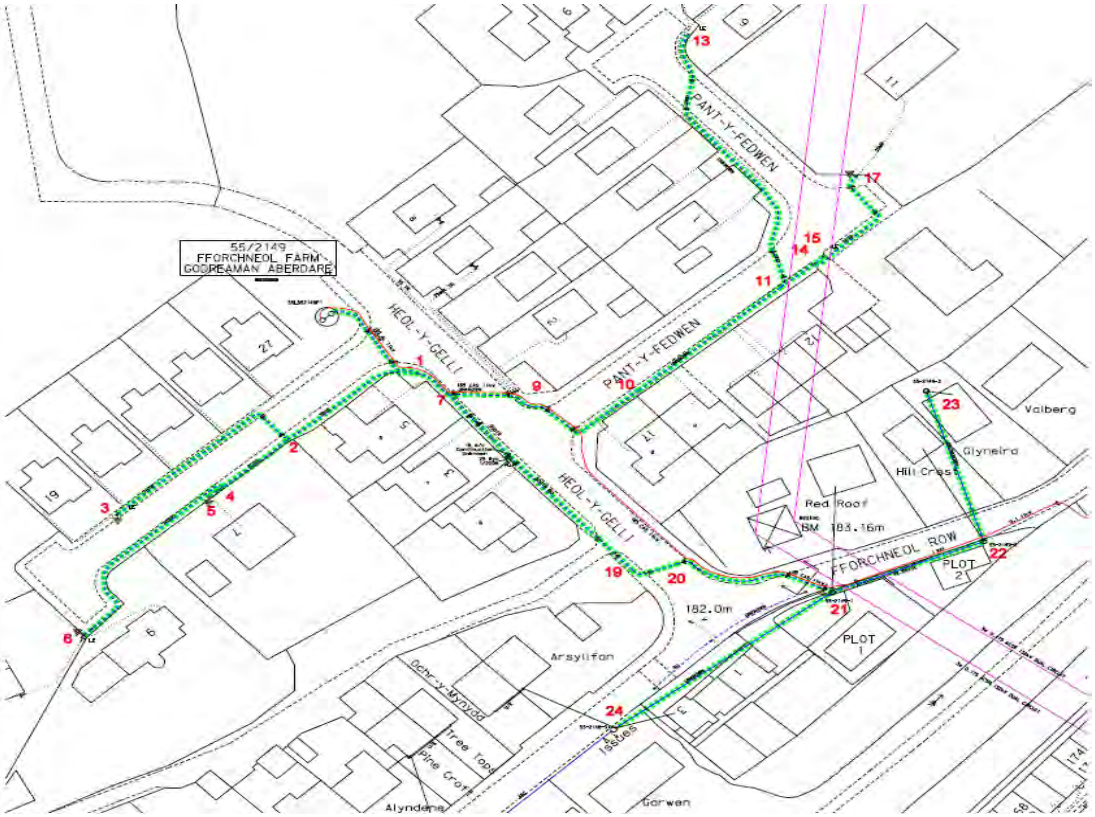

Figure 2.9 Map of Fforchneol Farm Godreaman network

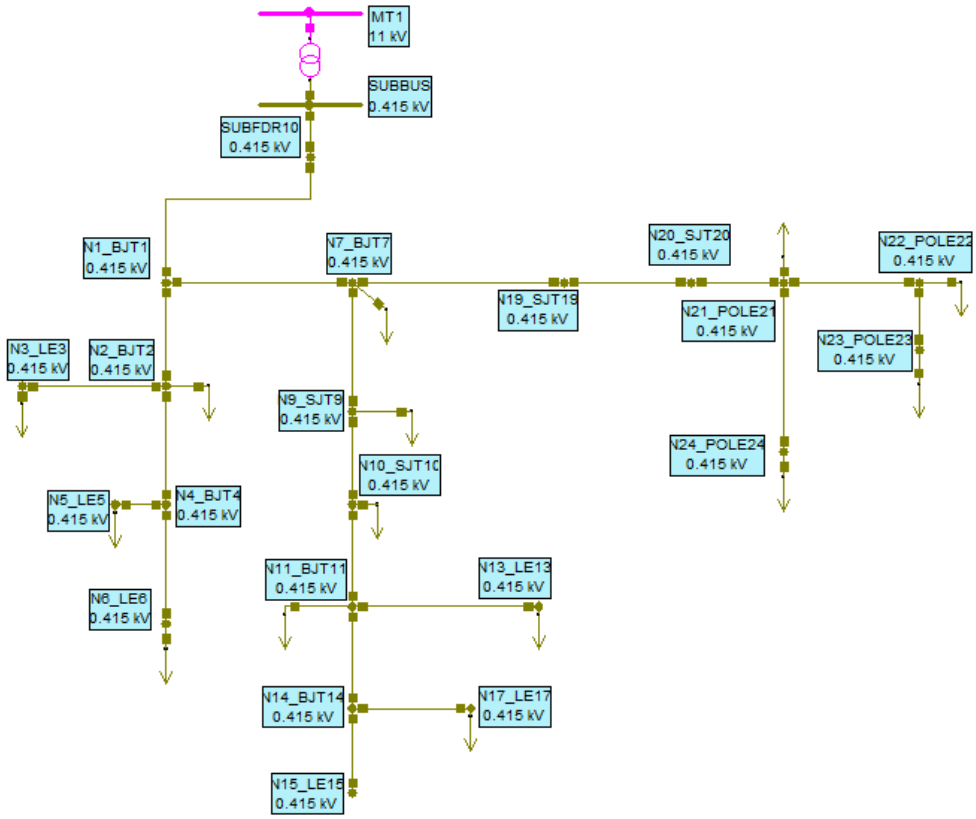

Figure 2.10 Line diagram of Fforchneol Farm Godreaman network

2.2 Types of cables and overhead lines of the networks

2.2.1 Low voltage underground cables

This section is dedicated to technical parameters and features of the underground cables and the overhead lines:

- PILCSTA (paper insulated lead covered steel tape armoured):
  - Three-phase 4 wire system (four core cable)
  - Stranded copper conductors
  - Paper core insulation
  - Lead sheathed
  - Steel tape armoured (STA[1]) and served
  - Three-phase 4 wire system
  - Maximum conductor temperature: 80°C
  - Suitable for 600/1000 [4]

[1] Before the '70s in UK it was common practice for 600/1000V cables to use STA [17]

Figure 2.10 PILCSTA underground cable [4]

- TR XLPE Al 3c SWA:
  - Three core cable
  - Shaped solid aluminium conductor
  - XLPE core insulation
  - Single layer of galvanised steel wires (armour) SWA
  - LSOH (low smoke zero halogen) sheath
  - Rated voltage 0.6/1 kV [5]

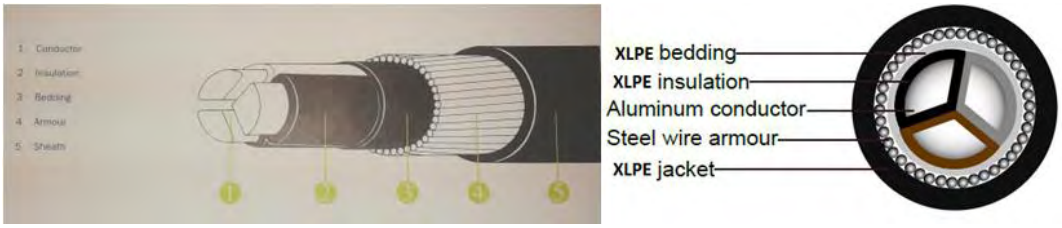

Figure 2.11 Details of TR XLPE Al 3c SWA underground cable. [5]

- WAVCON Al 3c:
  - CNE (combined neutral and earth) cable
  - Three core Aluminium cable + copper neutral wires
  - Solid shaped aluminium conductors
  - XLPE core insulation
  - Extruded PVC oversheath
  - Rubber anti-corrosion bedding
  - Rated voltage 0.6/1 kV [6]

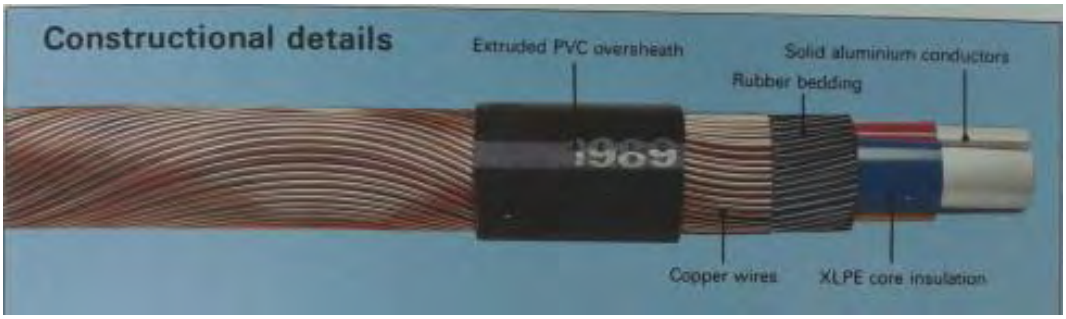

Figure 2.12 Shows a Wavcon Al 3c underground cable

Waveform cable is not a common three core shaped solid aluminium cable, in fact it has a distinctive trait from other cables inasmuch is a CNE cable (combined neutral and earth conductor).

The combined neutral and earth conductor consists of a concentric layer of either aluminium or copper applied in a sinusoidal formation. These wires, if of aluminium, are sandwiched between layers of unvulcanized synthetic rubber compound to give maximum protection against

corrosion. If of copper, the wires are partially embedded in the rubber compound without a rubber overbedding. The aluminium phase conductors and synthetic insulation provide a cable that is light in weight and clean and easy to handle. The most particularity feature of this cable is the simply jointing techniques because the neutral wires need not to be cut as they can be readily formed into a bunch on each side of the phase conductors. [6]

- 35 HYB Al (Hybrid Concentric Neutral HCN Cable):
  - Three phase and three core
  - Solid aluminium conductor
  - XLPE core insulation
  - Single rubber bedding
  - Copper wire helical concentric forming a combined neutral/earth conductor (CNE)
  - Rated voltage 0.6/1 kV
  - PVC sheathed overall [1]

2.2.2 Low voltage overhead lines data

- ABC (Aerial bundled cable):
  - Conductor Round, stranded and compacted aluminium conductor
  - Insulation Extruded black weather-resistant XLPE
  - The cable consists of insulated conductors stranded together where the direction of lay is right handed Z
  - Marking Core identification with longitudinal ridges
  - Advantage XLPE insulation allows high current carrying capacity
  - Rated voltage 0.6/1 kV [7]

Figure 2.14 Shows an Aerial bundled cable.

Aerial Bunched Cables (ABC) is an another way to supply by over head lines distribution systems. In comparison to the conventional bare conductor over head distribution system, ABC has an higher safety and reliability, lower power losses, lower maintenance and operative cost. This system may be used in a lot of contexts effectively, it is ideal for rural distribution in fact is used to replace the existing open wire over head lines, also is especially attractive for installation in difficult terrains such as hilly areas, forest areas, coastal areas etc..

- Open Wire:
  - Three-phase 4 wire system
  - Conductor material: copper (Cu)
  - Insulation not present
  - Rated voltage 0.6/1 kV

2.3 Transformers data

The networks analysed on this project are supplied by different types of transformers, table 2 shows the size of the transformer installed on each WPD network whereas table 3 shows, according to [8], the transformer electrical data considered in this project.

Table 2 Transformer types installed on the networks analysed

	Transformer data	
Network	**Size**	**Manufacturer**
Fforchneol Farm Godreaman Aberdare	100 kVA	Hawker Sideley
Rhos Wenallt Abernant Aberdare	100 kVA	Foster
Nettlefold Road	800 kVA	South Wales Tx
Stuttgart Street	500 kVA	South Wales Tx
Angus Street	1000 kVA	South Wales Tx

Table 3 Transformers electrical data [8]

Voltage ratio [kV]	Rating (kVA)	Number of phases	Short-Circuit Impedance (%)	Current nominal rating (A)
11/0.415	1000	3 Phase	4.75	1391
11/0.415	800	3 Phase	4.75	1113
11/0.415	500	3 Phase	4.75	696
11/0.415	100	3 Phase	4.75	139

Chapter 3

Balanced simulation results on four low voltage networks

3.1 Introduction

In this chapter, steady state power flow simulations are carried out on four Western Power Distribution (WPD) LV balanced networks using the OpenDSS simulation software, considering different operating conditions. These four LV networks have been modelled exploiting the WPD recorded data. The purpose of the balanced simulations is to assess the voltage profiles and thermal capability of the networks under various load conditions. The thermal and voltage assessment is extended to consider the ability of the networks to host embedded generation including renewable energy devices. The simulated network voltages are assessed against the statutory voltage limits and the thermal capability in terms of the individual cable ampacity.
The Open Distribution Simulator Software (OpenDSS) is a comprehensive electrical power system simulation tool intended primarily for the analysis of electric utility power distribution systems. The software enables sinusoidal steady-state analyses commonly performed on such systems. In particular, it has the facility of model unbalanced three-phases systems including unbalanced loads. This feature makes OpenDSS a particularly useful tool for analysis of low voltage systems. [9]

3.2 Stuttgarter Strasse network

3.2.1 Network description and relative parameters

OpenDSS can exploit the buses/nodes coordinates (in our case provided by WPD) in order to plot the semi-geographical network template. Figure 3.1 shows a semi-geographical network template of Stuttgarter Strasse network performed by OpenDSS. It can be noted that in this kind of network layout may be highlighted the loads and the nodes using dots and labels. This simulation tool program also may emphasised the power flow just varying the thickness and the colours of the lines. The nodes (buses) data are shown in Table 4, in which it can be seen that there is a single infeed at SUBBUS and only three main loads (3 phase, wye connection) are present at nodes: 4, 10 and 11; the real power magnitude at those buses have been estimated according to recorded data. Each bus and load characteristics are shown in table 5. In the network simulation cases carried out on chapter 3 and 4, the assumed load values at LV load points within the network have been set to correspond to the cumulative total maximum power measured at the network source (extreme case).

Table 4: Lines and transformer data of Stuttgarter Strasse network

Transformer Data		**P_{sc}**	**V_{sc}**	**Rating [KVA]**	**Ampacity [A]**	**Rated Voltage**	**type**
TR1		1%	4.75%	500	696	11kV/415V	Dyn11
Lines Data		**R**	**X**	**Ampacity [A]**		**Cable type**	
Feeders	**Lines**	**[Ω/Km]**	**[Ω/Km]**				
SUBTAIL	SUBBUS-n1_LE1	0.100	0.0725	496		300 TR XLPE Al 3c	
SUBFDR10	SUBBUS-n2_SJT2	0.100	0.0725	496		300 TR XLPE Al 3c	
	n2_SJT2- n3_BJT3	0.113	0.0689	395		0.25 4c Cu STA	
	n3_BJT3-n4_CUTOUT4	0.164	0.0740	335		185 Wavcon Al 3c	
	n3_BJT3- n5_BJT5	0.113	0.0689	395		0.25 4c Cu STA	
	n5_BJT5-n6_LE6	0.113	0.0689	395		0.25 4c Cu STA	
	n5_BJT5- n7_BJT7	0.113	0.0689	395		0.25 4c Cu STA	
	n7_BJT7- n8_LE8	0.113	0.0689	395		0.25 4c Cu STA	
	n7_BJT7- n9_LDB9	0.113	0.0689	395		0.25 4c Cu STA	
SUBFDR20	SUBBUS- n10_CUTOUT10	0.164	0.074	382		185 TR XLPE Al 3c	
SUBFDR30	SUBBUS- n11_CUTOUT11	0.100	0.0725	496		300 TR XLPE Al 3c	

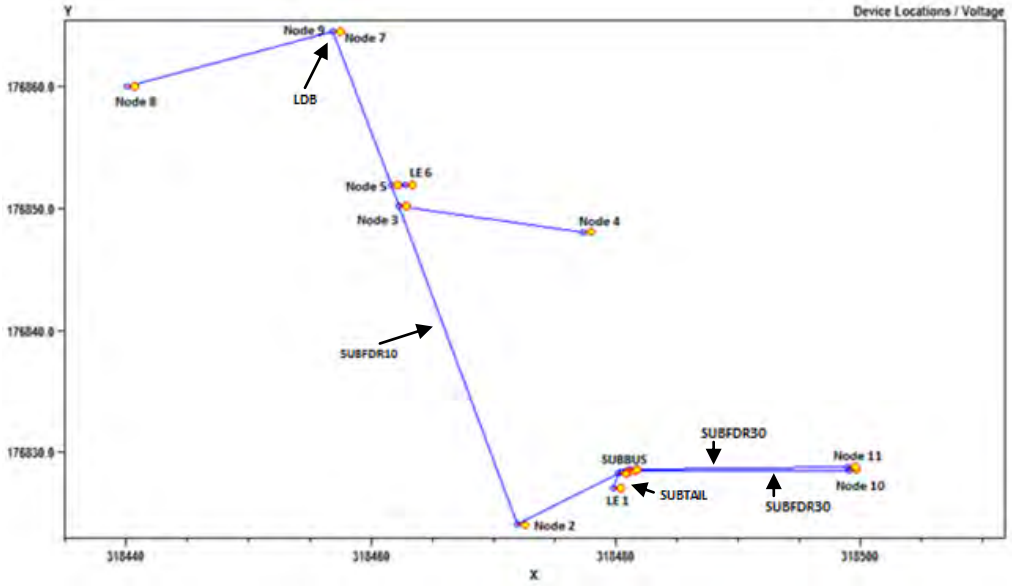

Figure 3.1 Semi-geographical network template (Stuttgarter Strasse) performed by OpenDSS

Table 5: Nodes/buses data of Stuttgarter Strasse network (base load case).

Bus Data	Base Loads		Source/Generator Rated Voltage L-N	
	P (Active Power) kW	Cosφ	kV	p.u.
mt1	/	/	6.3509	1
subbus	/	/	239.6	1
subfdr10	/	/	239.6	1
n2_sjt2	/	/	239.6	1
n3_bjt3	/	/	239.6	1
n4_cutout4	35	1	239.6	1
n5_bjt5	/	/	239.6	1
n6_le6	/	/	239.6	1
n7_bjt7	/	/	239.6	1
n8_le8	/	/	239.6	1
n9_ldb9	/	/	239.6	1
subfdr20	/	/	239.6	1
n10_cutout10	95	1	239.6	1
subfdr30	/	/	239.6	1
n11_cutout11	95	1	239.6	1
subtail	/	/	239.6	1
n1_le1	/	/	239.6	1

3.2.2 Simulation cases of Stuttgarter Strasse network

Stuttgarter Strasse is the first LV (urban) network that has been simulated by OpenDSS. The magnitude of the loads were estimated with the aid of the WPD directive [2] and assuming the maximum total load case from the WPD data provided. In order to assess the extreme cases of the network, it has been selected the maximum power value of the peak load day demand of the whole recorded data which is on 25th July 2012. As shown in table 6, different network operating scenarios has been simulated.

Table 6: Simulation cases analysed at Stuttgarter Strasse network.

Cases	Load Magnitude	Power Factor
1	Nominal load	Unity (1)
2	Nominal load	0.7 Lagging
3	150% of nominal load	Unity (1)

3.2.3 Result analysis of Stuttgarter Strasse simulations: voltage limits

The load cases analysed in the simulations are:

1) Case 1: PF=1

Figure 3.2 shows the voltage profiles voltages along the Stuttgarter Strasse feeders under base load and unity power factor. As can be seen in the graph, the voltage profiles are very flat.
There is a very small voltage drop across the transformer (11kV/415V) of about 0.5% V_n (1.14 V) and also, should be noted from figure 3.3 (with an expanded y-axis scale) that there is a negligible voltage drop along the feeders cables.

1) Case 2: Effects of power factor reduction

Figure 3.4 shows the resulting voltage profiles of the Stuttgarter Strasse feeders when the power factor is assumed about 0.7 (lagging). In this case, at the feeding point, the voltage drop across the transformer has increased of about 2.7% V_n (from 239.60 V to 233.17 V).
However, the voltage drop along the feeders is largely unaffected in fact at the feeder branch SUBBUS-N4_CUTOUT4, in which it is reached the maximum voltage drop on the network, the relative voltage drop value is 0.7 V. While on case 1 the same voltage drop magnitude is about 0.45 V. To highlight the marginally increasing of voltage drop along the feeders, figure 3.5 shows the zoom-in of feeder voltage profiles as function of distance.

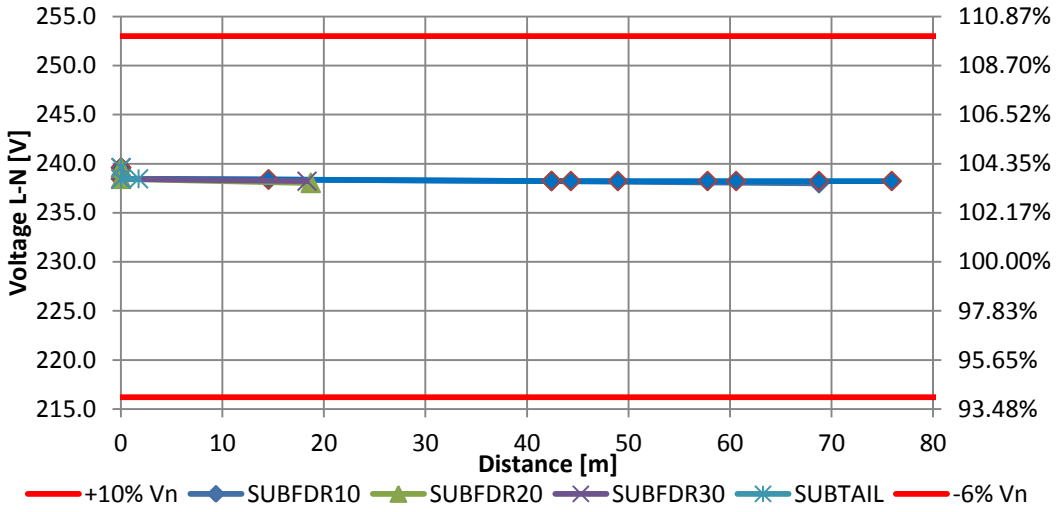

Figure 3.2 Voltage profile of Stuttgarter Strasse main feeders – Case 1: Base case load PF=1

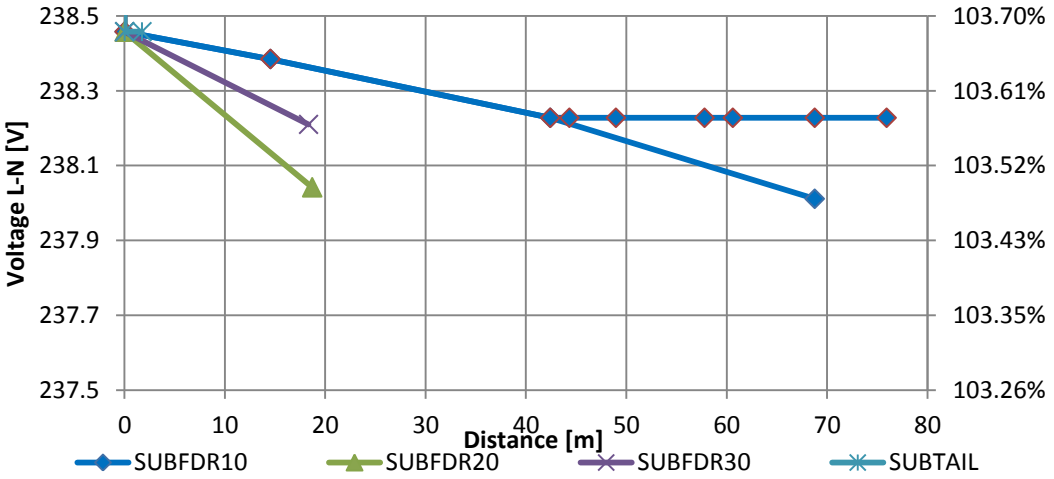

Figure 3.3 Voltage zoom-in profile of Stuttgarter Strasse main feeders – Case 1: Base case load PF=1

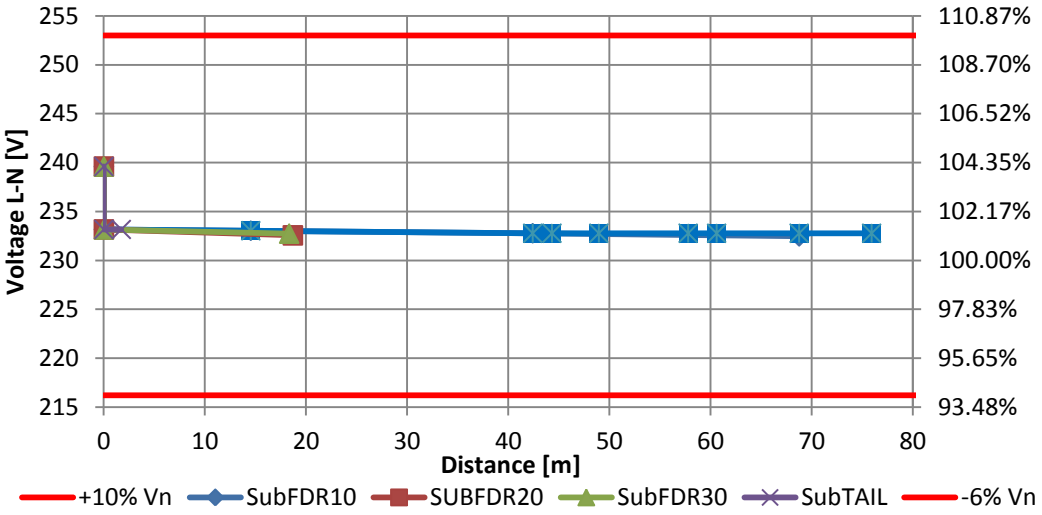

Figure 3.4 Voltage profile of Stuttgarter Strasse main feeders – case 2: Base load case PF=0.7

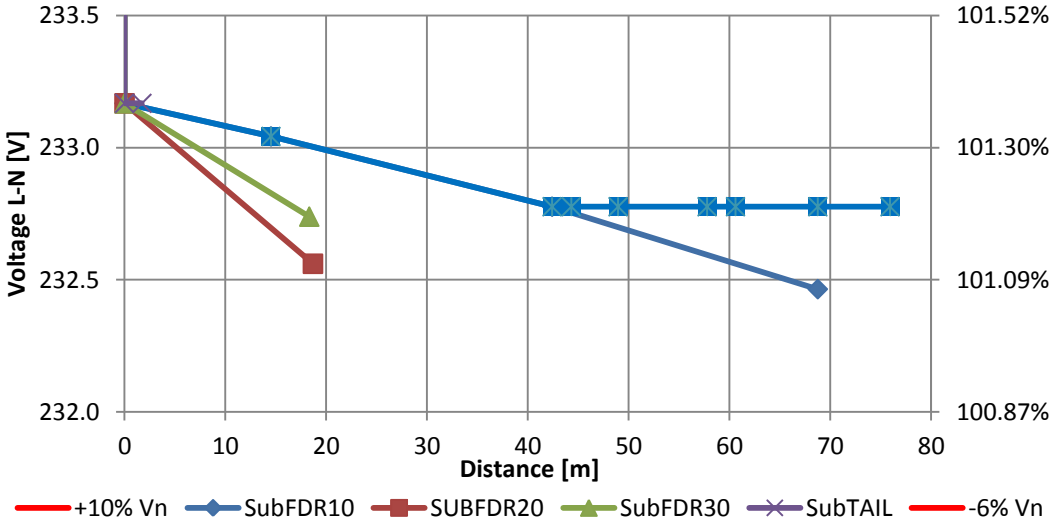

Figure 3.5 Voltage zoom-in profile of Stuttgarter Strasse main feeders – case 2: Base load case PF=0.7

2) Case 3: Effects of nominal real power increased (150% P_n)

Figure 3.6 shows the voltage profiles along the Stuttgarter Strasse feeders under increased loads power (150% P_n) and unity power factor. As can be seen in the graph, the voltage profiles are still very flat. There is a very small voltage drop across the 11kV/415V transformer of about 7.4‰ V_n and also a negligible drop along the feeders cables, indeed at the network branch SUBBUS-N4_CUTOUT4 the relative voltage drop value is 0.67 V while in case 1 the same voltage drop magnitude is about 0.45 V; with an expanded y-axis scale, as shown in Figure 3.7, it can be seen the voltage drop along individual feeders.

Further studies were carried out increasing the real power demand (PF=1) on the network, from the results of these simulations it was observed that the transformer and the feeders voltage drops were slowly increased; these behaviours are also still valid for large rise of load power magnitude. It has been found out that only a sensible PF decreasing can drastically reduced the voltage profile of the network. The consequences on the voltage changes are a possible violation of the relative statutory limits. The transformer voltage drop is the main cause on the voltage limits violations, in fact, along the feeders the voltage drop is not much relevant.

As can be seen in the previous voltage graphs, at the supply point of each feeder the voltage profile is more effected by the transformer voltage drop therefore a voltage regulation should be considered. In the case at issue, the network analysed is a traditionally passive top-down architecture where off-load tap changers are provided for voltage adjustment. [1]

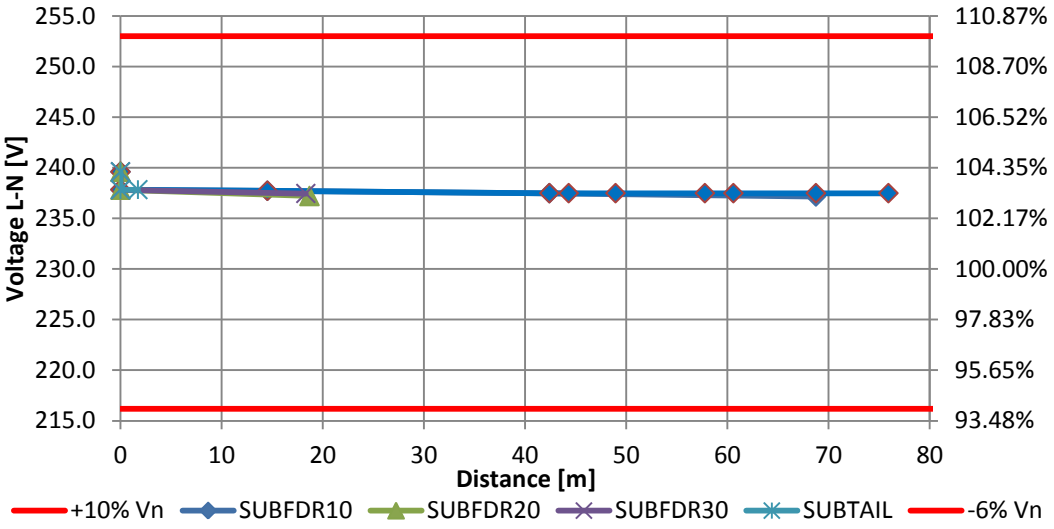

Figure 3.6 Voltage profile of Stuttgarter Strasse main feeders – case 3: 150% $P_{n,}$ PF=1

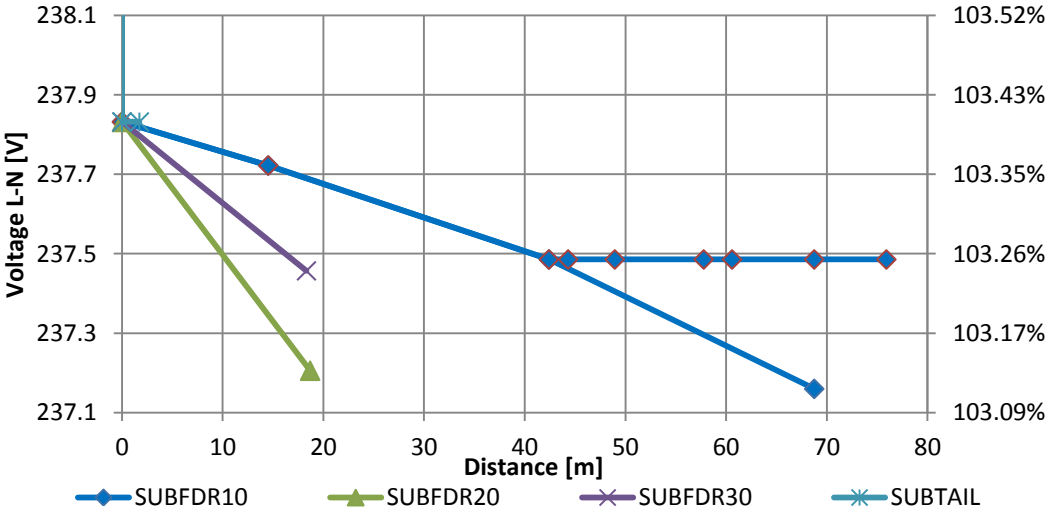

Figure 3.7 Voltage zoom-in profile of Stuttgarter Strasse main feeders – case 3: 150% $P_{n,}$ PF=1

3.2.4 Result analysis of Stuttgarter Strasse simulations: current limits

In the following graphs are analysed only the three active network branches of Stuttgarter Strasse because the other remaining are live end (LE) or inactive branches (see legend of appendix A).

1) Case 1: PF=1

Figure 3.8 shows the branch current profiles along the Nettlefold Road feeders under base load and unity power factor. In this simulation case the current magnitudes are not exceeding the cables ampacity (see Table 4) in fact the thermal limits are still far, especially for SUBFDR10-N4 and for the transformer nominal rating, which is 696 A; this last current limit has not been exceeded because the maximum current value at the main busbar is 314.2 A.

2) Case 2: Effects of power factor reduction

Figure 3.9 shows the profile currents along the Stuttgarter Strasse feeders under nominal load case and power factor of 0.7 (lagging). In this simulation case the transformer nominal rating is not overrun even if the current profile has been shifted up of about 142 A. Also the cables ampacity have been not exceeded by the feeder current.

Further studies were carried out increasing the nominal real power demand (PF=1) on the network in order to find out the network behaviours. With an increasing of 150% P_n the transformer current limit and the rating cables ampacity have been not exceeded. This simulation case is comparable to case 2.
From the simulations carried out so far and also in the following ones, it can be noted that the PF decreasing is affecting more the current magnitude than the voltage drop magnitude, therefore the thermal limit is always the first to be exceeded.

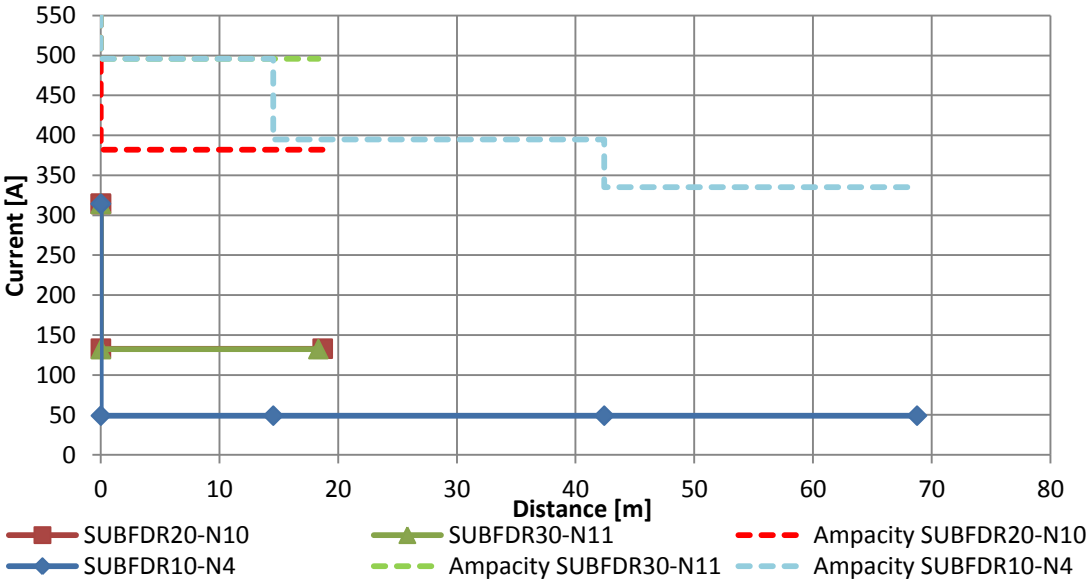

Figure 3.8 Current profile of Stuttgarter Strasse main feeders – Case 1: Base load case PF=1

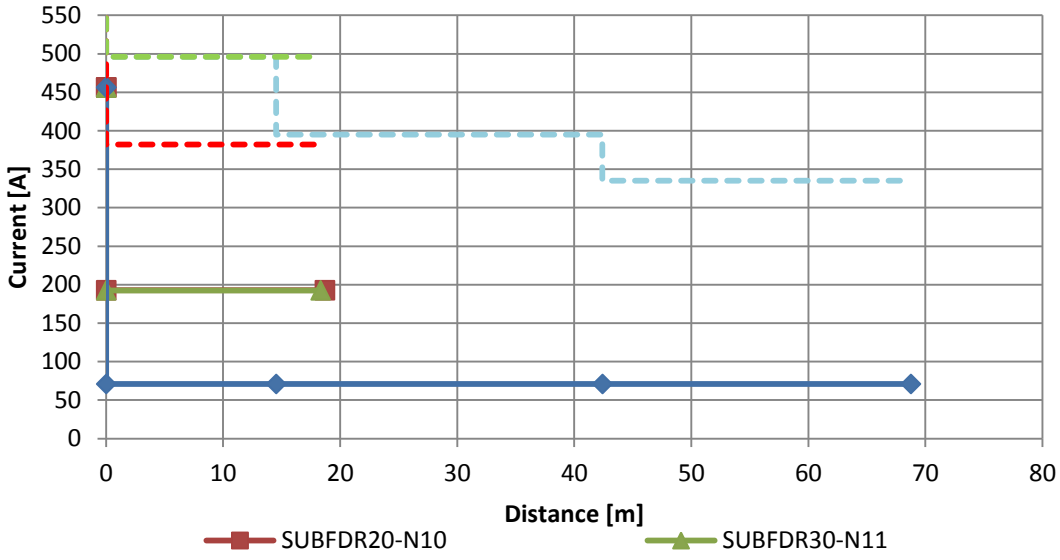

Figure 3.9 Current profile of Stuttgarter Strasse main feeders – case 2: Base load case PF=0.7

3.3 Nettlefold Road network

3.3.1 Network description and relative parameters

Figure 3.10 shows a semi-geographical network template of Nettlefold Road network performed by OpenDSS. As shown in table 7 and table 8, in which are described respectively the nodes/buses characteristics and the estimated loads magnitudes, there is a single infeed at SUBBUS and seven main loads tied to the network.

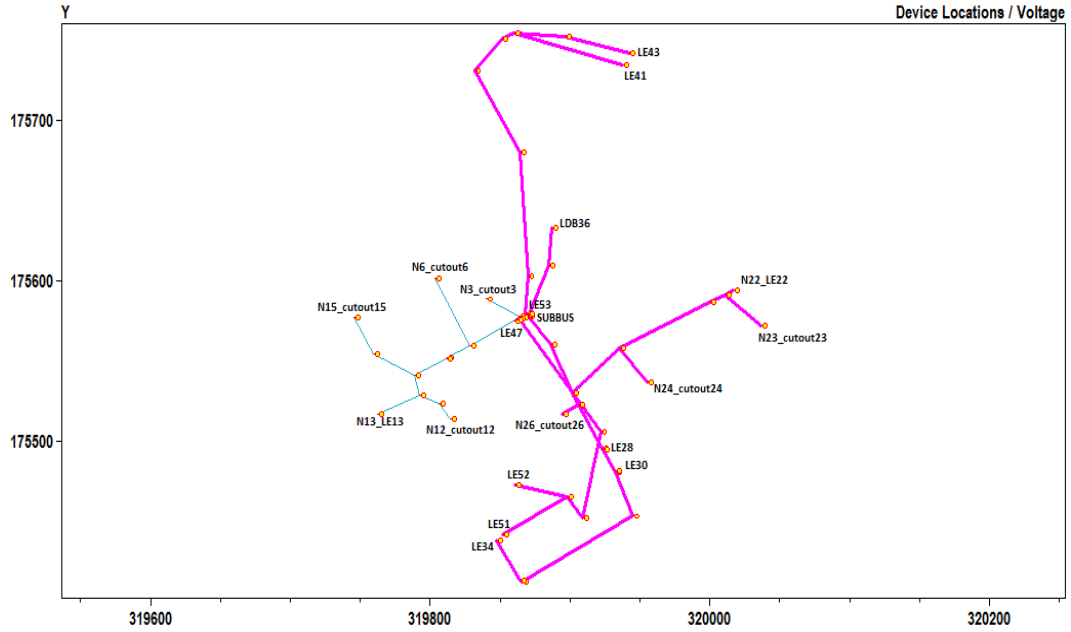

Figure 3.10 Semi-geographical network template (Nettlefold Road) plotted by OpenDSS

Table 7 (1/2): Lines and transformer data of Nettlefold Road network

Transformer Data		P_{sc}	V_{sc}	Rating [kVA]	Ampacity [A]	Rated Voltage	type
TR1		1%	4.75%	800	1113	11/0.415 kV	Dyn11
Lines Data		**R**	**X**	**Ampacity [A]**		**Cable type**	
Feeders	**Lines**	**[Ω/Km]**	**[Ω/Km]**				
SUBFDR10	SUBFDR10-N1_SJT1	0.1	0.0725	495		300 TR XLPE Al 3c	
	N1_SJT1-N2_BJT2	0.1	0.0725	495		300 TR XLPE Al 3c	
	N2_BJT2-N3_CUTOUT3	0.1	0.0725	495		300 TR XLPE Al 3c	
	N2_BJT2-N4_SJT4	0.1	0.0725	435		300 Wavcon Al 3c	
	N4_SJT4-N5_BJT5	0.1	0.0725	495		300 TR XLPE Al 3c	
	N5_BJT5-N6_CUTOUT6	0.164	0.074	335		185 Wavcon Al 3c	
	N5_BJT5-N7_SJT7	0.1	0.0725	495		300 TR XLPE Al 3c	
	N7_SJT7-N8_SJT8	0.1	0.0725	495		300 TR XLPE Al 3c	
	N8_SJT8-N9_BJT 9	0.1	0.0725	495		300 TR XLPE Al 3c	
	N9_BJT 9-N10_BJT 10	0.164	0.074	382		185 TR XLPE Al 3c	
	N11_SJT11-N12_CUT OUT 12	0.164	0.074	382		185 TR XLPE Al 3c	
	N10_BJT 10-N13_LE13	0.164	0.074	335		185 Wavcon Al 3c	
	N9_BJT 9-N14_SJT 14	0.164	0.074	382		185 TR XLPE Al 3c	
	N14_SJT 14-CUT OUT 15	0.164	0.074	335		185 Wavcon Al 3c	
SUBFDR20	SUBFDR20-N16_BJT 16	0.164	0.074	335		185 Wavcon Al 3c	
	N16_BJT 16-N17_DUMMY 17	0.1	0.0725	495		300 TR XLPE Al 3c	
	N17_DUMMY 17-N18_BJT 18	0.1	0.0725	495		300 TR XLPE Al 3c	
	N18_BJT 18-N19_BJT 19	0.1	0.0725	495		300 TR XLPE Al 3c	
	N19_BJT 19-N20_DUMMY 20	0.1	0.0725	495		300 TR XLPE Al 3c	
	N20_DUMMY 20-N21_BJT 21	0.1	0.0725	495		300 TR XLPE Al 3c	
	N21_BJT 21-N22_LE 22	0.1	0.0725	495		300 TR XLPE Al 3c	
	N21_BJT 21-N23_CUTOUT23	0.164	0.074	335		185 Wavcon Al 3c	
	N19_BJT 19-N24_CUTOUT24	0.164	0.074	382		185 TR XLPE Al 3c	
	N18_BJT 18-N25_BJT 25	0.1	0.0725	495		300 TR XLPE Al 3c	
	N25_BJT25-N26_CUT OUT 26	0.253	0.073	278		120 TR XLPE Al 3c	
	N25_BJT 25-N27_BJT 27	0.1	0.0725	495		300 TR XLPE Al 3c	
	N27_BJT 27-N28_LE 28	0.1	0.0725	495		300 TR XLPE Al 3c	

Table 7 (2/2): Lines and transformer data of Nettlefold Road network

Lines Data		R	X	Ampacity [A]	Cable type
Feeders	Lines	[Ω/Km]	[Ω/Km]		
SUBFDR20	N27_BJT 27-N29_BJT 29	0.1	0.0725	495	300 TR XLPE Al 3c
	N29_BJT 29-N30 LE 30	0.1	0.0725	495	300 TR XLPE Al 3c
	N29_BJT 29-N31_SJT 31	0.1	0.0725	495	300 TR XLPE Al 3c
	N31_SJT 31-N32_SJT 32	0.443	0.0755	203	70 TR XLPE Al 3c
	N32_SJT 32-N33_SJT 33	0.443	0.0755	203	70 TR XLPE Al 3c
	N33_SJT 33-N34_LE 34	0.1	0.0725	495	300 TR XLPE Al 3c
	N16_BJT 16-N35_SJT 35	0.1	0.0725	495	300 TR XLPE Al 3c
	N35_SJT 35-N36_LDB 36	0.1	0.0725	495	300 TR XLPE Al 3c
SUBFDR30	SUBFDR30_N36_SJT 36	0.1	0.0725	495	300 TR XLPE Al 3c
	N36_SJT 36-N37_SJT 37	0.1	0.0725	495	300 TR XLPE Al 3c
	N37_SJT 37-N38_SJT 38	0.1	0.0725	495	300 TR XLPE Al 3c
	N38_SJT 38-N39_DUMMY 39	0.1	0.0725	495	300 TR XLPE Al 3c
	N39_DUMMY 39-N40_BJT 40	0.1	0.0725	495	300 TR XLPE Al 3c
	N40_BJT 40-N41_LE 41	0.164	0.074	382	185 TR XLPE Al 3c
	N40_BJT 40-N42_SJT 42	0.1	0.0725	495	300 TR XLPE Al 3c
	N42_SJT 42-N43_LE 43	0.1	0.0725	495	300 TR XLPE Al 3c
SUBFDR40	SUB FDR 40-N44_BJT 44	0.1	0.0725	495	300 TR XLPE Al 3c
	N44_BJT 44-N45_SJT 45	0.1	0.0725	495	300 TR XLPE Al 3c
	N45_SJT 45-N46_BJT 46	0.1	0.0725	495	300 TR XLPE Al 3c
	N46_BJT 46-N47_LE 47	0.1	0.0725	495	300 TR XLPE Al 3c
	N46_BJT 46-N48_SJT 48	0.164	0.074	335	185 Wavcon Al 3c
	N48_SJT 48-N49_SJT 49	0.164	0.074	335	185 Wavcon Al 3c
	N49_SJT 49-N50_BJT 50	0.164	0.074	335	185 Wavcon Al 3c
	N50_BJT 50-N51_LE 51	0.164	0.074	335	185 Wavcon Al 3c
	N50_BJT 50-N51_LE 52	0.164	0.074	335	185 Wavcon Al 3c
	N44_BJT 44-N53_LE 53	0.164	0.074	335	185 Wavcon Al 3c

Table 8 (1/2): Nodes/buses data of Nettlefold Road network (base load case)

Bus Data	Base Loads		Source/Generator Rated Voltage L-N	
	P (Active Power) kW	Cosφ	kV	p.u.
mt1	/	/	6.3509	1
subbus	/	/	239.6	1
subfdr10	/	/	239.6	1
n1_sjt1	/	/	239.6	1
n2_bjt2	/	/	239.6	1
n3_cutout3	70	1	239.6	1
n4_sjt4	/	/	239.6	1
n5_bjt5	/	/	239.6	1
n6_cutout6	70	1	239.6	1
n7_sjt7	/	/	239.6	1
n8_sjt8	/	/	239.6	1
n9_bjt9	/	/	239.6	1
n10_bjt10	/	/	239.6	1
n11_sjt11	/	/	239.6	1
n12_cutout12	70	1	239.6	1
n13_le13	/	/	239.6	1
n14_sjt14	/	/	239.6	1
n15_cutout15	70	1	239.6	1
subfdr20	/	/	239.6	1
n16_bjt16	/	/	239.6	1
n17_dummy17	/	/	239.6	1
n18_bjt18	/	/	239.6	1
n19_bjt19	/	/	239.6	1
n20_dummy20	/	/	239.6	1
n21_bjt21	/	/	239.6	1
n22_le22	/	/	239.6	1
n23_cutout23	16	1	239.6	1
n24_cutout24	16	1	239.6	1
n25_bjt25	/	/	239.6	1
n26_cutout26	16	1	239.6	1
n27_bjt27	/	/	239.6	1
n28_le28	/	/	239.6	1
n29_bjt29	/	/	239.6	1
n30_le30	/	/	239.6	1

Table 8 (2/2): Nodes/buses data of Nettlefold Road network (base load case)

Bus Data	Base Loads		Source/Generator Rated Voltage L-N	
	P (Active Power) kW	Cosφ	kV	p.u.
n31_sjt31	/	/	239.6	1
n32_sjt32	/	/	239.6	1
n33_sjt33	/	/	239.6	1
n34_le34	/	/	239.6	1
n35_sjt35	/	/	239.6	1
n36_ldb36	/	/	239.6	1
subfdr30	/	/	239.6	1
n36_sjt36	/	/	239.6	1
n37_sjt37	/	/	239.6	1
n38_sjt38	/	/	239.6	1
n39_dummy39	/	/	239.6	1
n40_bjt40	/	/	239.6	1
n41_le41	/	/	239.6	1
n42_sjt42	/	/	239.6	1
n43_le43	/	/	239.6	1
subfdr40	/	/	239.6	1
n44_bjt44	/	/	239.6	1
n45_sjt45	/	/	239.6	1
n46_bjt46	/	/	239.6	1
n47_le47	/	/	239.6	1
n48_sjt48	/	/	239.6	1
n49_sjt49	/	/	239.6	1
n50_bjt50	/	/	239.6	1
n51_le51	/	/	239.6	1
n52_le52	/	/	239.6	1
n53_le53	/	/	239.6	1

3.3.2 Simulation cases of Nettlefold Road network

The second LV network simulated by OpenDSS is Nettlefold Road. With the intent of finding the extreme case of the network, it has been selected the maximum power value of the peak load demand day of the whole set recorded, which is on the 30th April 2012.
In Nettlefold Road network are present only seven main loads (3 phase, wye connection) which are connected only in two feeders SUBFDR10 and SUBFDR20. In order to obtain more information about the balanced three phase load flow some simulations were carried out considering different operating network scenarios, which are shown in Table 9.

Table 9: Simulation cases analysed at Nettlefold Road network

Cases	Load Magnitude	Power Factor
1	Nominal load	Unity (1)
2	Nominal load	0.8 Lagging
3	150% of nominal load	Unity (1)

3.3.3 Result analysis of Nettlefold Road simulations: voltage limits

The load cases analysed in these simulations are:

1) Case 1: PF=1

Figure 3.11 shows the voltage profiles along the Nettlefold Road feeders under nominal load case and unity power factor. As can be seen in the graph there is a very small voltage drop across the 11kV/415V transformer of about 4.5‰ V_n and a small drop along the feeders cables. In fact at SUBFDR10-n15_cutout15 branch, in which it is reached the maximum voltage drop on the network, the voltage drop value is about 1.51% V_{SUBBUS} (3.60 V). Figure 3.12 shows, with an expanded y-axis scale, the voltage drop along each individual feeder.

2) Case 2: Effects of power factor reduction

Figure 3.13 shows the resulting voltage profile of the Nettlefold Road feeders when the power factor is assumed 0.8 (lag). In this case the voltage drop across the transformer at the main busbar (SUBBUS) has slightly increased of about 2% V_n. Concerning the voltage drop along the feeders, at SUBFDR10-n15_cutout15 branch the voltage drop is increased of about 2.22% V_{SUBBUS} (5.07 V). Figure 3.14 shows the zoom-in of feeder voltage profiles as function of distance in which it can be seen that the voltage drop along the feeders is just increasing marginally (i.e. for SUBFDR10-n15_cutout15 there is a low voltage drop rise of about 1.47 V).

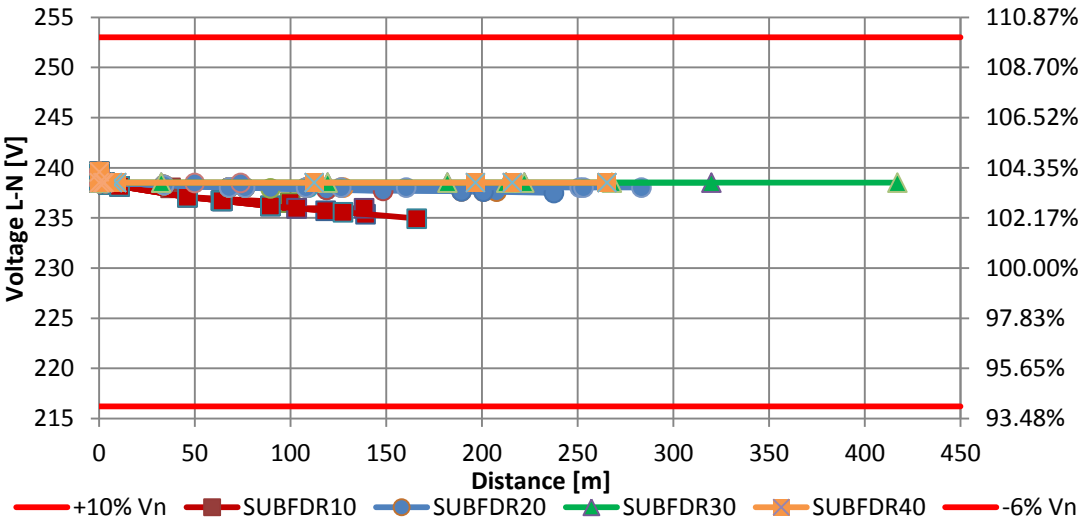

Figure 3.11 Voltage profile of Nettlefold Road main feeders – case 1: Base load case PF=1

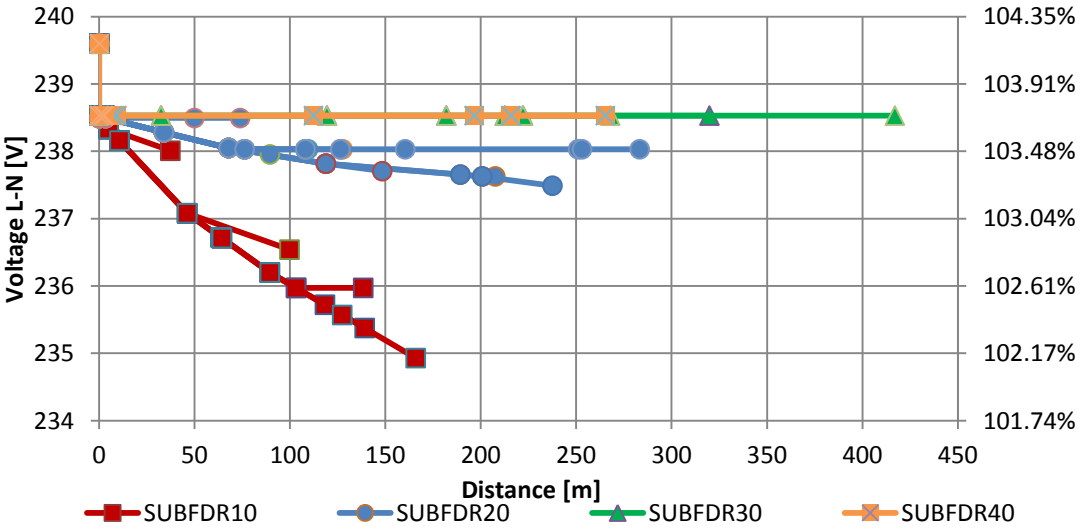

Figure 3.12 Voltage zoom-in profile of Nettlefold Road main feeders – Case 1: Base case load PF=1

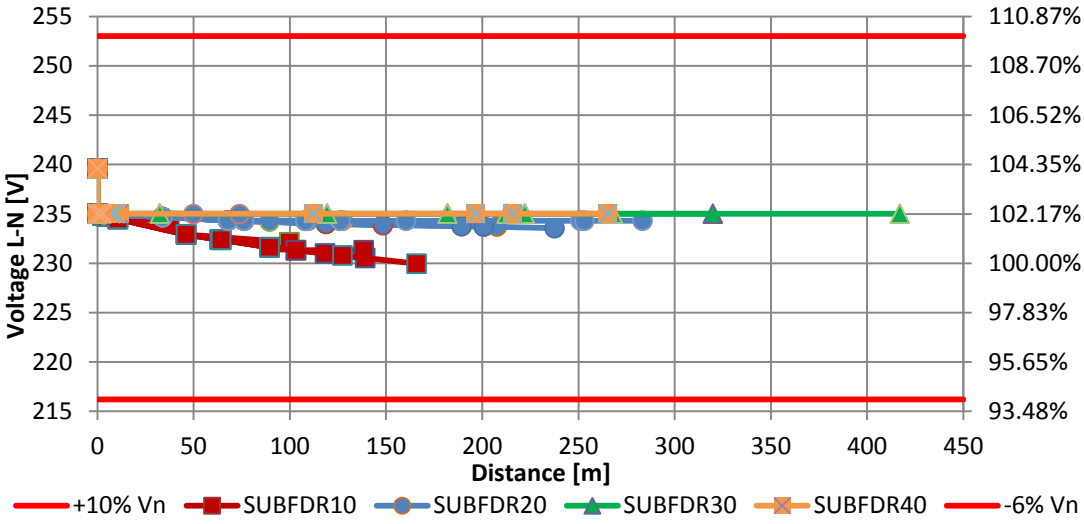

Figure 3.13 Voltage profile of Nettlefold Road main feeders – case 2: Base load case PF=0.8

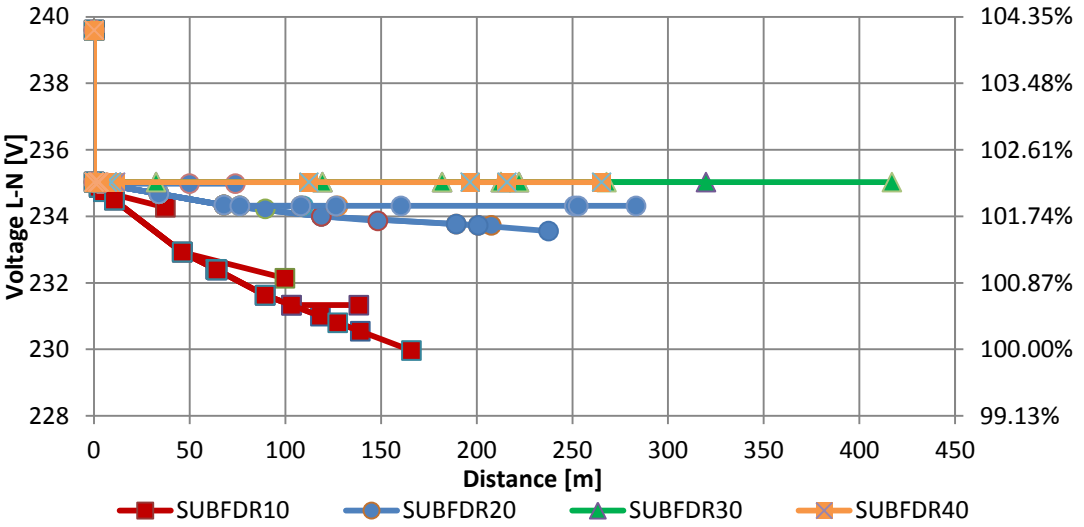

Figure 3.14 Voltage zoom-in profile of Nettlefold Road main feeders – Case 2 Base case load PF=0.8

3) Case 3: Effect of nominal real power increased (150% P_n)

Figure 3.15 shows the voltage profiles along the Nettlefold Road feeders under nominal load increased (150% P_n) and unity power factor. As can be seen in the graph, the voltage profiles of SUBFDR20, SUBFDR30, SUBFDR40 are very flat, should be noted that the last two feeders are not connected with any load. Contrariwise SUBFDR10 is relevant affected by voltage drop, however the statutory limits are not violated.

The voltage drop across the 11kV/415V transformer is still very small about 7‰ V_n and also there is a small voltage drop along the feeders, in fact at SUBFDR10-n15_cutout15 branch the voltage drop value is about 2.3% V_{SUBBUS} (5.5 V). Figure 3.16 shows, with an expanded y-axis scale, the voltage drop along each individual feeder.

Further studies were carried out increasing the real power demand (PF=1) on the network. From the simulation results was observed that the transformer and the feeders voltage drops were slowly increased, these behaviours are also still valid for large rise of load power magnitude, as might be 200% P_n for each load.

Even in this urban network it was found that only a sensible PF variation can relevant vary the voltage profile of the network and therefore a possible statutory voltage limits violation. In comparison with the previous urban network, the voltage drop along the feeder is greater than that of transformer. A reason why of this behaviour might be caused to the different types of transformers that are supplying the networks, indeed the relative power rating of Nettlefold Road's transformer is higher than Stuttgarter Strasse's transformer.

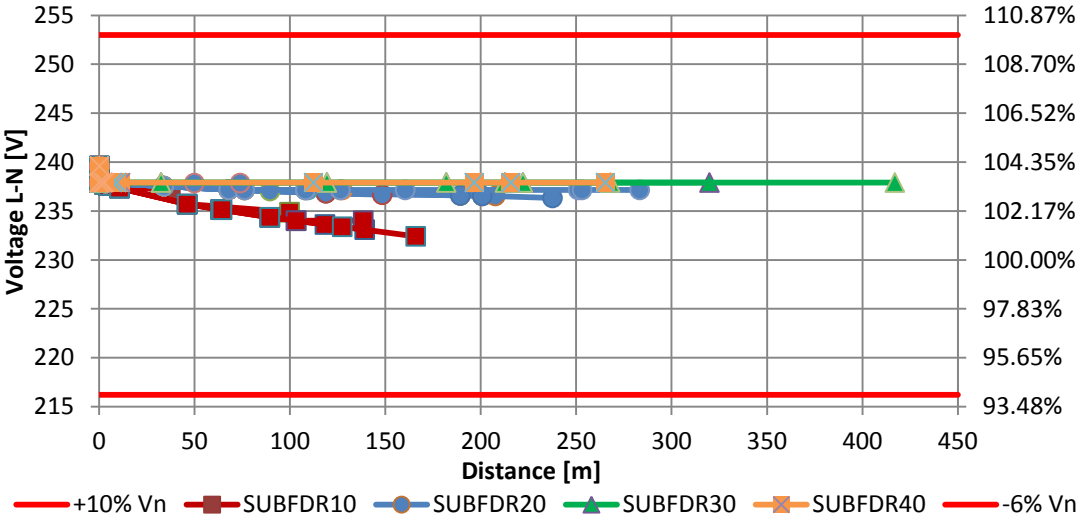

Figure 3.15 Voltage profile of Nettlefold Road main feeders – case 3: 150% P_n, PF=1

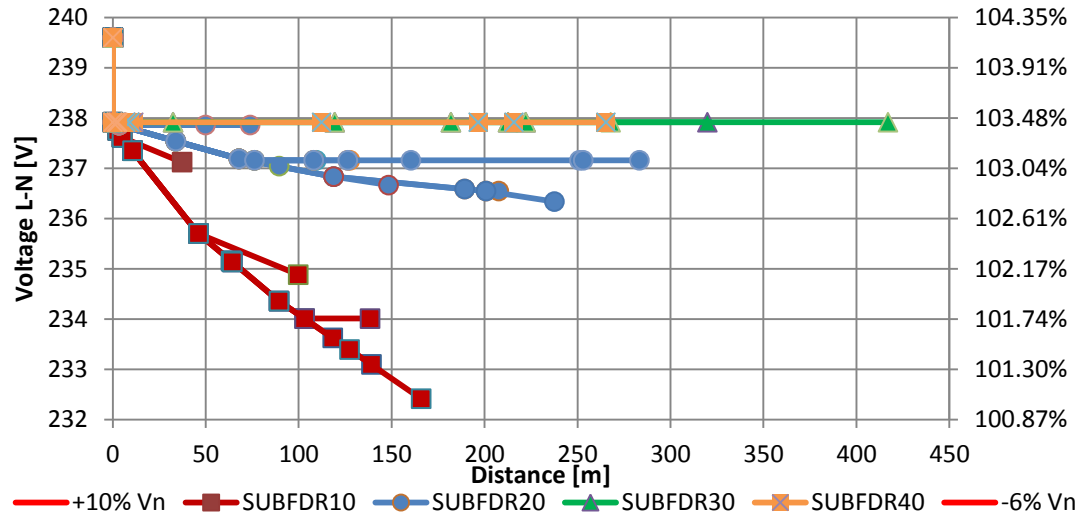

Figure 3.16 Voltage zoom-in profile of Nettlefold Road main feeders – case 3: 150% P_n, PF=1

3.3.3 Result analysis of Nettlefold Road simulations: current limits

In the following graphs are analysed only the seven active branches of the network because the other remaining are live end (LE) cable (see appendix A) or just inactive branches.

1) Case 1: PF=1

Figure 3.17 and 3.18 show the branch current profiles along the Nettlefold Road feeders under nominal load case and unity power factor. In this simulation case the cables ampacity and the transformer nominal rating are not exceeded (see Table 7) in fact the thermal limits are rather high if compared with the operating currents, especially for SUBFDR20 in which there are very

low current values. While at SUBBUS the relative current value is 461.96 A, which is not much low compared to the transformer current rating (696 A). In both figures 3.17 and 3.18 are shown the current profiles of each active feeder branch of SUBFDR10 and SUBFDR20 respectively.

2) Case 2: Effects of power factor reduction

Figure 3.19, 3.20 and 3.21 shows the branch current profiles along the Nettlefold Road feeders under base load case and power factor value of 0.8 (lagging). In this simulation case the transformer rating is still not violated because the current value at the network feeding point is about 573.4 A. Also at the network branches analysed their thermal limits are always not violated but in this operating scenario the actual currents values are very close to the rated cables ampacity. In fact, for instance at the first bus of SUBFDR10 the current trend is perilously approaching the cable ampacity (495 A) with a relative value of 490.15 A. Whereas concerning the cables ampacity of the other feeder considered in figure 3.21 (SUBFDR20), the relative current trends are very low: 83.28 A. Therefore the thermal limits on SUBBUS20 will never exceeded.
It has been also simulated case 3 but it was observed that the resulting current values of the network are comparable to case 2.

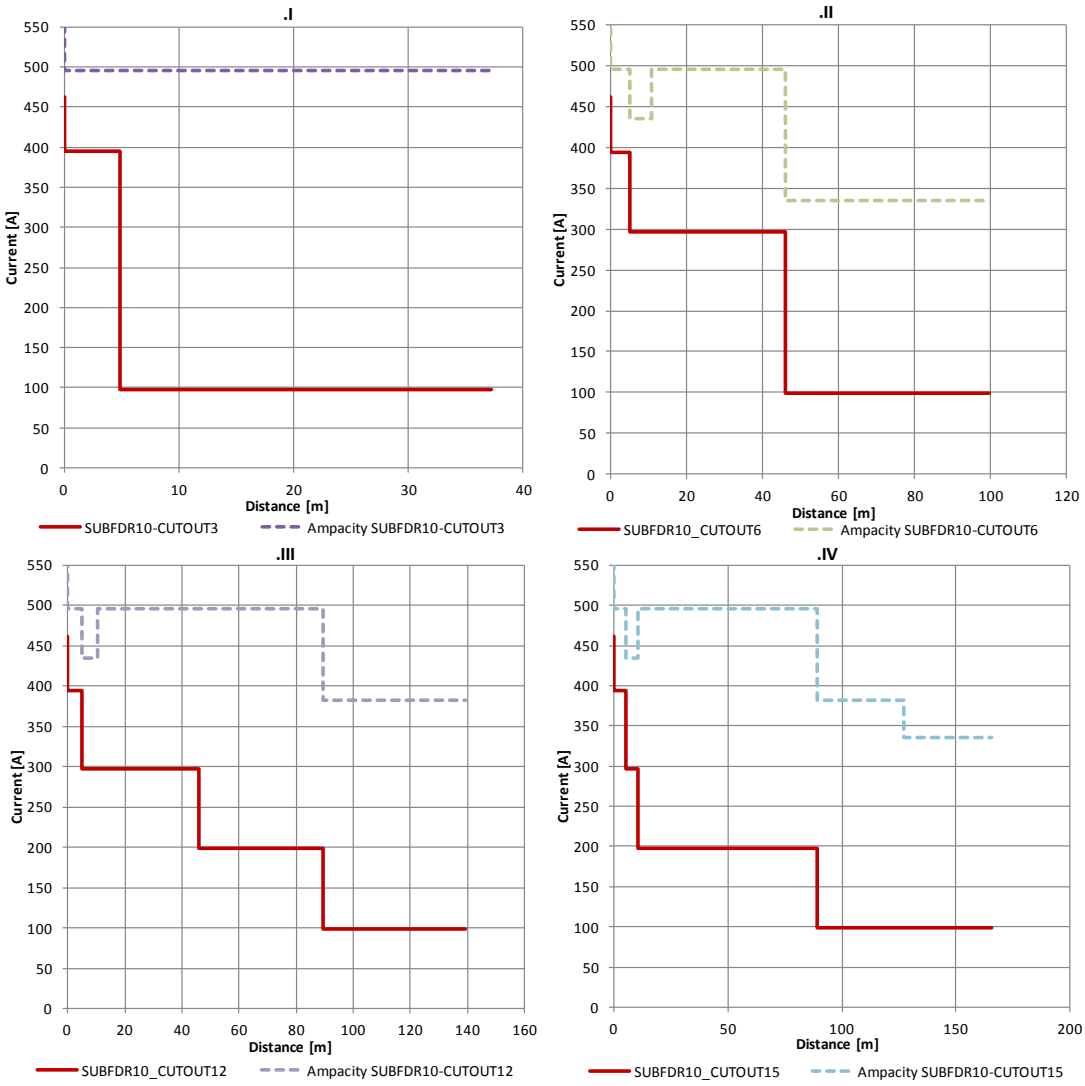

Figure 3.17 Branch current profiles of SUBFDR10 at Nettlefold Road– Case 1: Base load case PF=1: .I SUBFDR10-CUTOUT3, .II SUBFDR10-CUTOUT6, .III SUBFDR10-CUTOUT12 and .IV SUBFDR10-CUTOUT15

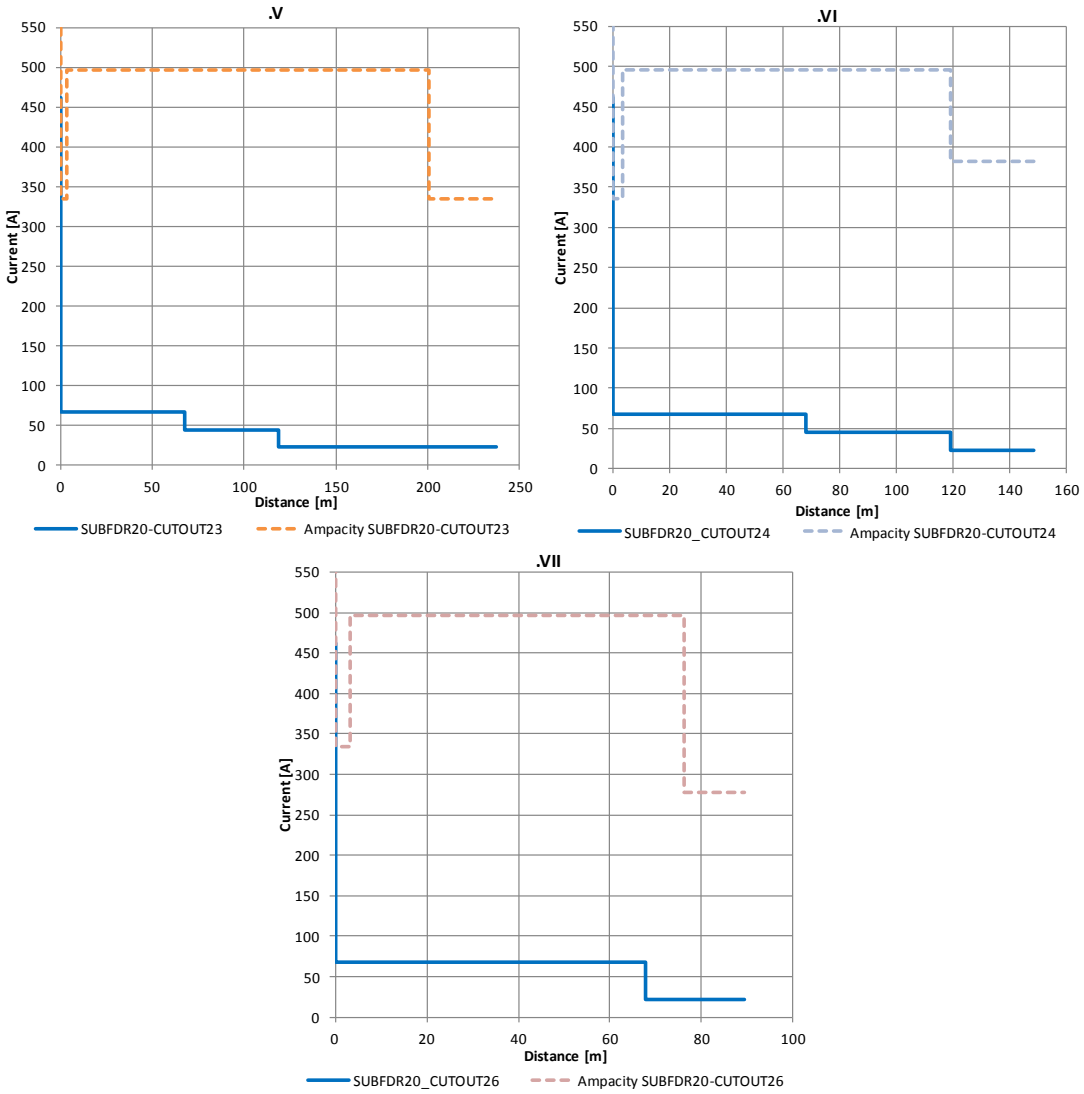

Figure 3.18 Branch current profiles of SUBFDR20 at Nettlefold Road– Case 1: Base load case PF=1: .V SUBFDR20-CUTOUT23, .VI SUBFDR10-CUTOUT24 and .VII SUBFDR10-CUTOUT26

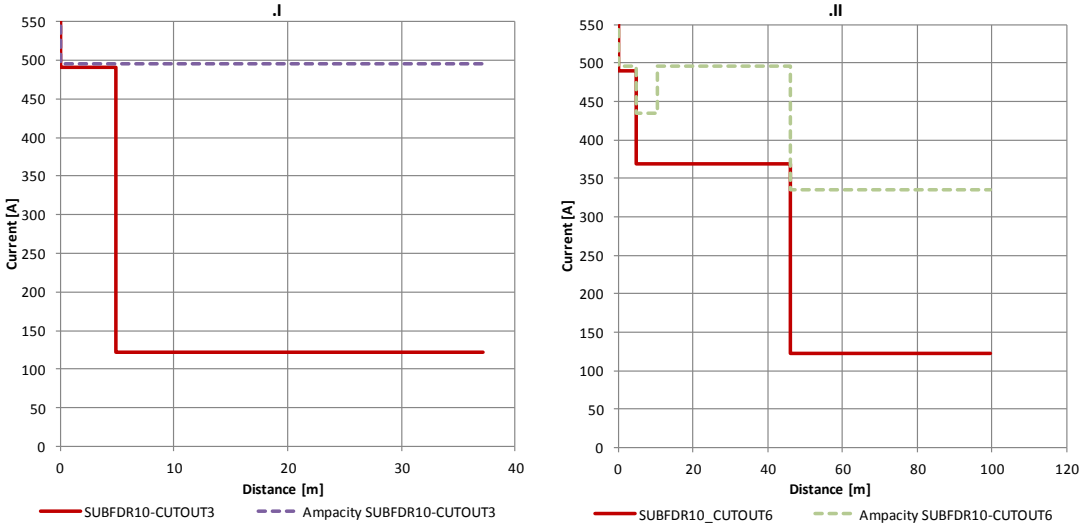

Figure 3.19 Branch current profiles of SUBFDR10 at Nettlefold Road– Case 2: Base load case PF=0.8: .I SUBFDR10-CUTOUT3 and .II SUBFDR10-CUTOUT6

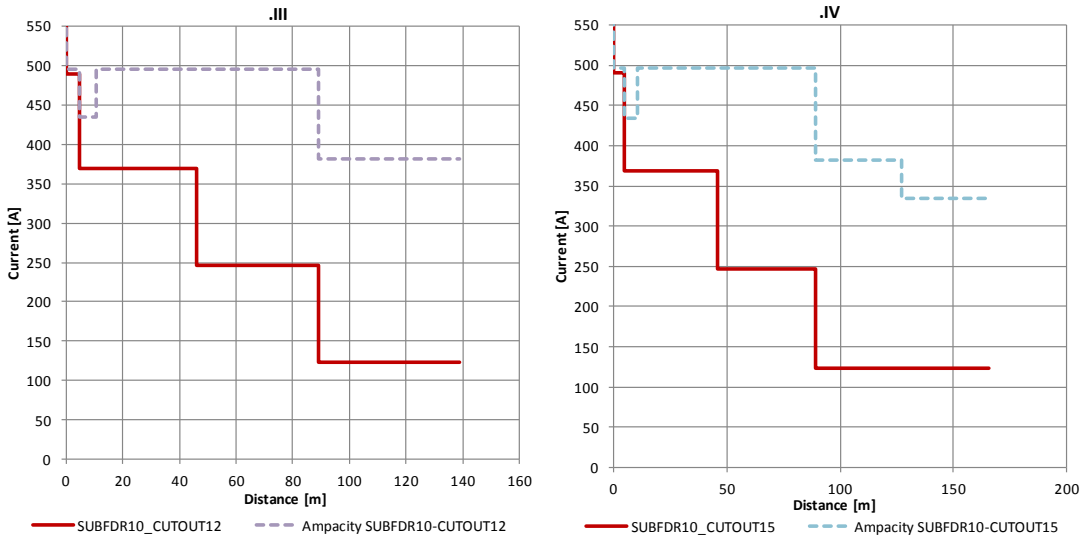

Figure 3.20 Branch current profiles of SUBFDR10 at Nettlefold Road– Case 2: Base load case PF=0.8: .III SUBFDR10-CUTOUT12 and .IV SUBFDR10-CUTOUT15

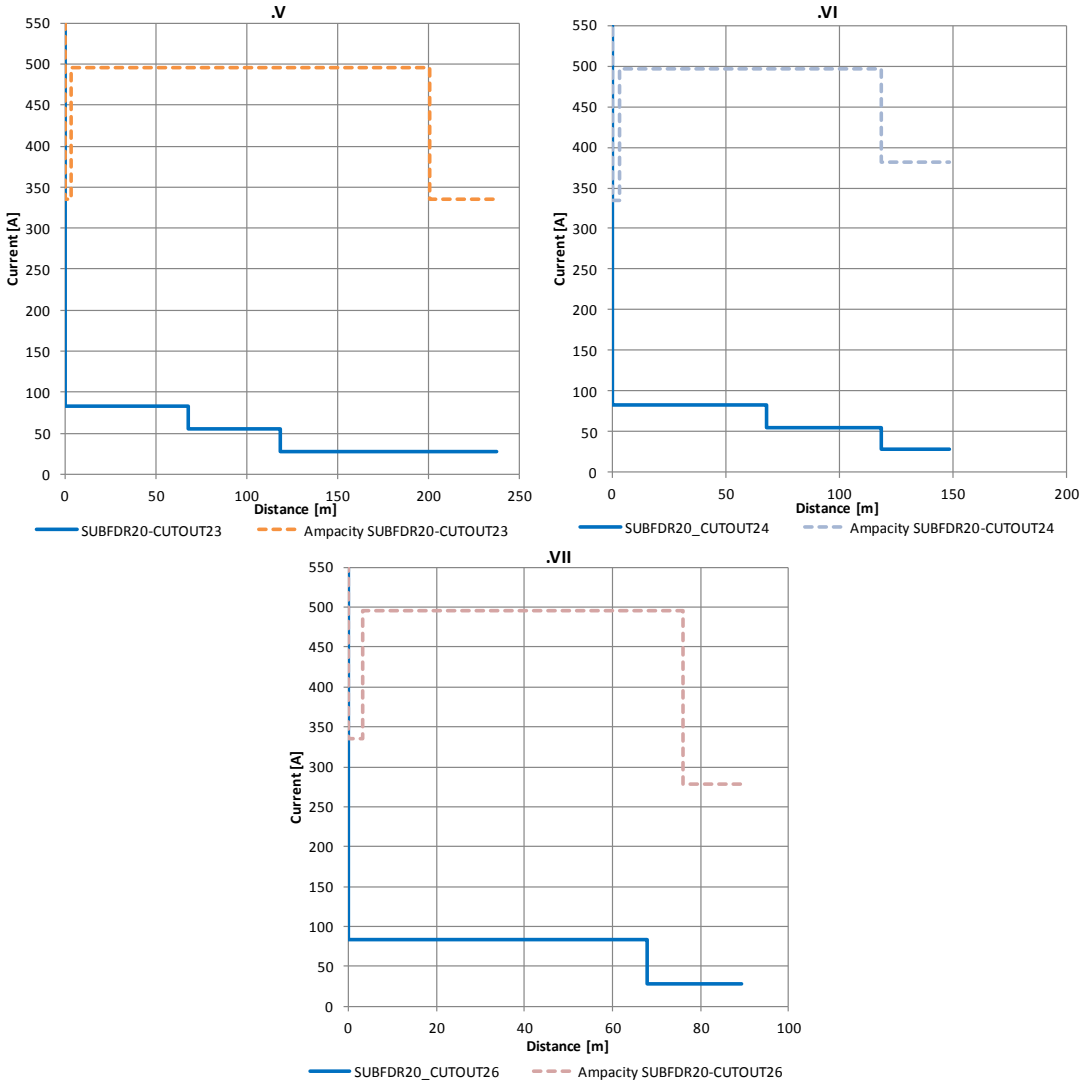

Figure 3.21 Branch current profiles of SUBFDR20 at Nettlef old Road– Case 2: Base load case PF=0.8: .VI SUBFDR10-CUTOUT24 and .VII SUBFDR10-CUTOUT26

3.4 Rhos Wenallt Abernant network

3.4.1 Network description and relative parameters

Figure 3.22 shows a semi-geographical network template of Rhos Wenallt Abernant network performed by OpenDSS. from table 10 and 11, in which are described respectively the nodes/buses characteristics and the estimated loads magnitudes, should be noted that there is a single infeed at the network supply point (SUBBUS) and seven main loads connected to the network.

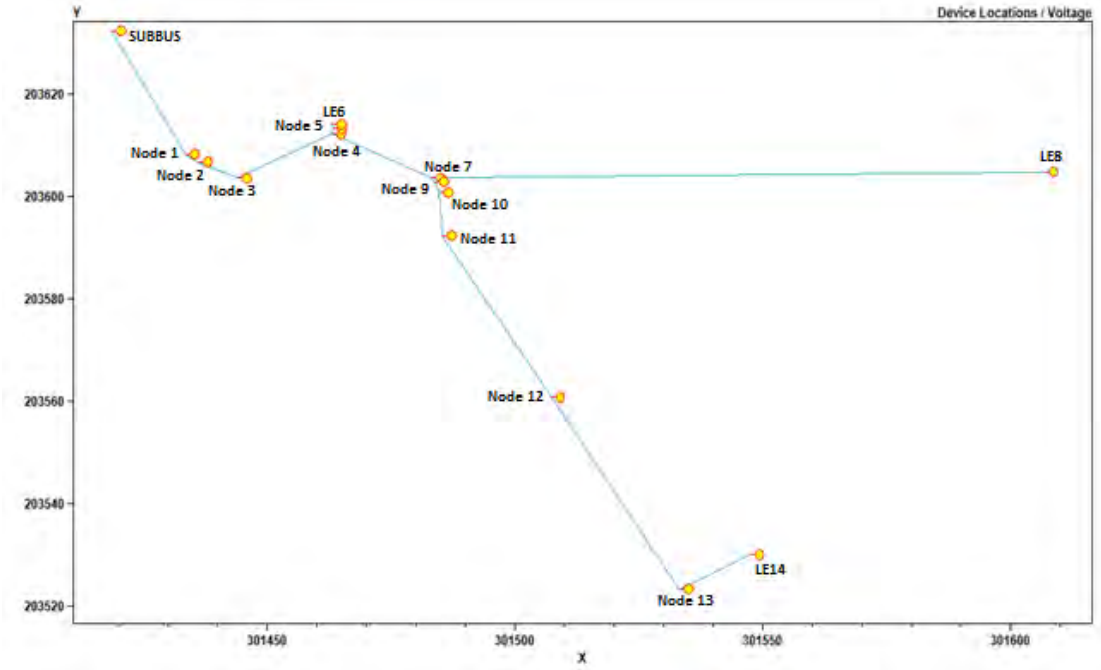

Figure 3.22 Semi-geographical network template (Rhos Wenallt Abernant) performed by OpenDSS

Table 10: Lines and transformer data of Rhos Wenallt Abernant network

Transformer Data		P_{sc}	V_{sc}	Rating [kVA]	Ampacity [A]	Rated Voltage	type
TR1		1%	0.0475	100	139	11kV/415V	Dyn11
Lines Data		**R**	**X**	**Ampacity [A]**		**Cable type**	
Feeder		**[Ω/Km]**	**[Ω/Km]**				
SUBFDR10	subfdr10-n1_sjt1	0.253	0.073	278		120 TR XLPE Al 3c	
	n1_sjt1-n2_sjt2	0.253	0.073	278		120 TR XLPE Al 3c	
	n2_sjt2-n3_sjt3	0.253	0.073	278		120 TR XLPE Al 3c	
	n3_sjt3-n4_bjt4	0.253	0.073	278		120 TR XLPE Al 3c	
	n4_bjt4-n5_sjt5	0.253	0.073	278		120 TR XLPE Al 3c	
	n5_sjt5-n6_le6	0.253	0.073	278		120 TR XLPE Al 3c	
	n4_bjt4-n7_bjt7	0.253	0.073	278		120 TR XLPE Al 3c	
	n7_bjt7-n8_le8	0.1	0.0725	496		300 TR XLPE Al 3c	
	n7_bjt7-n9_sjt9	0.253	0.073	278		120 TR XLPE Al 3c	
	n9_sjt9-n10_sjt10	0.253	0.073	278		120 TR XLPE Al 3c	
	n10_sjt10-n11_sjt11	0.443	0.0755	203		70 TR XLPE Al 3c	
	n11_sjt11-n12_sjt12	0.443	0.0755	203		70 TR XLPE Al 3c	
	n12_sjt12-n13_sjt13	0.443	0.0755	203		70 TR XLPE Al 3c	
	n13_sjt13-n14_le14	0.443	0.0755	203		70 TR XLPE Al 3c	

Table 11: Nodes/buses data of Rhos Wenallt Abernant network (base load case)

Bus Data	Base Loads		Source/Generator Rated Voltage L-N	
	P (Active Power) kW	Cosφ	kV	p.u.
mt1	/	/	6.3509	1
subbus1	/	/	239.6	1
subbus	/	/	239.6	1
subfdr10	/	/	239.6	1
n1_sjt1	7	1	239.6	1
n2_sjt2	/	/	239.6	1
n3_sjt3	/	/	239.6	1
n4_bjt4	/	/	239.6	1
n5_sjt5	/	/	239.6	1
n6_le6	5	1	239.6	1
n7_bjt7	/	/	239.6	1
n8_le8	1	1	239.6	1
n9_sjt9	/	1	239.6	1
n10_sjt10	5	1	239.6	1
n11_sjt11	5	1	239.6	1
n12_sjt12	5	1	239.6	1
n13_sjt13	5	1	239.6	1
n14_le14	5	1	239.6	1

3.4.2 Simulation cases of Rhos Wenallt Abernant network

The first LV (rural) network simulated by OpenDSS is Rhos Wenallt Abernant. The selected date in which are based the simulations is on the 14th October 2012.
In Rhos Wenallt Abernant network are connected eight main loads (3 phase, wye connection) at one feeder (SUBFDR10). In order to obtain more information about the balanced three phase load flow some simulations were carried out considering different operating network scenarios which are shown in Table 12.

Table 12: Simulation cases analysed at Rhos Wenallt Abernant network

Cases	Load Magnitude	Power Factor
1	Nominal load	Unity (1)
2	Nominal load	0.6 Lagging
3	150% of nominal load	Unity (1)

3.4.3 Result analysis of Rhos Wenallt simulations: voltage limits

The load cases analysed in the simulations are:

1) Case 1: PF=1

Figure 3.23 shows the voltage profiles along the Rhos Wenallt Abernant Aberdare feeder under nominal load and unity power factor. As can be seen in the graph, the voltage profiles are quite flat.
There is a very small voltage drop across the 11kV/415V transformer about 4‰V_n and also a small drop along the feeder. In fact at SUBFDR10-LE14 branch, in which it is reached the maximum voltage drop on the network, the voltage drop is about 8‰ V_{SUBBUS} (1.91 V). Figure 3.24 shows, with an expanded y-axis scale, the voltage drop along each individual branch.

2) Case 2: Effects of power factor reduction

Figure 3.25 shows the resulting voltage profile of the Rhos Wenallt Abernant feeder when the power factor is assumed 0.6 lagging (extreme case).
In this simulation case the voltage drop across the transformer at the main busbar is increased of about 2.8% V_n (from 239.6 V to 232.9 V). Concerning the voltage drop along the feeder, it is

slightly increased, in fact in SUBFDR10-LE14 branch the voltage drop value now is 9‰ $V_{SUBFDR10}$ (≈2.1 V).
Figure 3.26 shows the zoom-in of the feeder voltage profiles as function of distance, as can be seen from the graph the voltage drop along the network branches is not relevant increased if compared with case 1 (i.e. for SUBFDR10-LE14 voltage rise of only 0.14 V).

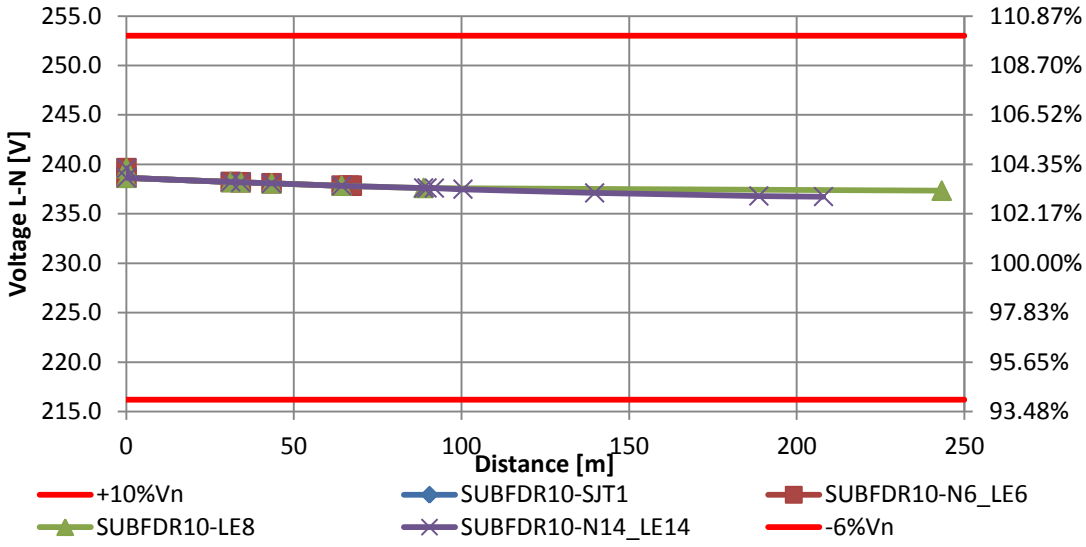

Figure 3.23 Voltage profile of Rhos Wenallt Abernant network main feeders – case 1: Base load case PF=1

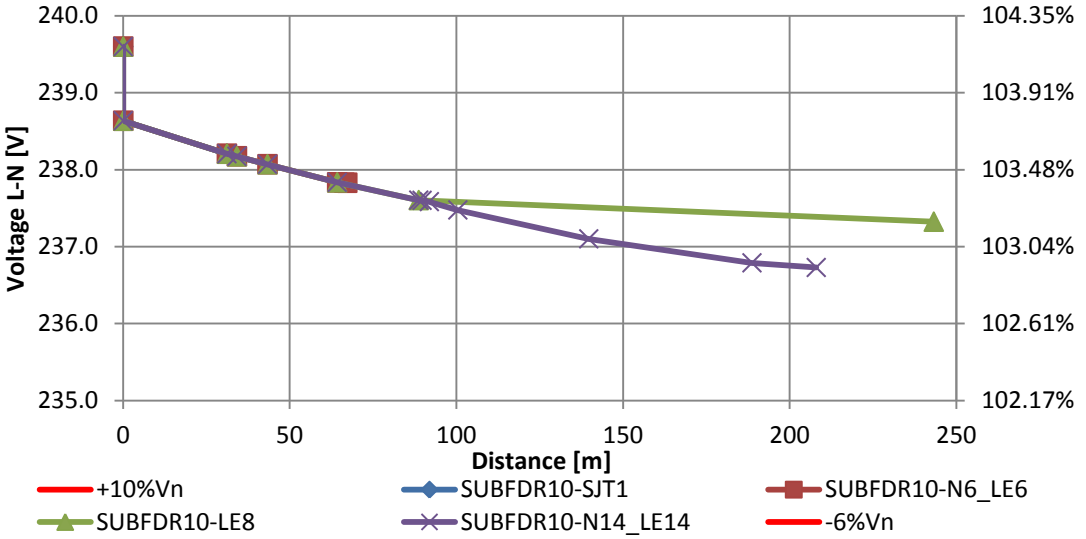

Figure 3.24 Voltage zoom-in profile of Rhos Wenallt Abernant main feeders – Case 1: Base case load PF=1

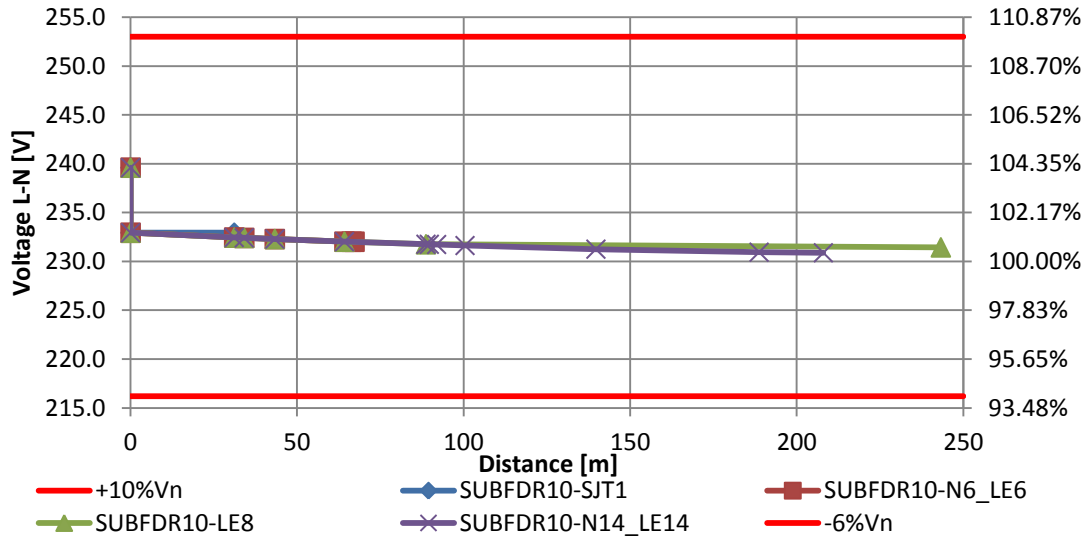

Figure 3.25 Voltage zoom-in profile of Rhos Wenallt Abernant main feeders – Case 2: Base case load PF=0.6

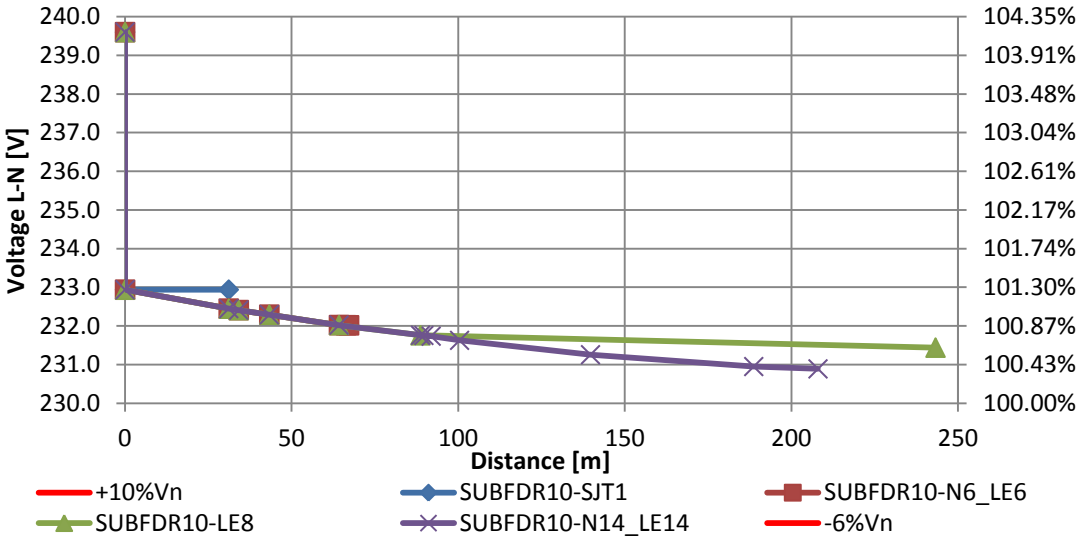

Figure 3.26 Voltage zoom-in profile of Rhos Wenallt Abernant main feeders – Case 2: Base case load PF=0.6

3) Case 3: Effects of nominal real power increased (150% P_n)

Figure 3.27 shows the voltage profiles along the Rhos Wenallt Abernant feeder under nominal load increased (150% P_n) and unity power factor. As can be seen in the graph, the voltage profiles of SUBFDR10 are still very flat.

The voltage drop across the 11kV/415V transformer is very small 6‰ V_n and also there is a small rise of drop voltage along the network branches if compared with the previous cases examined, indeed at SUBFDR10-LE14 branch the voltage drop value is about 1.2% $V_{SUBFDR10}$ (2.88 V).

Figure 3.28 shows, with an expanded y-axis scale, the voltage drop along each individual feeder branches.

Further studies were carried out gradually increasing the real power demand (PF=1) on the network but the transformer and the feeder voltage drops were varying very slowly compared with the previous result cases.

In this first rural network it was found out that only a sensible decreasing of PF may boost the transformer voltage drop to violate the voltage statutory limits without tap changing voltage regulation.

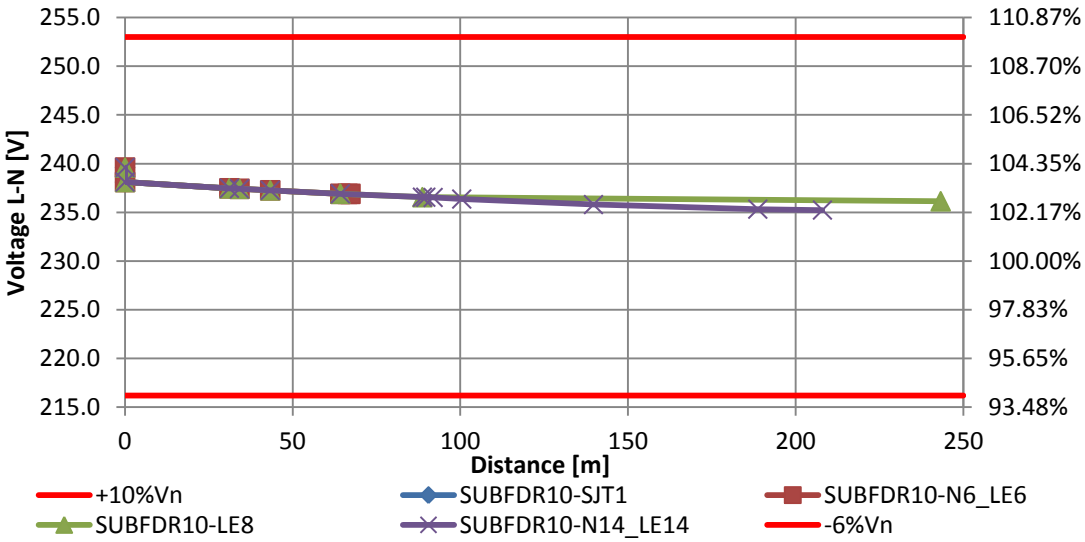

Figure 3.28 Voltage profile of Rhos Wenallt Abernant Aberdare main feeders – case 3: 150% P_n and PF=1

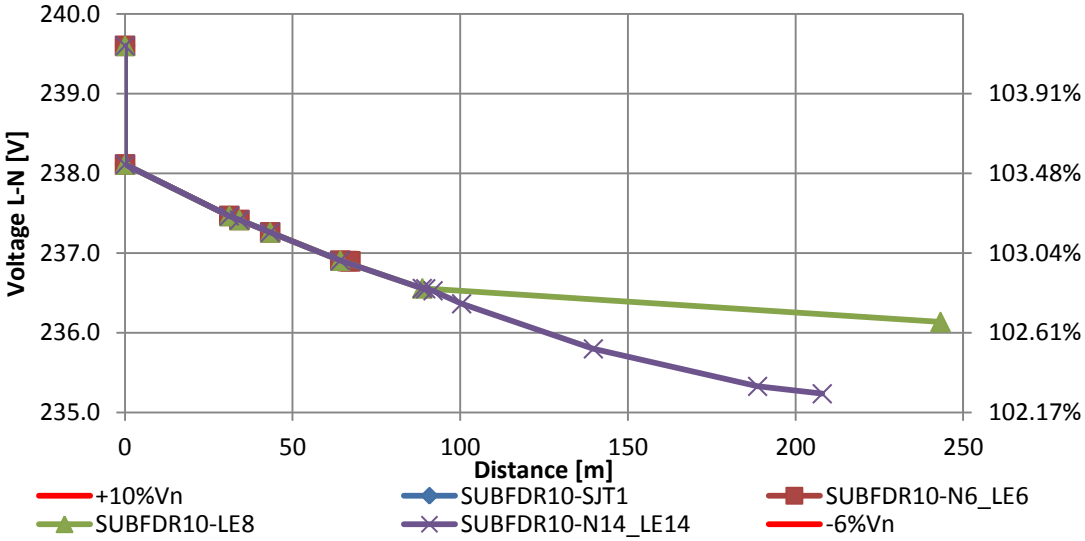

Figure 3.29 Voltage zoom-in profile of Rhos Wenallt Abernant Aberdare main feeders – case 3: 150% P_n and PF=1

3.4.4 Result analysis of Rhos Wenallt simulations: current limits

In the following graphs are analysed the current behaviours on SUBFDR10 and on its relative branches:

1) Case 1: PF=1

Figure 3.30 shows the branch current profiles along the Rhos Wenallt Abernant feeder under nominal load case and unity power factor. In this simulation case the current values are not exceeding the cables ampacity (see Table 10) indeed the thermal limits are still far. Figure 3.31 shows, with an expanded y-axis scale, the current profile along each SUBFDR10 branch.

2) Case 2: Effects of power factor reduction

Figure 3.32 shows the branch current profiles along the Wenallt Abernant feeder under nominal load case but with a power factor value of 0.6 (lagging). In this simulation the current trends are only approaching the transformer thermal limit (139 A) with a value of 83.57 A, because the cables ampacity are higher than the transformer nominal rating.

It has been also simulated case 3 (150% P_n) but it was not much relevant because it was observed that the resulting current values of the network are comparable to case 2 (PF=0.6).

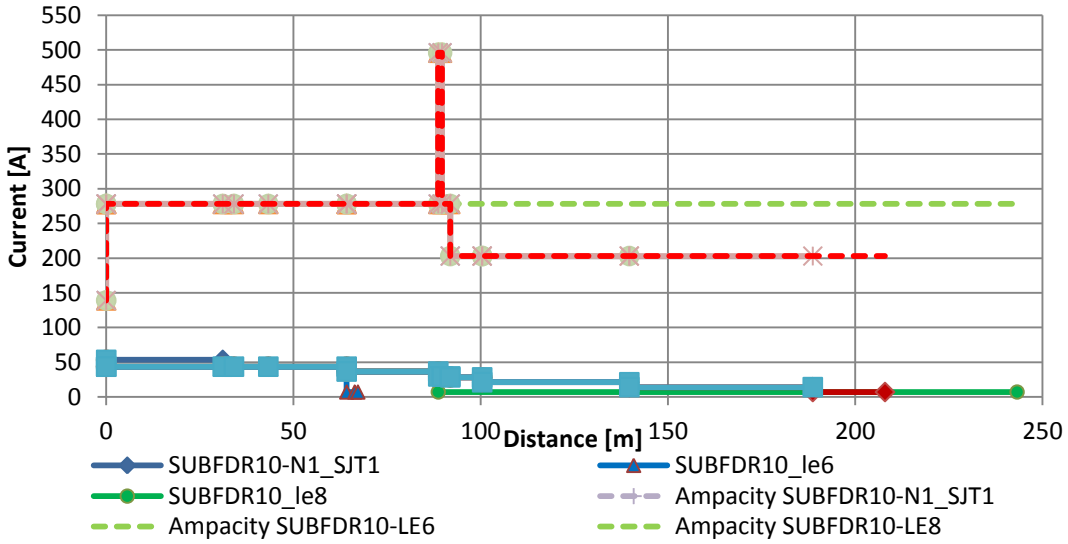

Figure 3.30 Current profiles of SUBFDR10 at Rhos Wenallt Abernant Aberdare – Case 1: Base load case and PF=1

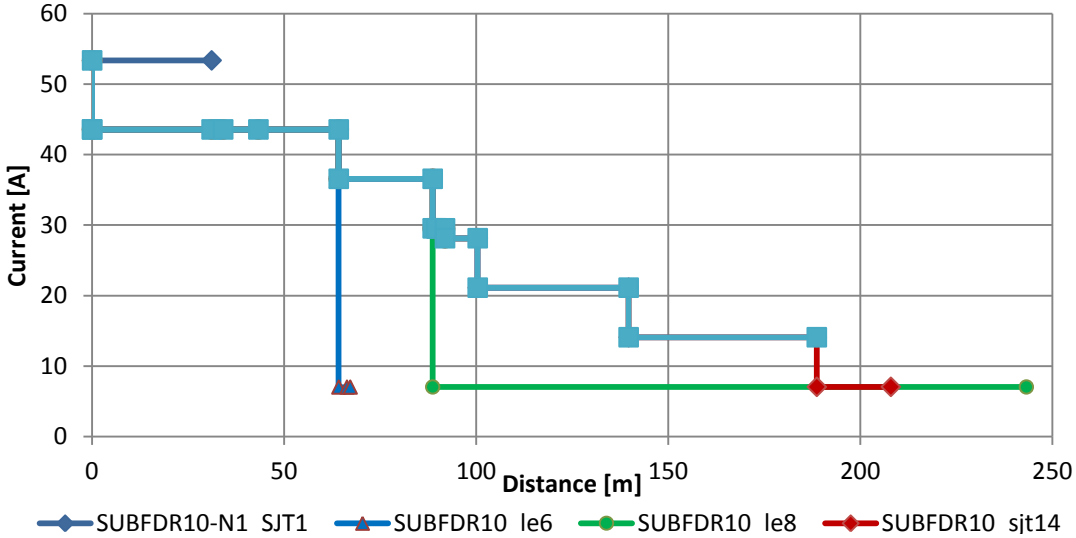

Figure 3.31 Current zoom-in profiles of SUBFDR10 at Rhos Wenallt Abernant Aberdare – Case 1: Base load case and PF=1

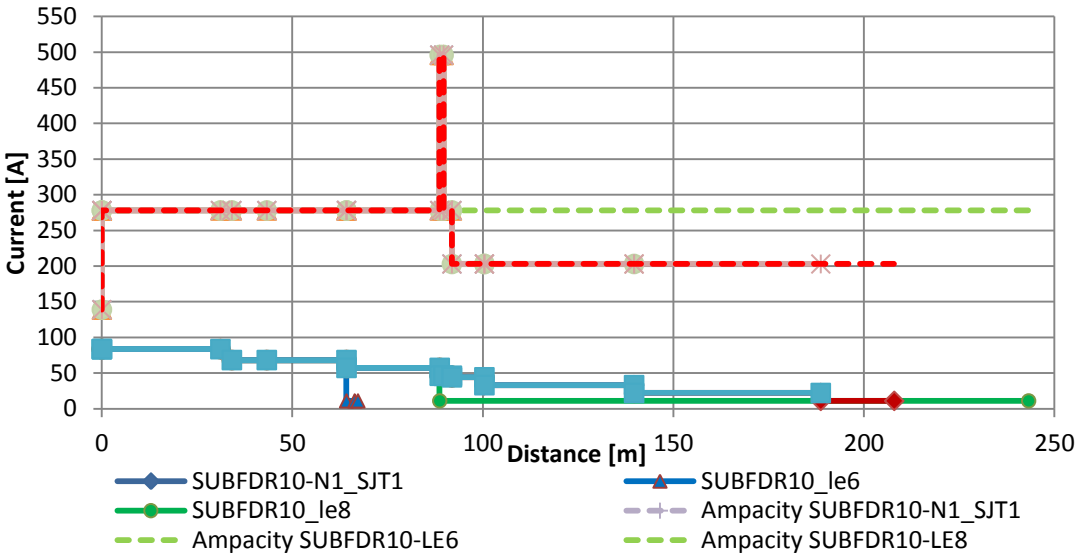

Figure 3.32 Current profiles of SUBFDR10 at Rhos Wenallt Abernant Aberdare – Case 2: Base load case and PF=0.6

3.5 Fforchneol Farm Godreaman network

3.5.1 Network description and relative parameters

Figure 3.33 shows a semi-geographical network template of Fforchneol Farm Godreaman network performed by OpenDSS.

As for the previous network simulated there is a single infeed at SUBBUS and fourteen main loads are tied to the network. From table 13 and table 14 are described respectively the nodes/buses characteristics and the estimated loads magnitude.

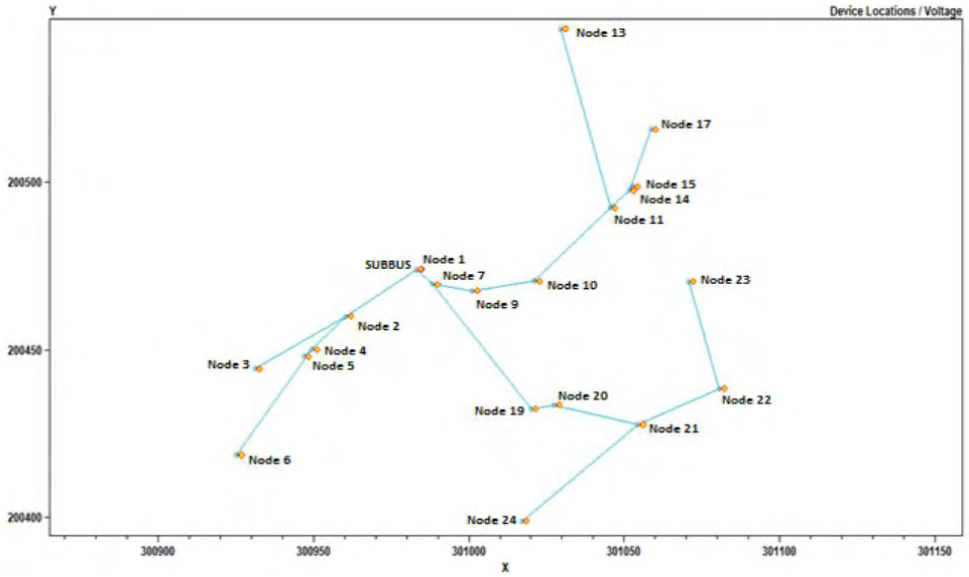

Figure 3.33 Semi-geographical network template (Fforchneol Farm Godreaman) performed by OpenDSS

Table 13: Lines and transformer data of Fforchneol Farm Godreaman network

Transformer Data		P_{sc}	V_{sc}	Rating [KVA]	Ampacity [A]	Rated Voltage	type
TR1		1%	4.75%	100	139	11/0.415 kV	Dyn11
Lines Data		**R**	**X**	**Ampacity [A]**		**Cable type**	
Feeder	**Lines**	**[Ω/Km]**	**[Ω/Km]**				
SUBFDR 10	subfdr10-n1_bjt1	0.1	0.0725	496		300TR-XLPE	
	n1_bjt1-n2_bjt2	0.443	0.0755	203		70TR-XLPE	
	n2_bjt2-n3_le3	0.443	0.0755	203		70TR-XLPE	
	n2_bjt2-n4_bjt4	0.443	0.0755	203		70TR-XLPE	
	n4_bjt4-n5_LE5	0.443	0.0755	203		70TR-XLPE	
	n4_bjt4-n6_le6	0.443	0.0755	203		70TR-XLPE	
	n1_bjt1-n7_bjt7	0.1	0.0725	496		300TR-XLPE	
	n7_bjt7-n9_sjt9	0.1	0.0725	496		300TR-XLPE	
	n9_sjt9-n10_sjt10	0.1	0.0725	496		300TR-XLPE	
	n10_sjt10-n11_bjt11	0.443	0.0755	203		70TR-XLPE	
	n11_bjt11-n13_le13	0.443	0.0755	203		70TR-XLPE	
	n11_bjt11-n14_bjt14	0.443	0.0755	203		70TR-XLPE	
	n14_bjt14-n15_le15	0.443	0.0755	203		70TR-XLPE	
	n14_bjt14-n17_le17	0.443	0.0755	203		70TR-XLPE	
	n7_bjt7-n19_sjt19	0.1	0.0725	496		300TR-XLPE	
	n19_sjt19-n20_sjt20	0.1	0.0725	496		300TR-XLPE	
	n20_sjt20-n21_pole_552149-1_21	0.443	0.0755	203		70TR-XLPE	
	n21_pole_552149-1_21-n22_pole_552149-2_22	0.868	0.086	120		ABC 4X35XLPE	
	n22_pole_552149-2_22-n23_pole_552149-3_23	0.541	0.297	159		4W 0.05	
	n21_pole_552149-1_21-n24_pole_552148-31_24	0.868	0.086	120		ABC 4X35XLPE	

Table 14: Nodes/buses data of Fforchneol Farm Godreaman network (base load case)

Bus Data	Base Loads		Source/Generator Rated Voltage L-N	
	P (Active Power) kW	Cosφ	kV	p.u.
subfdr10	/	/	6.3509	1
n1_bjt1	/	/	239.6	1
n2_bjt2	3.5	1	239.6	1
n3_le3	2.5	1	239.6	1
n4_bjt4	/	/	239.6	1
n5_le5	1.5	1	239.6	1
n6_le6	2.5	1	239.6	1
n7_bjt7	5	1	239.6	1
n9_sjt9	5	1	239.6	1
n10_sjt10	7.5	1	239.6	1
n11_bjt11	5	1	239.6	1
n13_le13	6	1	239.6	1
n14_bjt14	/	/	239.6	1
n15_le15	/	/	239.6	1
n17_le17	1.5	1	239.6	1
n19_sjt19	/	/	239.6	1
n20_sjt20	/	/	239.6	1
n21_pole_552149-1_21	1.5	1	239.6	1
n24_pole_552148-31_24	6	1	239.6	1
n22_pole_552149-2_22	1.5	1	239.6	1
n23_pole_552149-3_23	1.5	1	239.6	1

3.5.2 Simulation cases of Fforchneol Farm Godreaman network

The second LV rural network simulated by OpenDSS is Fforchneol Farm Godreaman. The selected day in which are based the simulations is on the 29th April 2012. In Fforchneol Farm Godreaman network are connected fourteen main loads (3 phase, wye connection) at one feeder (SUBFDR10). As for the previous rural network studied, the balanced three phase load flow simulations were carried out considering different operating network scenarios which are shown in Table 12.

3.5.3 Result analysis of Fforchneol Farm Godreaman simulations: voltage limits

The load cases analysed in the simulations are:

1) Case 1: PF=1

Figure 3.34 shows the voltage profiles along the Fforchneol Farm Godreaman feeder under nominal load and unity power factor. As can be seen in the graph, the voltage profiles are very flat. In fact, there is a very small voltage drop across the 11kV/415V transformer of about 4.5‰ V_n and a small drop along the feeders cables.
At SUBFDR10-N24 branch, where is reached the maximum voltage drop of the whole network, its relative voltage drop value is very low: about 3.5‰ V_{SUBBUS} (0.83 V).
Figure 3.35 shows, with an expanded y-axis scale, the voltage drop along each individual branch.

2) Case 2: Effects of power factor reduction

Figure 3.36 shows the resulting voltage profile of the Fforchneol Farm Godreaman feeder when the power factor is assumed to be 0.6 (extreme case).
In this case the voltage drop across the transformer at the main busbar rise until a value of about 3.7% V_n (from 239.6 V to 230.762 V). Concerning the voltage drop along the feeder, it is slightly increased, in fact in SUBFDR10-N24 branch the voltage drop value now is 4.7‰ $V_{SUBFDR10}$ (≈1.1 V).
Figure 3.37 shows the zoom-in of the feeder voltage profiles as function of distance, moreover it can be seen that the voltage drop along the branch feeders is not much increased in comparison with case 1, for instance at SUBFDR10-N24 the voltage drop value is about 0.26 V.

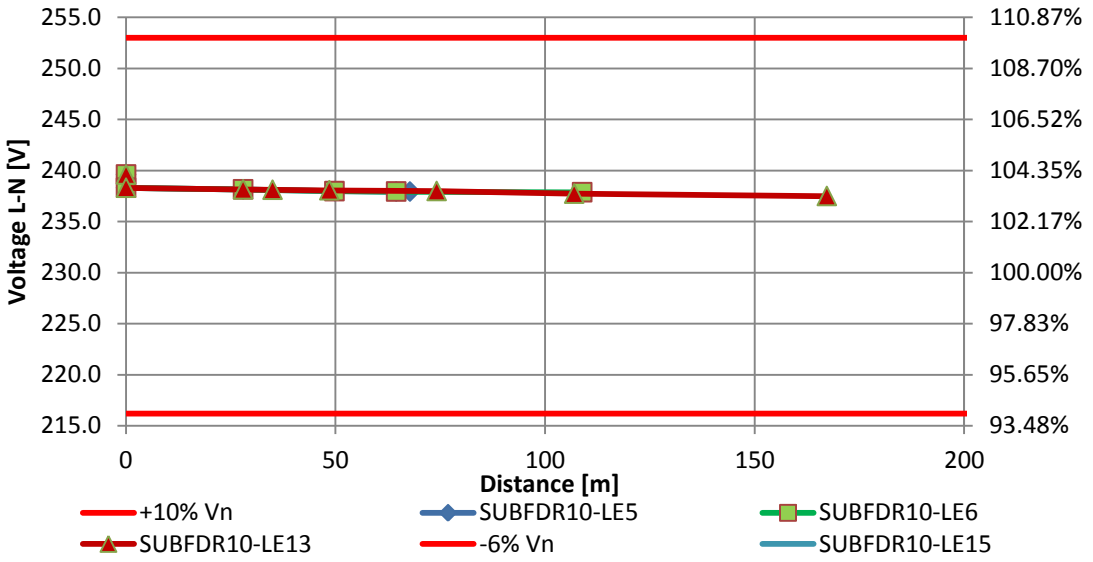

Figure 3.34 Voltage profile of Fforchneol Farm Godreaman Aberdare main feeders – Case 1: Base case load and PF=1

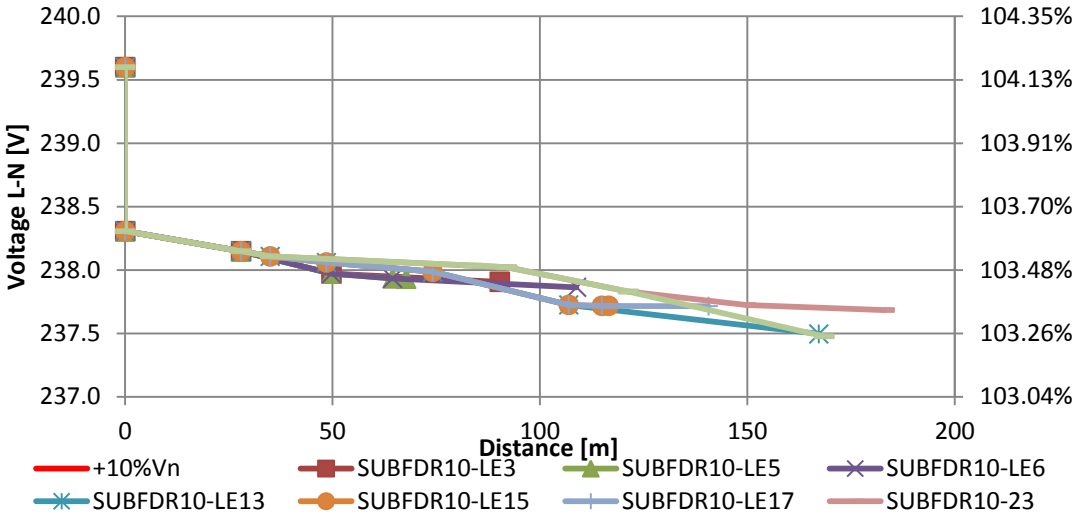

Figure 3.35 Voltage zoom-in profile of Fforchneol Farm Godreaman Aberdare main feeders – Case 1: Base case load and PF=1

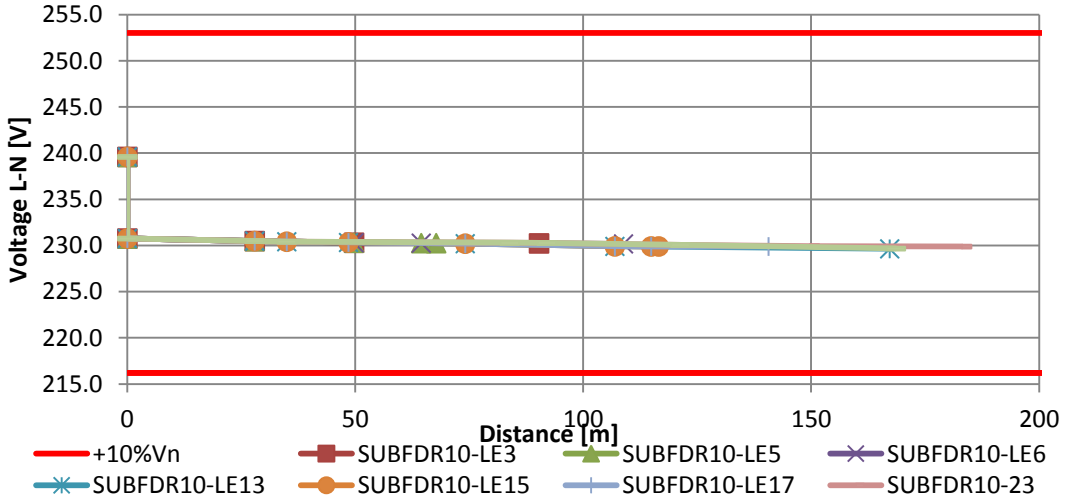

Figure 3.36 Voltage profile of Fforchneol Farm Godreaman Aberdare main feeders – Case 2: Base case load and PF=0.6

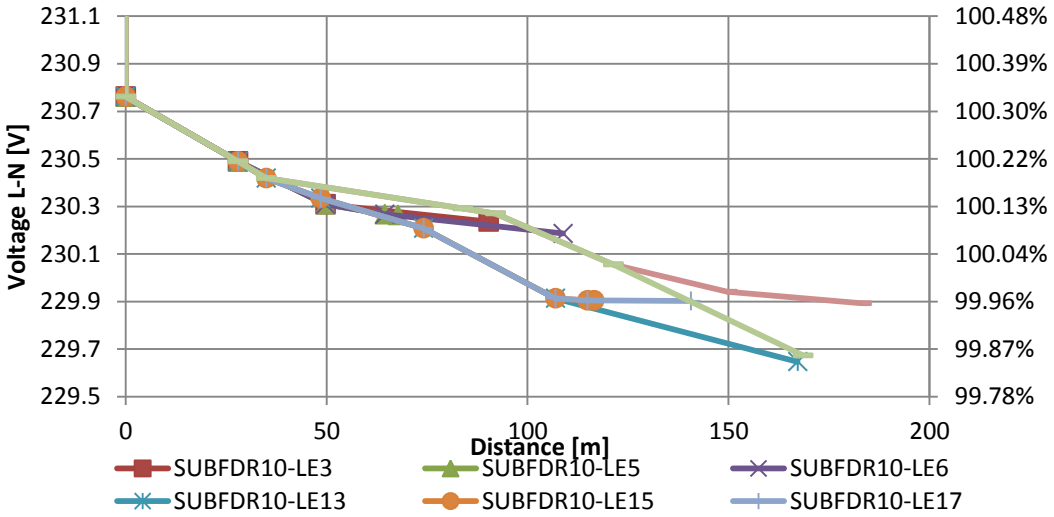

Figure 3.37 Voltage zoom-in profile of Fforchneol Farm Godreaman Aberdare main feeders – Case 2: Base case load and PF=0.6

3) Case 3: Effects of real power increased (150% P_n)

In this case is analysed the voltage profiles along the Fforchneol Farm Godreaman feeder under increased loads power (150% P_n) and unity power factor. Also in this scenario the voltage profiles are still very flat. The voltage drop across the 11kV/415V transformer remain very small, 8.4‰ V_n, while there is a not relevant increasing of drop voltage along the branch feeders; for instance at SUBFDR10-N24 branch the maximum voltage drop value is about 5.3‰ $V_{SUBFDR10}$ (≈1.25 V).

In both rural networks simulations results have been found out that the voltage trends have about the same behaviours, in fact also at Fforchneol Farm Godreaman network it was found that a sensible PF decreasing can only raise the voltage drop of the transformer. Therefore the voltage statutory limit might be violated only because of the transformer voltage drop.

3.5.4 Result analysis of Fforchneol Farm Godreaman network simulations: current limits

In the following graphs are analysed the current behaviours on SUBFDR10 and on its relative branches:

1) Case 1: PF=1

Figure 3.38 and 3.39 shows the branch current profiles along the Fforchneol Farm Godreaman network under nominal load case and unity power factor. In this simulation case the current trends of each network branch are not exceeding the cables ampacity (see Table 13).

2) Case 2: Effects of power factor reduction

Figure 3.41 and 3.42 shows the branch current profiles along the Fforchneol Farm Godreaman feeder under the base load case and power factor value of 0.6 (lagging). In this simulation case the current values are perilously approaching only the transformer thermal limit with a current value of 115.1 A, because the cables ampacity are higher than the actual current trends.

It has been also simulated case 3 (150% P_n) but, as for the previous rural network, the relative results were not much relevant because it was observed that the resulting current values of the network are comparable to case 2 (PF=0.6).

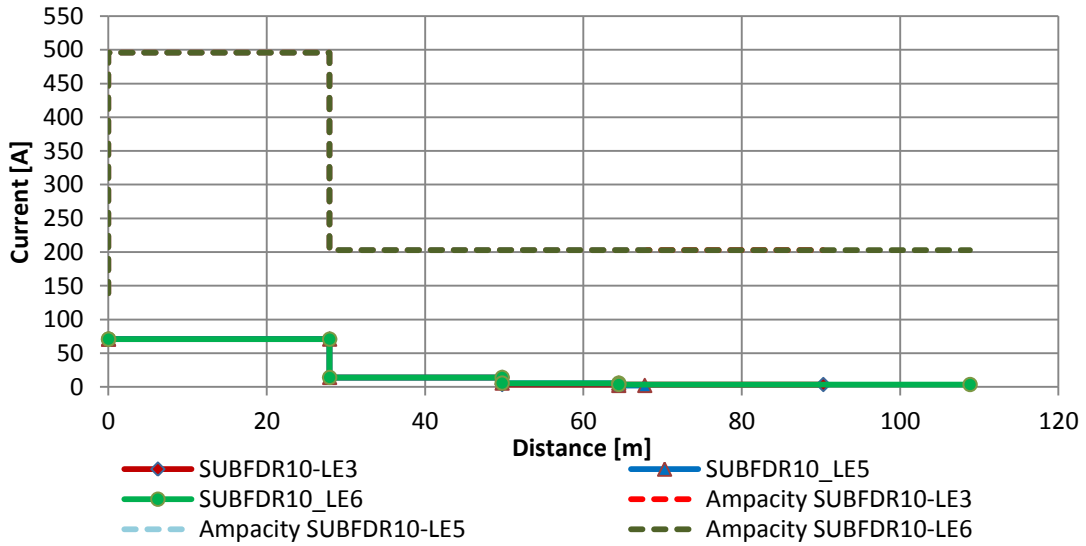

Figure 3.38 Current branches profiles of SUBFDR10 at Fforchneol Farm Godreaman Aberdare – Case 1: Base load case and PF=1

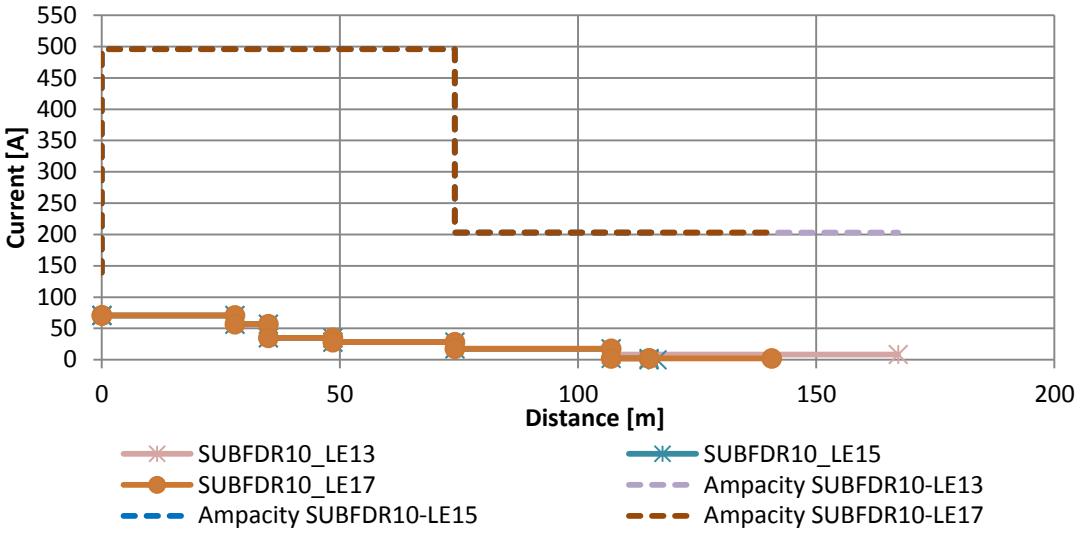

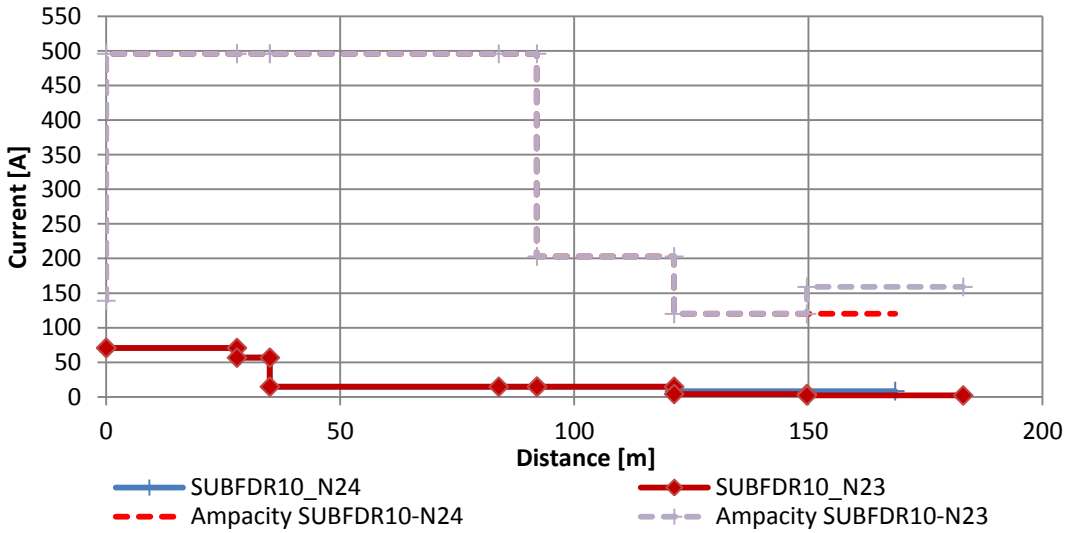

Figure 3.39 Current branches profiles of SUBFDR10 at Fforchneol Farm Godreaman Aberdare–Case 1: Base load case PF=1

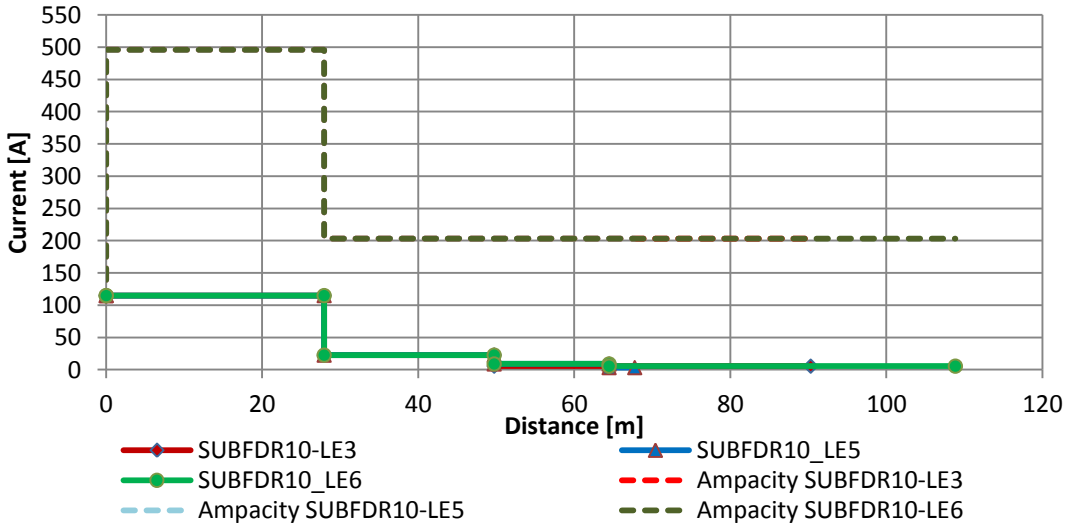

Figure 3.40 Current profiles of SUBFDR10 at Fforchneol Farm Godreaman Aberdare – Case 2: Base load case and PF=0.6

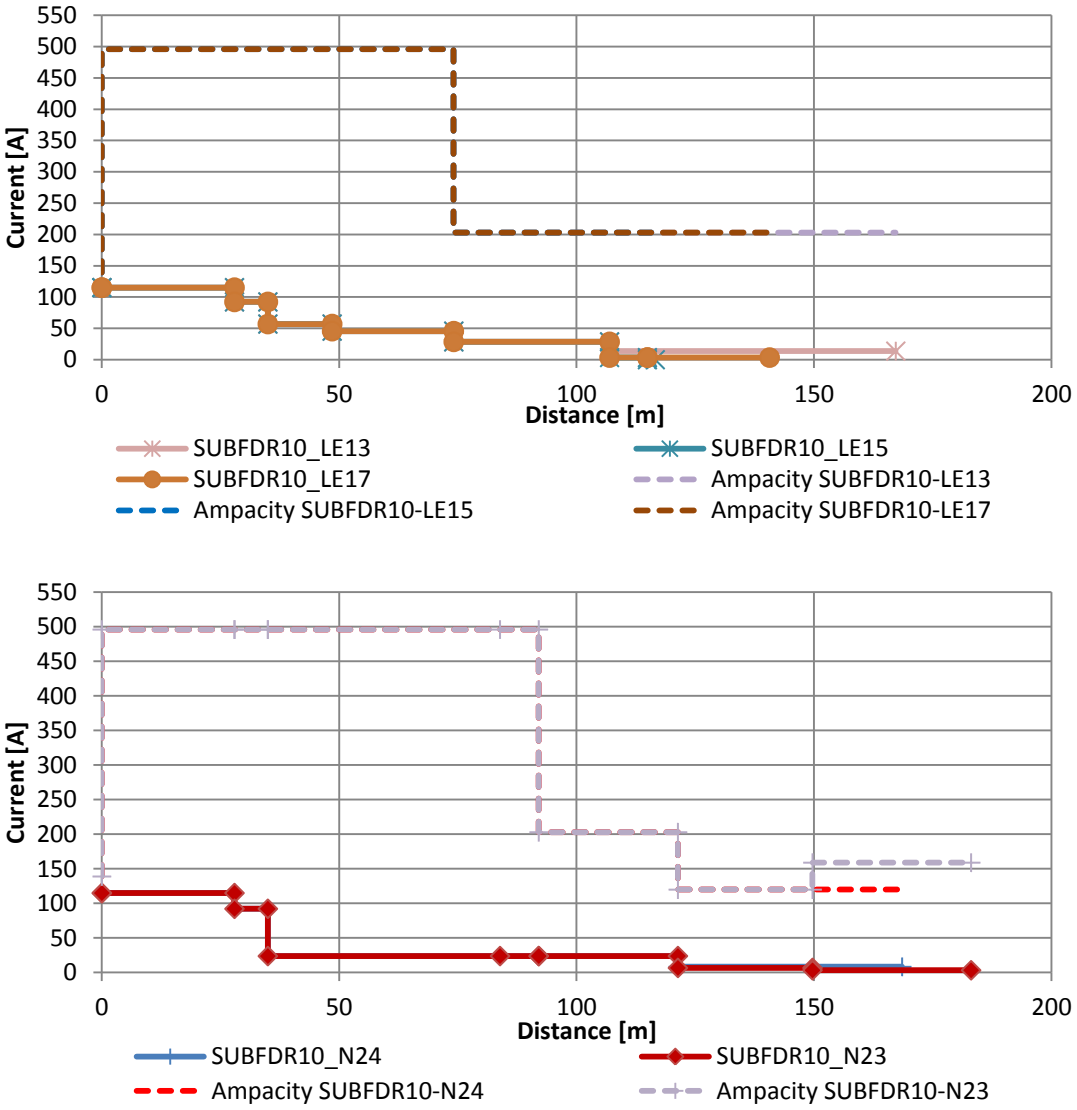

Figure 3.41 Current profiles of SUBFDR10 at Fforchneol Farm Godreaman Aberdare – Case 2: Base load case and PF=0.6

Chapter 4

Unbalanced simulation results on a low voltage network

4.1 Aim of the simulations

In this chapter, steady state power flow simulations are carried out on a Western Power Distribution (WPD) low voltage networks, which is strongly unbalanced, using the OpenDSS simulation software. The purpose of these simulations is to assess the network voltage profiles and thermal capability under different load conditions. The simulation results are shown with similar modality used on chapter 3, indeed it is focused on the profiles voltage restrictions (-6%/+10% of 230 V) [2] and on the relative thermal capability in terms of the individual cable ampacity. The network analysed, Angus Street, has initially been simulated considering only passive loads in order to assess its real network operating conditions, according to recorded data provided. Afterwards it has been connected some renewable generator devices in four customer locations to understand the possible alterations on the network during normal and extreme cases.

4.2 Angus Street network

4.2.1 Network description and relative parameters

Figure 4.1 shows a semi-geographical network template of Angus Street performed by OpenDSS.
The nodes/buses characteristics are shown in table 15, while the estimated loads magnitude are shown in table 16. From these tables and the figure can be seen that there is a single in-feed at SUBBUS and fifty-three loads are present.

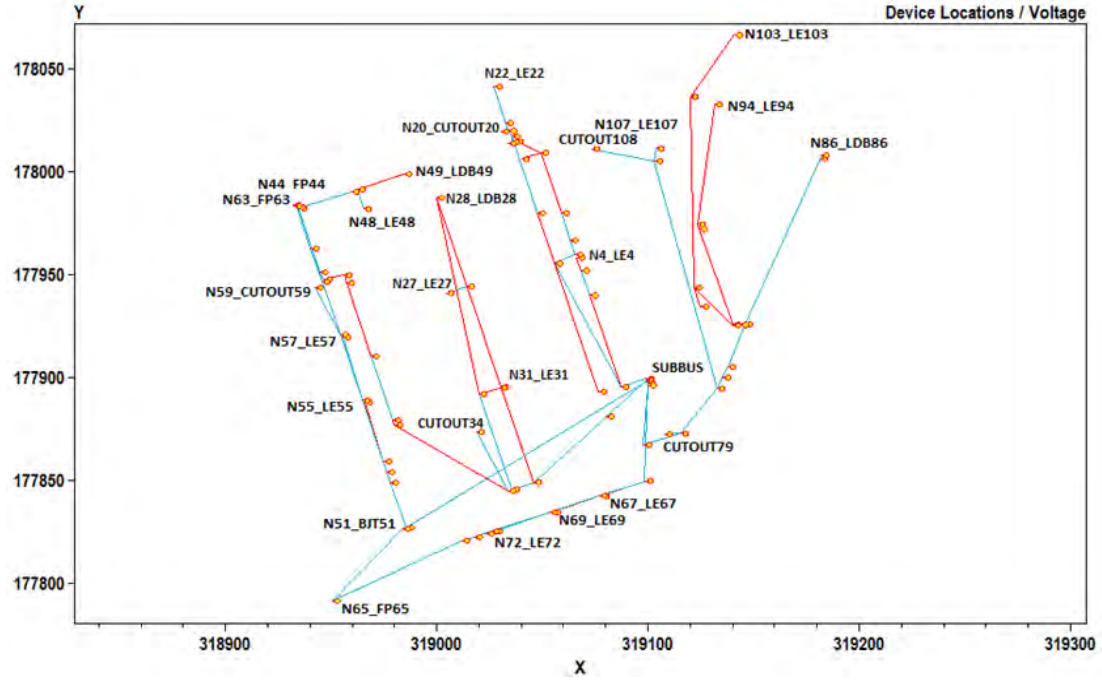

Figure 4.1 Semi-geographical network template (Angus Street) performed by OpenDSS

Table 15 (1/2): Lines and transformer data of Angus Street network

Transformer Data		P_{sc}	V_{sc}	Rating [KVA]	Ampacity [A]	Rated Voltage	type
TR1		1%	4.75%	1000	1391	11/0.415 kV	Dyn11
Lines Data		**R**	**X**	**Ampacity [A]**		**Cable type**	
Feeders	**Lines**	**[Ω/Km]**	**[Ω/Km]**				
SUBFDR10	subFDR10-n1_bjt1	0.142	0.0689	345		0.2 4c Cu STA	
	n1_bjt1-n2_sjt2	0.188	0.07	290		0.15 2c Cu STA	
	n2_sjt2-n3_sjt3	0.188	0.07	290		0.15 2c Cu STA	
	n3_sjt3-n4_le4	0.188	0.07	290		0.15 2c Cu STA	
	n1_bjt1-n5_bjt5	0.142	0.0689	345		0.2 4c Cu STA	
	n5_bjt5-n6_sjt6	0.276	0.0733	250		0.1 2c Cu STA	
	n6_sjt6-n7_sjt7	0.276	0.0733	250		0.1 2c Cu STA	
	n7_sjt7-n8_sjt8	0.276	0.0733	250		0.1 2c Cu STA	
	n8_sjt8-n10_bjt10	0.276	0.0733	250		0.1 2c Cu STA	
	n10_bjt10-n11_le11	0.276	0.0733	250		0.1 2c Cu STA	
	n10_bjt10-n12_le12	0.276	0.0733	250		0.1 2c Cu STA	
	n5_bjt5-n13_bjt13	0.142	0.0689	345		0.2 4c Cu STA	
	n13_bjt13-n14_le14	0.188	0.07	290		0.15 2c Cu STA	
	n13_bjt13-n16_bjt16	0.188	0.07	290		0.15 4c Cu STA	
	n16_bjt16-n17_sjt17	0.188	0.07	290		0.15 4c Cu STA	
	n17_sjt17-n18_ldb18	0.188	0.07	290		0.15 4c Cu STA	
	n16_bjt16-n19_bjt19	0.188	0.07	290		0.15 4c Cu STA	
	n19_bjt19-n20_cutout20	0.188	0.07	290		0.15 4c Cu STA	
	n19_bjt19-n21_sjt21	0.188	0.07	290		0.15 4c Cu STA	
	n21_sjt21-n22_le22	0.188	0.07	290		0.15 4c Cu STA	
SUBFDR20	subFDR20-n23_sjt23	0.142	0.0689	345		0.2 4c Cu STA	
	n23_sjt23-n24_bjt24	0.142	0.0689	345		0.2 4c Cu STA	
	n24_bjt24-n25_sjt25	0.276	0.0733	250		0.1 2c Cu STA	
	n25_sjt25-n26_bjt26	0.276	0.0733	250		0.1 2c Cu STA	
	n26_bjt26-n27_le27	0.276	0.0733	250		0.1 2c Cu STA	
	n26_bjt26-n28_ldb28	0.276	0.0733	250		0.1 2c Cu STA	
	n24_bjt24-n29_bjt29	0.276	0.0733	250		0.1 4c Cu STA	
	n29_bjt29-n30_bjt30	0.276	0.0733	250		0.1 2c Cu STA	
	n30_bjt30-n31_le31	0.276	0.0733	250		0.1 2c Cu STA	
	n30_bjt30-n28_ldb28	0.276	0.0733	250		0.1 2c Cu STA	
	n29_bjt29-n33_bjt33	0.142	0.0689	345		0.2 4c Cu STA	
	n33_bjt33-n34_cutout34	0.443	0.0755	203		70 TR XLPE Al 3c	
	n33_bjt33-n36_sjt36	0.188	0.07	290		0.15 2c Cu STA	
	n36_sjt36-n37_sjt37	0.32	0.0735	235		95 Wavcon Al 3c	
	n37_sjt37-n38_sjt38	0.188	0.07	290		0.15 2c Cu STA	
	n38_sjt38-n39_sjt39	0.188	0.07	290		0.15 2c Cu STA	
	n39_sjt39-n40_sjt40	0.188	0.07	290		0.15 2c Cu STA	
	n40_sjt40-n41_sjt41	0.188	0.07	290		0.15 2c Cu STA	
	n41_sjt41-n42_sjt42	0.188	0.07	290		0.15 2c Cu STA	
	n42_sjt42-n43_bjt43	0.188	0.07	290		0.15 4c Cu STA	
	n43_bjt43-n44_fp44	0.164	0.074	335		185 Wavcon Al 3c	
	n43_bjt43-n45_sjt45	0.164	0.074	335		185 Wavcon Al 3c	
	n45_sjt45-n46_sjt46	0.276	0.0733	250		0.1 2c Cu STA	
	n46_sjt46-n47_bjt47	0.276	0.0733	250		0.1 2c Cu STA	
	n47_bjt47-n48_le48	0.276	0.0733	250		0.1 2c Cu STA	
	n47_bjt47-n49_ldb49	0.276	0.0733	250		0.1 2c Cu STA	
SUBFDR30	subFDR30-n51_bjt51	0.092	0.0678	445		0.3 4c Cu STA	
	n51_bjt51-n52_sjt52	0.276	0.0733	250		0.1 4c Cu STA	
	n52_sjt52-n53_sjt53	0.32	0.0735	235		95 Wavcon Al 3c	
	n53_sjt53-n54_bjt54	0.276	0.0733	250		0.1 4c Cu STA	
	n54_bjt54-n55_le55	0.188	0.07	290		0.15 2c Cu STA	
	n54_bjt54-n56_bjt56	0.276	0.0733	250		0.1 4c Cu STA	
	n56_bjt56-n57_le57	0.188	0.07	290		0.15 2c Cu STA	
	n56_bjt56-n58_bjt58	0.276	0.0733	250		0.1 4c Cu STA	
	n58_bjt58-n59_cutout59	0.188	0.07	290		0.15 2c Cu STA	
	n58_bjt58-n60_sjt60	0.276	0.0733	250		0.1 4c Cu STA	
	n60_sjt60-n61_sjt61	0.188	0.07	290		0.15 2c Cu STA	
	n61_sjt61-n62_sjt62	0.188	0.07	290		0.15 4c Cu STA	
	n62_sjt62-n63_fp63	0.164	0.074	335		185 Wavcon Al 3c	
	n51_bjt51-n64_sjt64	0.092	0.0678	445		0.3 4c Cu STA	
	n64_sjt64-n65_fp65	0.113	0.0689	395		0.25 4c Cu STA	
SUBFDR40	subFDR40-n66_bjt66	0.142	0.0689	345		0.2 4c Cu STA	
	n66_bjt66-n67_le67	0.276	0.0733	250		0.1 2c Cu STA	
	n66_bjt66-n68_bjt68	0.142	0.0689	345		0.2 4c Cu STA	
	n68_bjt68-n69_le69	0.276	0.0733	250		0.1 2c Cu STA	
	n68_bjt68-n70_bjt70	0.142	0.0689	345		0.2 4c Cu STA	
	n70_bjt70-n71_sjt71	0.276	0.0733	250		0.1 2c Cu STA	
	n71_sjt71-n72_le72	0.276	0.0733	250		0.1 2c Cu STA	
	n70_bjt70-n73_sjt73	0.142	0.0689	345		0.2 4c Cu STA	
	n73_sjt73-n74_sjt74	0.142	0.0689	345		0.2 4c Cu STA	
	n74_sjt74-n75_sjt75	0.142	0.0689	345		0.2 4c Cu STA	
	n75_sjt75-n65_fp65	0.113	0.0689	395		0.25 4c Cu STA	

Table 15 (2/2): Lines and transformer data of Angus Street network

Lines Data		R [Ω/Km]	X [Ω/Km]	Ampacity [A]	Cable type
Feeders	Lines				
SUBFDR50	subFDR50-n77_sjt77	0.142	0.0689	345	0.2 4c Cu STA
	n77_sjt77-n78_bjt78	0.113	0.0689	395	0.25 4c Cu STA
	n78_bjt78-n79_cutout79	0.32	0.0735	235	95 Wavcon Al 3c
	n78_bjt78-n80_bjt80	0.113	0.0689	395	0.25 4c Cu STA
	n80_bjt80-n81_sjt81	0.113	0.0689	395	0.25 4c Cu STA
	n81_sjt81-n82_sjt82	0.164	0.074	335	185 Wavcon Al 3c
	n82_sjt82-n83_ldb83	0.113	0.0689	395	0.25 4c Cu STA
	n83_ldb83-n85_sjt85	0.113	0.0689	395	0.25 4c Cu STA
	n85_sjt85-n86_ldb86	0.113	0.0689	395	0.25 4c Cu STA
	n83_ldb83-n87_sjt87	0.32	0.0735	235	95 Wavcon Al 3c
	n87_sjt87-n88_sjt88	0.32	0.0735	235	95 Wavcon Al 3c
	n88_sjt88-n90_sjt90	0.276	0.0733	250	0.1 2c Cu STA
	n90_sjt90-n91_sjt91	0.276	0.0733	250	0.1 2c Cu STA
	n91_sjt91-n94_le94	0.276	0.0733	250	0.1 2c Cu STA
	n83_ldb83-n95_sjt95	0.32	0.0735	235	95 Wavcon Al 3c
	n95_sjt95-n96_sjt96	0.32	0.0735	235	95 Wavcon Al 3c
	n96_sjt96-n98_bjt98	0.276	0.0733	250	0.1 2c Cu STA
	n98_bjt98-n99_le99	0.276	0.0733	250	0.1 2c Cu STA
	n98_bjt98-n101_sjt101	0.276	0.0733	250	0.1 2c Cu STA
	n101_sjt101-n103_le103	0.276	0.0733	250	0.1 2c Cu STA
	n80_bjt80-n106_bjt106	0.164	0.074	382	185 TR XLPE Al 3c
	n106_bjt106-n107_le107	0.164	0.074	382	185 TR XLPE Al 3c
	n106_bjt106-n108_cutout108	0.443	0.0755	203	70 TR XLPE Al 3c

Table 16 (1/2): Nodes/buses data of Angus Street network (base load case)

Bus Data	Base Loads			Source/Generator Rated Voltage L-N	
	P (Active Power) kW	Cosφ	n-phase	kV	p.u.
mt1	/	/	/	6.3509	1
subbus	/	/	/	239.6	1
subfdr10	/	/	/	239.6	1
n1_bjt1	/	/	/	239.6	1
n1bis_bjt1	/	/	/	239.6	1
n2_sjt2	/	/	/	239.6	1
n3_sjt3	/	/	/	239.6	1
n4_le4	2.5	0.982	1	239.6	1
n5_bjt5	/	/	/	239.6	1
n5bis_bjt5	/	/	/	239.6	1
n6_sjt6	/	/	/	239.6	1
n7_sjt7	/	/	/	239.6	1
n8_sjt8	/	/	/	239.6	1
n10_bjt10	/	/	/	239.6	1
n11_le11	/	/	/	239.6	1
n12_le12	6.5	0.982	1	239.6	1
n13_bjt13	/	/	/	239.6	1
n14_le14	10.5	0.982	1	239.6	1
n16_bjt16	/	/	/	239.6	1
n17_sjt17	/	/	/	239.6	1
n18_ldb18	1.5	0.982	1	239.6	1
n19_bjt19	/	/	/	239.6	1
n20_cutout20	1.5	0.982	1	239.6	1
n20_cutout20	1.5	0.982	1	239.6	1
n20_cutout20	1.7	0.982	1	239.6	1
n21_sjt21	/	/	/	239.6	1
n22_le22	5.8	0.982	1	239.6	1
subfdr20	/	/	/	239.6	1
n23_sjt23	3.8	0.982	1	239.6	1
n24_bjt24	/	/	/	239.6	1
n25_sjt25	/	/	/	239.6	1
n26_bjt26	3.5	0.982	1	239.6	1
n27_le27	/	/	/	239.6	1
n28_ldb28	3.5	0.982	1	239.6	1
n29_bjt29	/	/	/	239.6	1
n30_bjt30	/	/	/	239.6	1
n31_le31	2.3	/	/	239.6	1
n33_bjt33	/	/	/	239.6	1
n34_cutout34	2.3	0.982	1	239.6	1
n34_cutout34	2.3	0.982	1	239.6	1
n34_cutout34	2.5	0.982	1	239.6	1
n36_sjt36	/	/	/	239.6	1
n37_sjt37	5	0.982	1	239.6	1
n38_sjt38	/	/	/	239.6	1

Table 16 (2/2): Nodes/buses data of Angus Street network (base load case)

Bus Data	Base Loads			Source/Generator Rated Voltage L-N	
	P (Active Power) kW	Cosφ	n-phase	kV	p.u.
n39_sjt39	4	0.982	1	239.6	1
n40_sjt40	4	0.982	1	239.6	1
n41_sjt41	4	0.982	1	239.6	1
n42_sjt42	/	/	/	239.6	1
n43_bjt43	/	/	/	239.6	1
n44_fp44	2.5	0.982	1	239.6	1
n45_sjt45	/	/	/	239.6	1
n46_sjt46	/	/	/	239.6	1
n47_bjt47	4	0.982	1	239.6	1
n48_le48	/	/	/	239.6	1
n49_ldb49	2	0.982	1	239.6	1
subfdr30	/	/	/	239.6	1
n51_bjt51	/	/	/	239.6	1
n52_sjt52	/	/	/	239.6	1
n53_sjt53	/	/	/	239.6	1
n54_bjt54	/	/	/	239.6	1
n55_le55	11.5	0.982	1	239.6	1
n56_bjt56	/	/	/	239.6	1
n57_le57	/	/	/	239.6	1
n58_bjt58	9.5	0.982	1	239.6	1
n59_cutout59	/	/	/	239.6	1
n60_sjt60	/	/	/	239.6	1
n61_sjt61	9.5	0.982	1	239.6	1
n62_sjt62	/	/	/	239.6	1
n63_fp63	9.2	0.982	1	239.6	1
n64_sjt64	16	0.982	1	239.6	1
n64_sjt64	20.5	0.982	1	239.6	1
n64_sjt64	17.5	0.982	1	239.6	1
n65_fp65	10	0.982	1	239.6	1
subfdr40	/	/	/	239.6	1
n66_bjt66	/	/	/	239.6	1
n67_le67	28.5			239.6	1
n68_bjt68	/	/	/	239.6	1
n69_le69	18.5	0.982	1	239.6	1
n69_le69	18.5	0.982	1	239.6	1
n69_le69	18.5	0.982	1	239.6	1
n70_bjt70	/	/	/	239.6	1
n71_sjt71	/	/	/	239.6	1
n72_le72	36.5	0.982	1	239.6	1
n73_sjt73	/	/	/	239.6	1
n74_sjt74	17.5	0.982	1	239.6	1
n74_sjt74	17.5	0.982	1	239.6	1
n75_sjt75	/	/	/	239.6	1
subfdr50	/	/	/	239.6	1
n77_sjt77	/	/	/	239.6	1
n78_bjt78	/	/	/	239.6	1
n79_cutout79	2	0.982	1	239.6	1
n79_cutout79	2	0.982	1	239.6	1
n79_cutout79	2.5	0.982	1	239.6	1
n80_bjt80	/	/	/	239.6	1
n81_sjt81	/	/	/	239.6	1
n82_sjt82	/	/	/	239.6	1
n83_ldb83	/	/	/	239.6	1
n85_sjt85	/	/	/	239.6	1
n86_ldb86	102	0.982	1	239.6	1
n87_sjt87	/	/	/	239.6	1
n88_sjt88	/	/	/	239.6	1
n90_sjt90	15	0.982	1	239.6	1
n91_sjt91	23	0.982	1	239.6	1
n94_le94	24	0.982	1	239.6	1
n95_sjt95	/	/	/	239.6	1
n96_sjt96	/	/	/	239.6	1
n98_bjt98	24	0.982	1	239.6	1
n99_le99	24	0.982	1	239.6	1
n101_sjt101	18	0.982	1	239.6	1
n103_le103	20	0.982	1	239.6	1
n106_bjt106	/	/	/	239.6	1
n107_le107	10	0.982	1	239.6	1
n108_cutout108	7	0.982	1	239.6	1
n108_cutout108	7	0.982	1	239.6	1
n108_cutout108	7	0.982	1	239.6	1

4.2.2 Simulation cases of Angus Street network

In this modelled network four possible operating scenarios were investigated. As reported in table 17, in the first two simulation cases only passive loads are connected to the network, which are set to their nominal values and with two different power factor magnitude. Whereas in the third and fourth cases distributed generation units (DGs) have been connected to the network. Five single-phase Photovoltaic Systems (PVs) are tied in four key customer locations of each feeder. These PVs are placed on the relative feeder branches most affected by drop voltage. Concerning an embedded generation simulation, a typical extreme case is when the passive loads are at the minimum operating condition (lower energy demand) while the DGs are at the higher generation level.

Table 17: Simulation cases analysed at Angus Street network

Cases	Load type	Load Magnitude	Load Power Factor	
1	Passive loads	Nominal load: P=624.75 kW, Q=128.5 kVAr	0.982 Lagging	
2	Passive Loads	Nominal load P=624.75 kW, Q=128.5 kVAr	0.9 Lagging	
3	Distributed Generations & passive loads	Nominal Load P=624.75 kW, Q=128.5 kVAr, P_{PV}=96.5 kW	1	0.982 Lagging
4	Distributed Generations & passive loads	310% Nominal load: P=624.75 kW, Q=128.5 kVAr, P_{PV}=300 kW	1	0.982 Lagging

4.2.3 Result analysis of Angus Street simulations: voltage limits

The load cases analysed in the simulations are:

1) Case 1: PF=0.982

Figure 4.2 and 4.3 show the resulting voltage profiles (L-N) of network branches at Angus Street under nominal load case and power factor 0.982 (lagging). In the graphs are plotted the three phases of each branch that is most affected by drop voltage, as can be seen in .I, .II, .IV and .V of figure 4.2 and 4.3 are emphasized the single-phase lines tendencies. There is a very small voltage drop across the 11kV/415V transformer at the main busbar (SUBBUS) of about 1.3% V_n (average value of the three phases) and also a not negligible drop along the feeders, in fact at SUBFDR50-N103_LE103 branch, where is reached the maximum voltage drop of the whole network, the voltage drop value at phase 3 (single-phase line from N96_SJT96 until N103_LE103) is about 6.5% V_{SUBBUS} (15.3 V). Being the simulations strongly unbalanced it may be possible to have neutral point potential shifting, for this reason is present a very small voltage rise on the phases, for instance this behaviour can be seen in figure 4.2 at graph .IV on the third phase.

2) Case 2: Effect of the power factor

Figure 4.4 and 4.5 show the resulting voltage profiles of network branches at Angus Street when the power factor is assumed to be 0.9 lag (extreme scenario in accordance with Western Power Distribution). In this case the voltage drop across the transformer has slightly increased 2.13% V_n. Even along the feeders the voltage drop is increased indeed at SUBFDR50-N103_LE103 branch is about 7.4% V_{SUBBUS} (17.2 V). At SUBFDR50-N103_LE103 branch, the statutory voltage limits is very close at end line (N103_LE103) on phase 3.

3) Case 3: Effects of the renewable units connected to the network (low PV penetration: 96.5kW)

This simulation case is a possible embedded generation scenario of Angus Street network with a low PV penetration on the nominal operating condition of the network (case 1). Figure 4.6 and 4.7 show the voltage profiles (L-N) along the Angus Street feeders in which are tied photovoltaic systems (single-phase). In this scenario the transformer and the feeder voltage drops are almost equivalent to the relative ones of case 1, therefore the network behaviours of the these two

cases are slightly different. In fact, the voltage drop across the 11kV/415V transformer is about 1.2% V_n while along SUBFDR50-N103_LE103 branch, at phase 3, the voltage drop is about 5.2% V_{SUBBUS} (12.4 V). A comparison between case 1 and 3 reveal that when DGs are connected to the network there is a general enhancement of the voltage profiles. However, in some cases if massive PV penetration is present on the grid, it may cause relevant alterations on the maximum voltage magnitude of the buses, thus a voltage control systems might be required (see chapter 5).

4) Case 4: Effect of the renewable units connected to the network (high PV penetration: 300 kW)

To comprehend the network behaviours on the embedded generation extreme scenario it has been simulated a maximum PV penetration for Angus Street. This DGs installable quantity correspond to the maximum hosting capacity of Angus Street which is 300 kW in accordance with [10] and [11]. Figure 4.8 and 4.9 show the voltage profiles (L-N) along the Angus Street feeders in which photovoltaic systems, with a PV penetration of 300kW, are tied to the network. In this case the behaviour of the network is quite different in comparison to the previous case. As a matter of fact, from the simulation results the transformer voltage drop magnitude is halved compared to case 3, in fact the relative value is about 0.67% V_n while the voltage drop along SUBFDR50-N103_LE103 branch, at phase 3, is about 3.5% V_{SUBBUS} (8.3 V).
The comparison between the embedded scenarios reveal that even with an high PV penetration the network may has advantages in terms of voltage losses reduction. However to attest the real benefits and the drawbacks of the embedded generation at this LV network should carry out also other studies to evaluate the power quality, for instance the harmonic flow analyses.

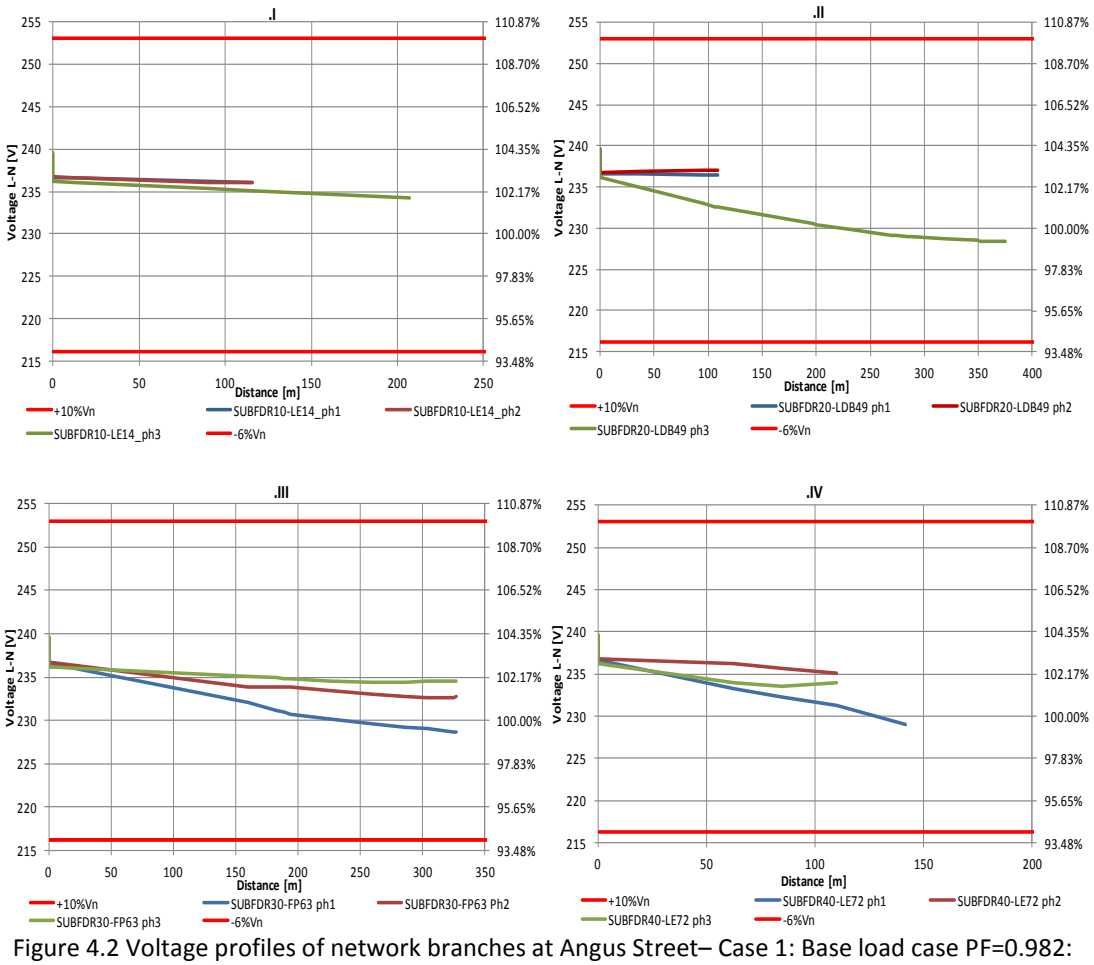

Figure 4.2 Voltage profiles of network branches at Angus Street– Case 1: Base load case PF=0.982: .I SUBFDR10-LE14, .II SUBFDR20-LDB49, .III SUBFDR30-FP63 and .IV SUBFDR40-LE72

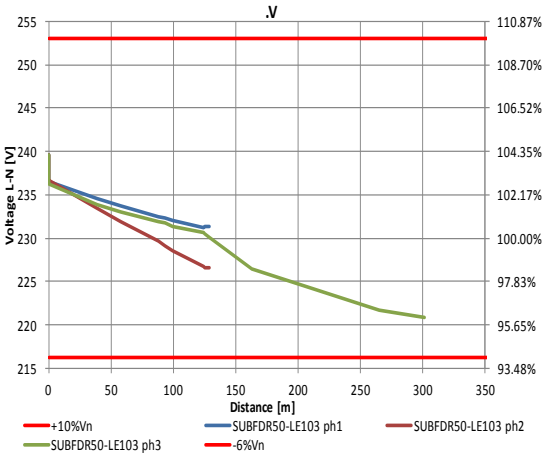

Figure 4.3 Voltage profiles of network branches at Angus Street– Case 1: Base load case PF=0.982: .V SUBFDR50-LE103

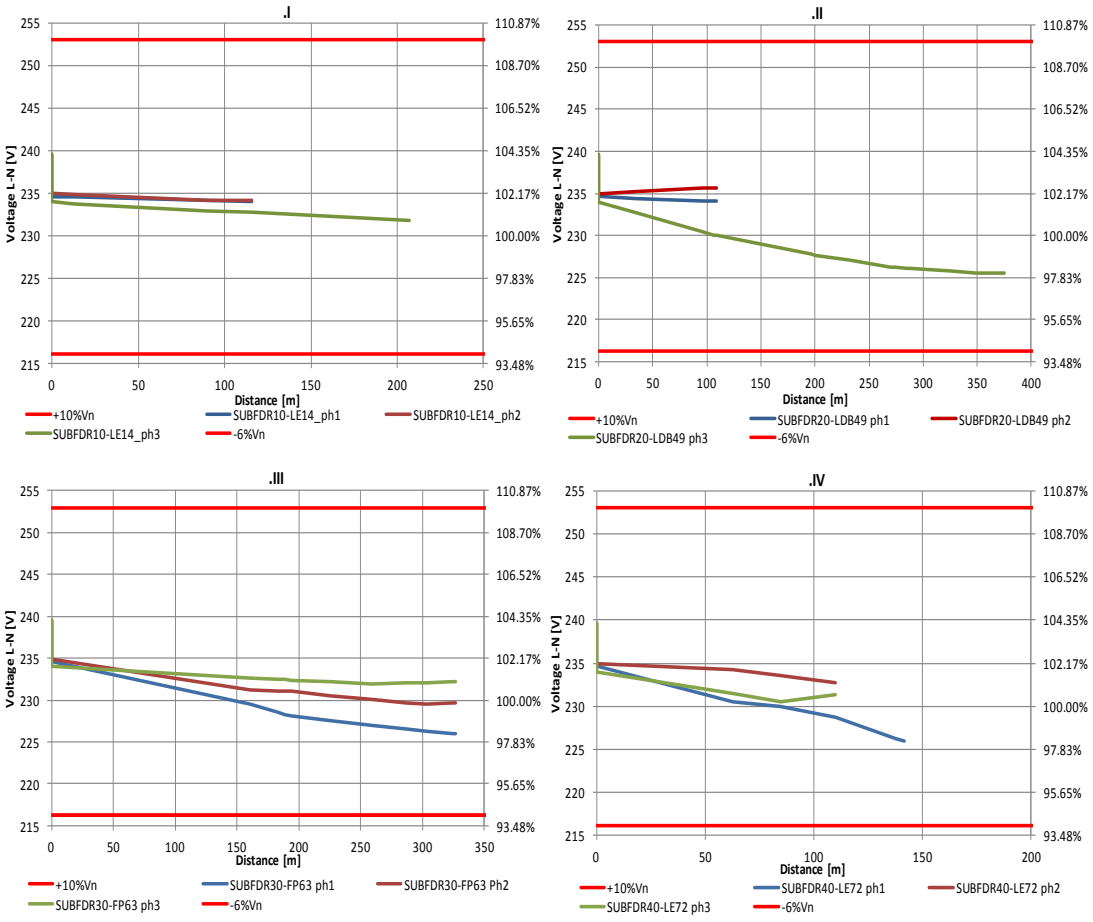

Figure 4.4 Voltage profiles of network branches at Angus Street– Case 2: Base load case PF=0.9: .I SUBFDR10-LE14, .II SUBFDR20-LDB49, .III SUBFDR30-FP63 and .IV SUBFDR40-LE72

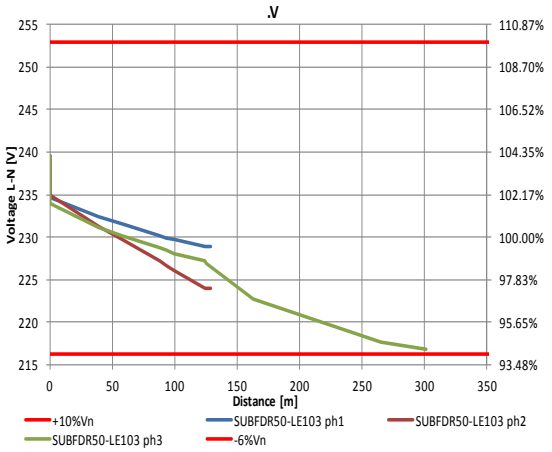

Figure 4.5 Voltage profiles of network branches at Angus Street– Case 2: Base load case PF=0.9: .V SUBFDR50-LE103

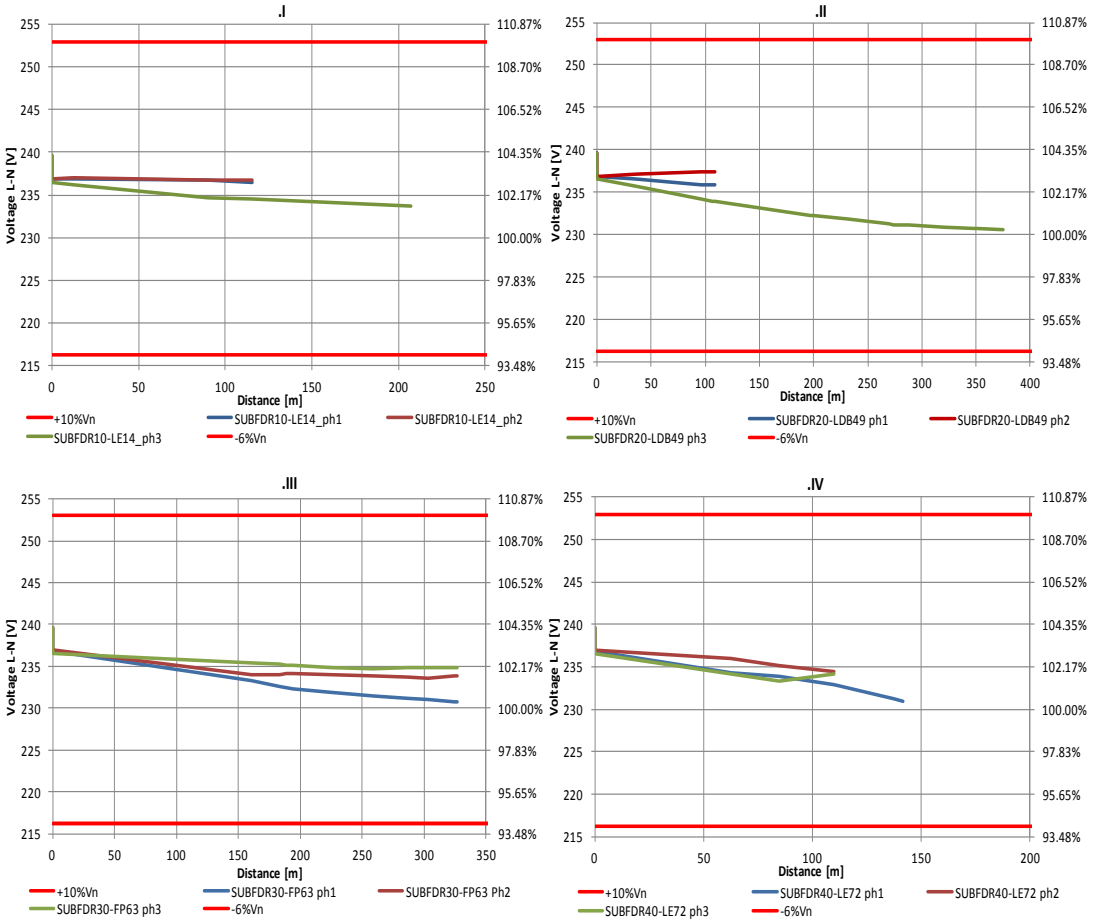

Figure 4.6 Voltage profiles of network branches at Angus Street with renewable units connected Case 3: Renewable loads connected (low PV penetration): .I SUBFDR10-LE14, .II SUBFDR20-LDB49, .III SUBFDR30-FP63 and .IV SUBFDR40-LE72

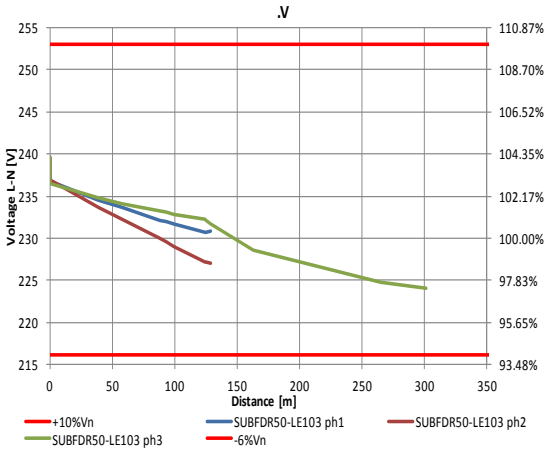

Figure 4.7 Voltage profiles of network branches at Angus Street with renewable units connected Case 3: Renewable loads connected (low PV penetration): .V SUBFDR50-LE103

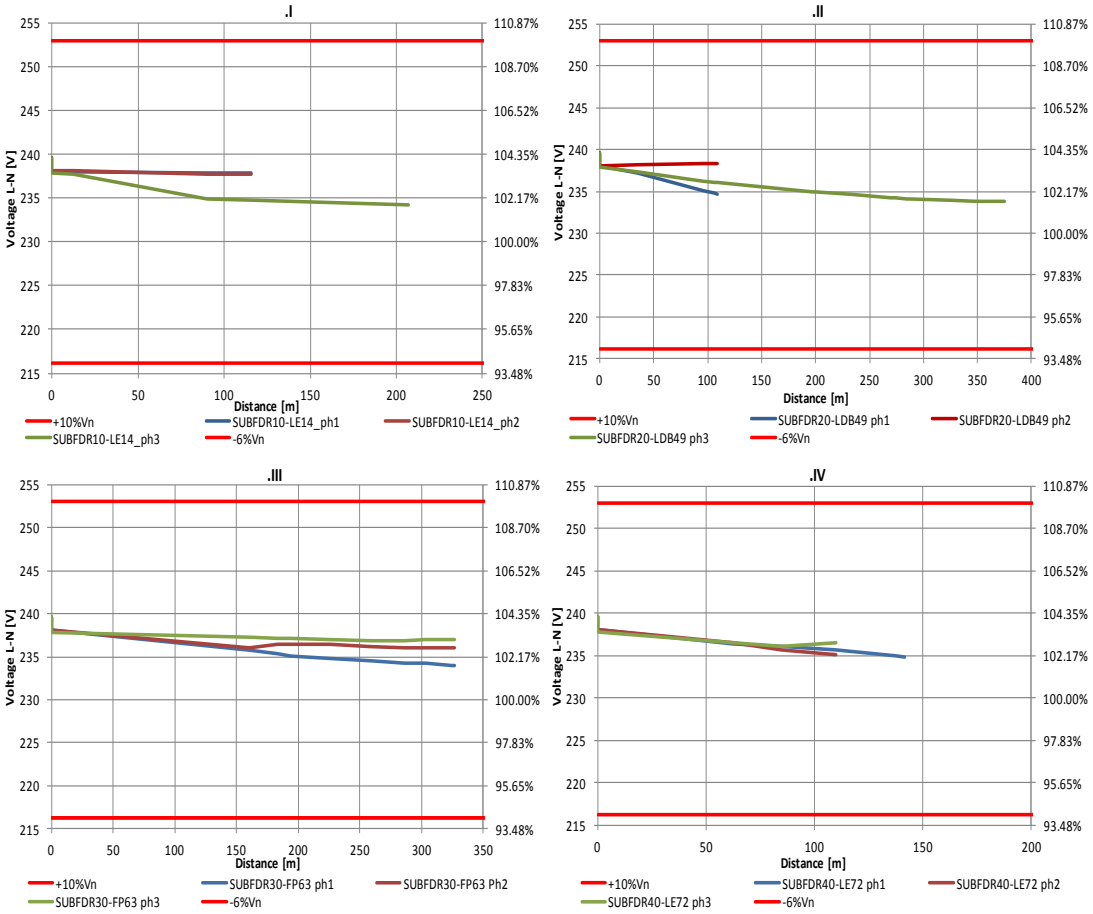

Figure 4.8 Voltage profiles of network branches at Angus Street with renewable units connected – Case 4: Renewable loads connected (high PV penetration):
.I SUBFDR10-LE14, .II SUBFDR20-LDB49, .III SUBFDR30-FP63 and .IV SUBFDR40-LE72

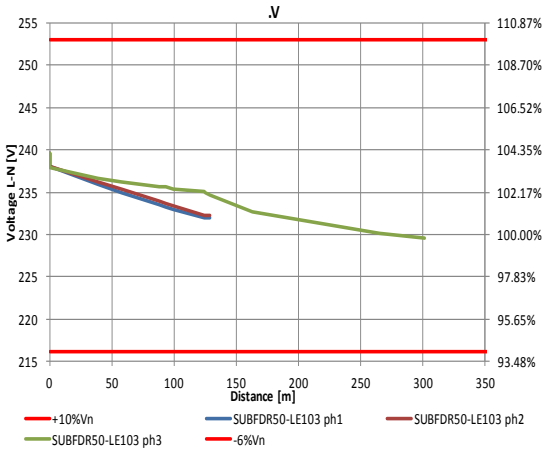

Figure 4.9 Voltage profiles of network branches at Angus Street with renewable units connected – Case 4: Renewable loads connected (high PV penetration): .V SUBFDR50-LE103

4.2.4 Result analysis of Angus Street simulations: current limits

In this section are analysed the same network branches of the previous voltage simulations but focusing on the phase current tendencies:

1) Case 1: PF=0.982

   Figure 4.10 and 4.11 shows the current profiles along Angus Street network under nominal load case with power factor value of 0.982 (lagging). In this simulation case the phase currents trends are exceeding the cables ampacity (see Table 15) only at SUBFDR50-LE103 branch. As shown in the relative branch graph on figure 4.11, two phases are violating the cables thermal limits already at the initial feeding point. Phases 2 and 3 are exceeding the limits of about one hundred amps whereas phase 1 is just barely under the thermal capability. However, in all of the network branches of this scenario and also in the others cases depicted below, the nominal transformer rating (current limit: 1391 A) has never been violated.

2) Case 2: Effects of the power factor reduction

   Figure 4.12 and 4.13 shows the current profiles along Angus Street network under the nominal load case with power factor value of 0.9 (lagging). In this case the phase currents trends are still exceeding the cables ampacity only at SUBFDR50-LE103. At this stage all of the three phases are violating the cables thermal limits already at the initial supply point. The approximate current gap between ampacity limit and phase is about 130 - 140 A for phase 2 and 3, whereas for phase 1 is just less than 20 A. Also in this urban network, as the previous ones analysed in chapter 3, can be noted that the PF decreasing is affecting more the current magnitude than the voltage drop across the transformer and the cable lines.

3) Case 3: Effects of the renewable units connected to the network (low PV penetration: 96.5 kW)

   Figure 4.14 and 4.15 shows the current profiles along the Angus Street feeders in which photovoltaic systems, with low PV penetration 96.5 kW, are tied to the network. In this case the DG units (single-phase) substantially reduce the current flowing in the relative interconnected conductors.
   In this simulation case the phase currents trends are exceeding the cables ampacity only at SUBFDR50-LE103 almost like the pattern of the first simulation scenario but with an enhancement on phase 3. In fact the thermal violation now is less compared with case 1 of about 50 A. Therefore in this kind of simulation when DG units are tied to the network there is a general

reduction of the current magnitude in the relative conductors. However a massive quantity of PV systems connected may significant affect the total harmonic distortion (THD) of the network.

4) Case 4: Effects of the renewable units connected to the network (PV penetration: 300 kW)

To comprehend the current behaviours of a network with high PV penetration (300 kW), it has been simulated an extreme case, in which the passive loads are set up according to the minimum energy demand level of the network during the day time, that is when the PV systems may work (i.e. 9.00 – 17.00).
Figure 4.16 and 4.17 shows the phase current profiles along the Angus Street feeders in which photovoltaic systems, with a PV penetration of 300kW, are tied to the grid. In this network operating scenario the most interesting branch is SUBFDR20-N49_LDB49 because of its strongly phase unbalance and also for the current magnitude at phase 3 that has drastically been increased causing the thermal limit violation at end line. Can be noted that the current values at the third phase are doubled if compared with those of case 3. While on SUBFDR10-N14_LE14 branch at phase 2, in which are connected the single-phase PV systems, the current raise and cause an important unbalance respect the other two phases. In contrary of the previous branch described the ampacity is not violated. Therefore on branches with lower energy demand there is a general worsening on the network unbalanced indeed, in the other branches analysed, where is present an high energy demand, there is a substantial improvement on the general current unbalance.

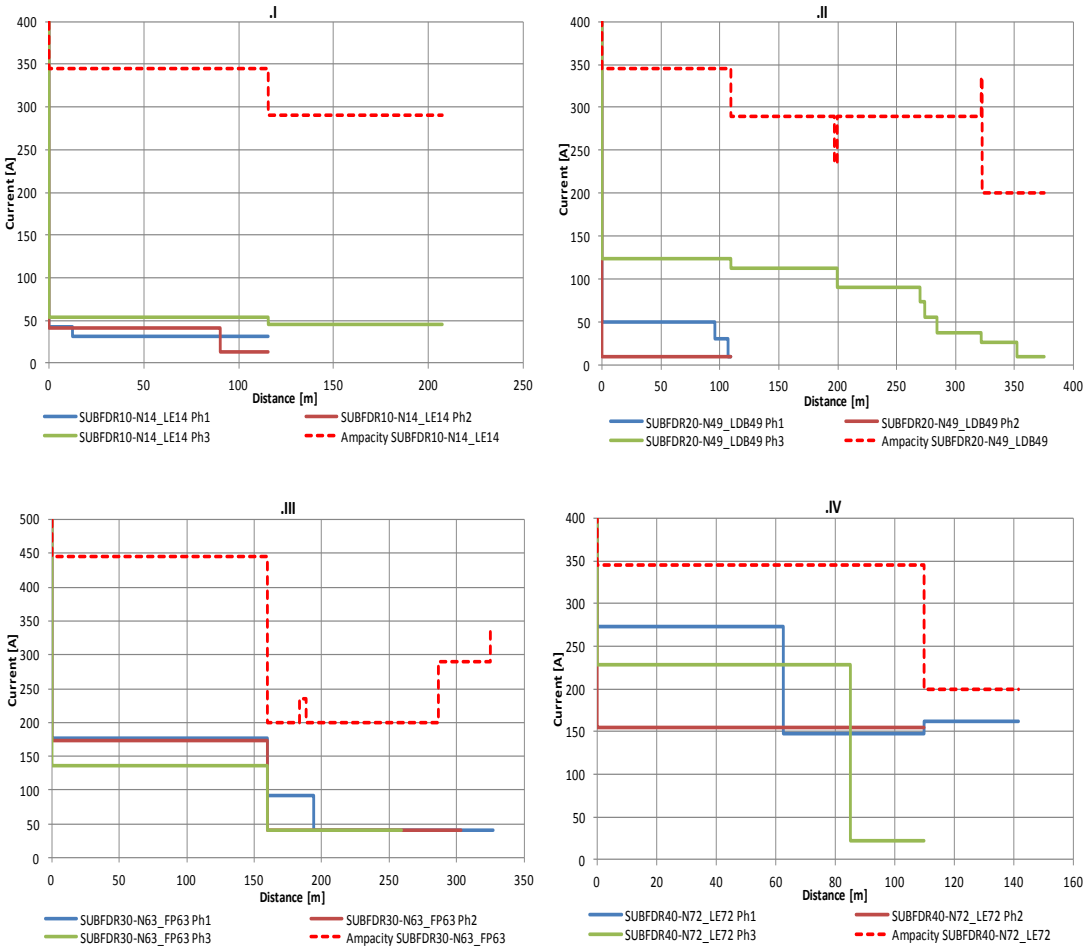

Figure 4.10 Current profiles of the network branches at Angus Street– Case 1: Base load case and PF=0.982:
.I SUBFDR10-LE14, .II SUBFDR20-LDB49, .III SUBFDR30-FP63 and .IV SUBFDR40-LE72

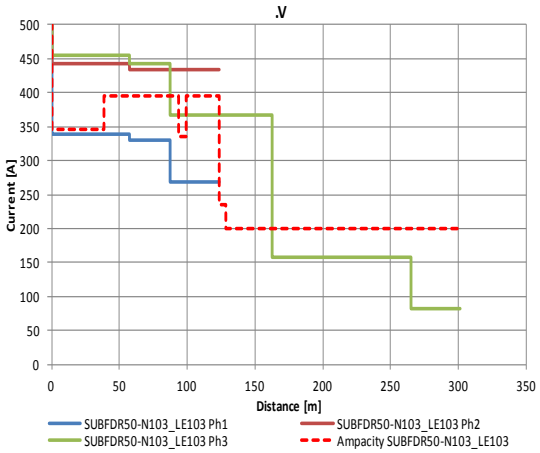

Figure 4.11 Current profiles of the network branches at Angus Street– Case 1: Base load case and PF=0.982:.V SUBFDR50-LE103

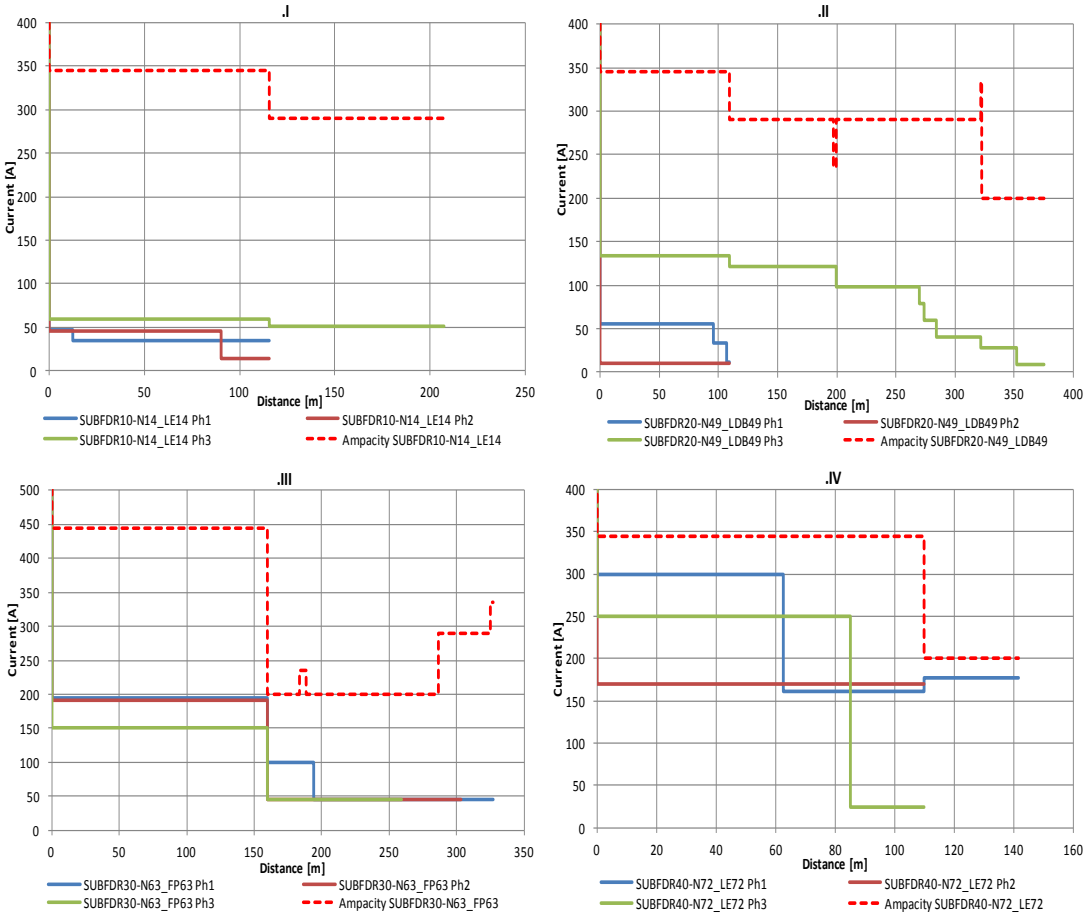

Figure 4.12 Current profiles of network branches at Angus Street– Case 2: Base load case PF=0.9: .I SUBFDR10-LE14, .II SUBFDR20-LDB49, .III SUBFDR30-FP63 and .IV SUBFDR40-LE72

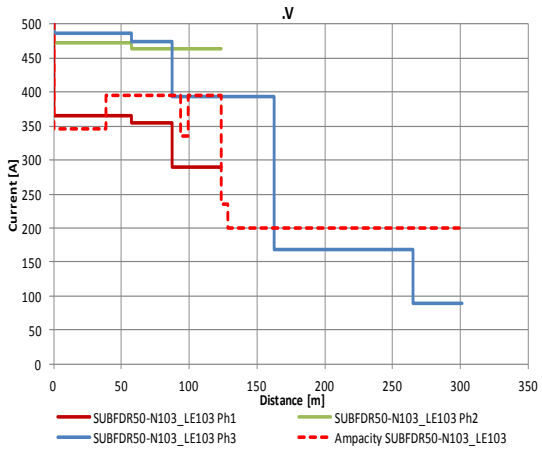

Figure 4.13 Current profiles of network branches at Angus Street – Case 2: Base load case and PF=0.9: .V SUBFDR50-LE103

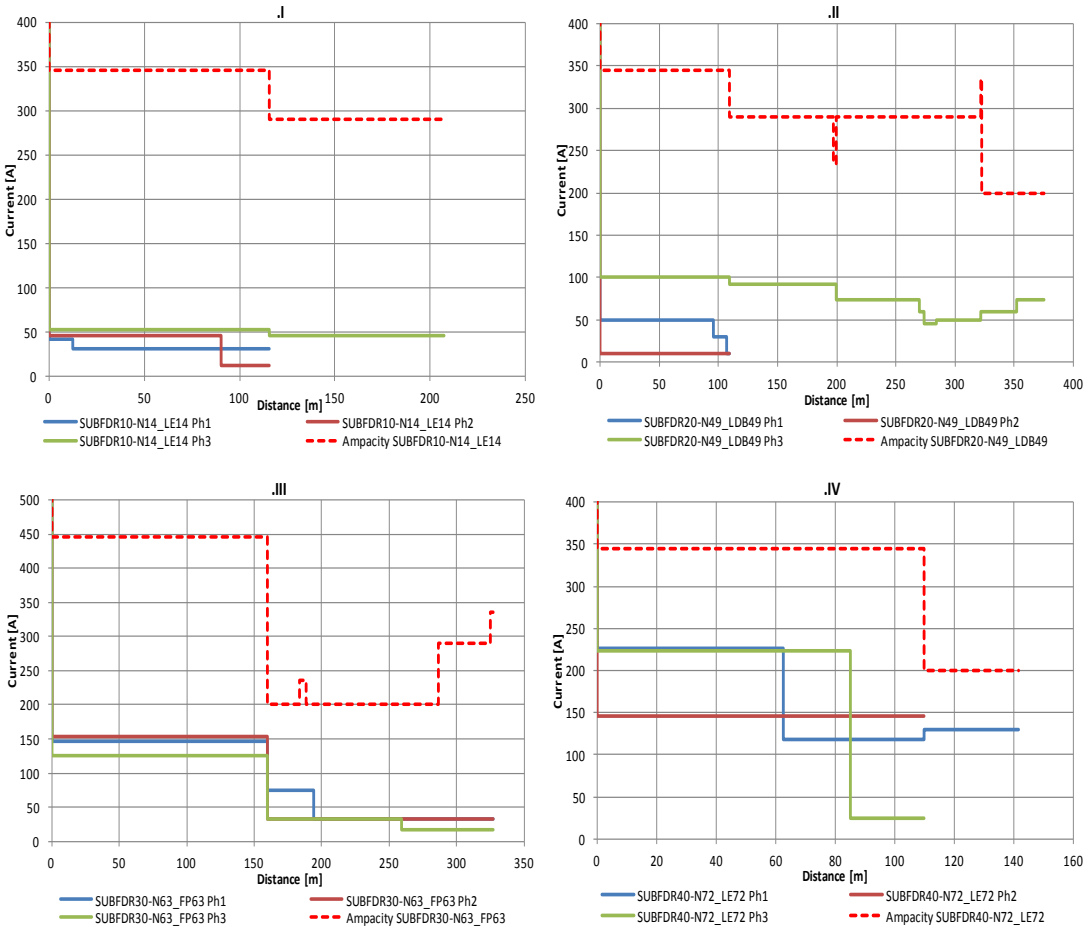

Figure 4.14 Current profiles of network branches at Angus Street – Case 3: Renewable units connected (Low PV penetration 100 kW): .I SUBFDR10-LE14, .II SUBFDR20-LDB49, .III SUBFDR30-FP63 and .IV SUBFDR40-LE72

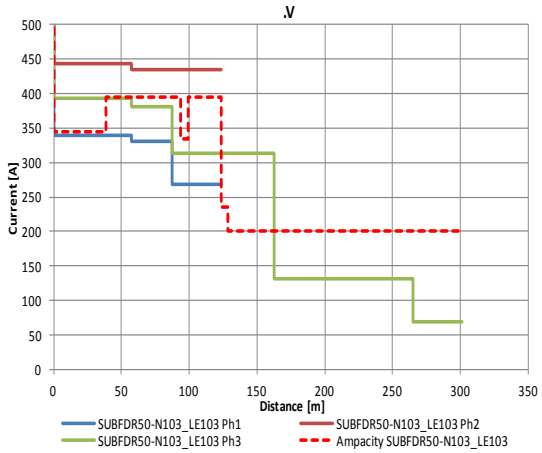

Figure 4.15 Current profiles of network branches at Angus Street – Case 3: Renewable units connected (Low PV penetration 100 kW): .V SUBFDR50-LE103

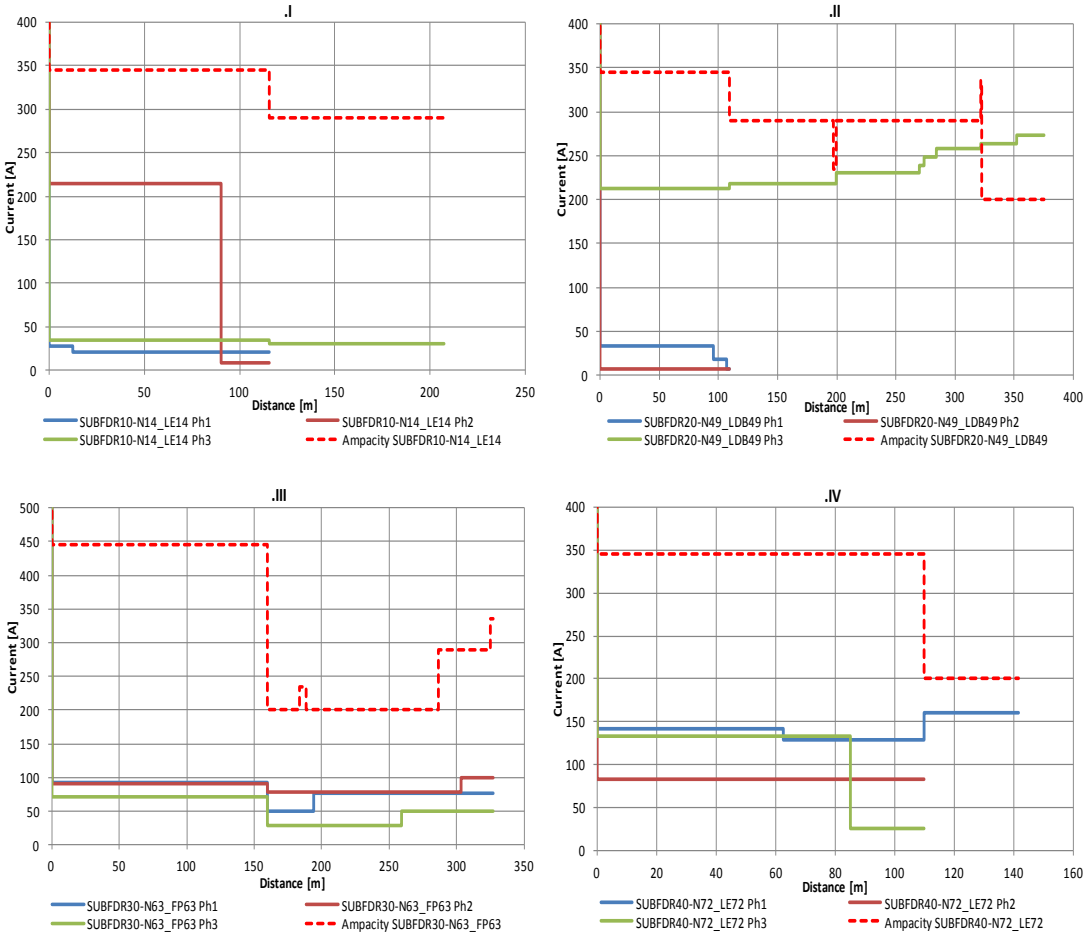

Figure 4.16 Current profiles of network branches at Angus Street – Case 4: Renewable units connected (High PV penetration 300 kW): .I SUBFDR10-LE14, .II SUBFDR20-LDB49, .III SUBFDR30-FP63 and .IV SUBFDR40-LE72

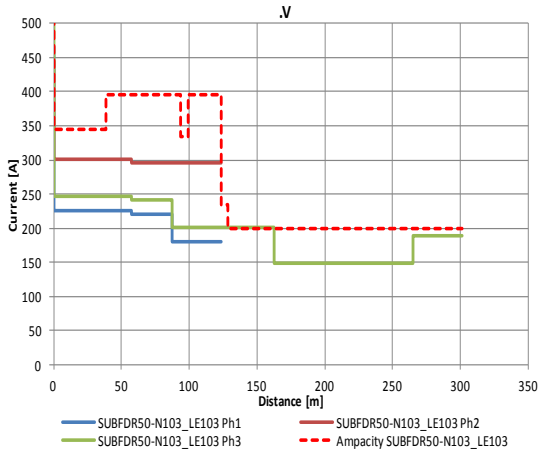

Figure 4.17 Current profiles of network branches at Angus Street – Case 4: Renewable units connected (High PV penetration 300 kW): .V SUBFDR50-LE103

Chapter 5

Types, effects and simulation results of reactive power compensation

5.1 Effects of reactive power compensation

A Correct design of an electrical network permits reducing energy wastefulness, but especially a rational use of the electrical energy with ensuing optimization of the correlated costs. One fundamental characteristic to minimizing expenses related to the purchase of energy is to reduce losses, starting from generation and on to distribution and use. In order to accomplish this objective a powerful action that make it possible is the reactive power compensation or reactive power control; it may be used for energy savings as it: limits energy losses due to the Joule effect along the cables, limits voltage drops along the cables, reduces plant engineering costs for users (conductors with a smaller cross-section) and voltage control.
Several techniques could be used to have the benefits depicted above. Some possibilities that works as a controllable current source are: shunt capacitors and inverter interfaced DG units.
The first technique has been adopted on the reactive power compensation simulations which are carried out in 5.3.1 and 5.3.2. The second one will be considered and explained in section 5.5.
A shunt capacitor of suitable size can accomplish a power factor correction in different ways depending on the various applications and needs. The types of power factor correction can be differentiated into: individual power factor correction, centralized power factor correction, mixed power factor correction and power factor correction per groups.
In this chapter has been presented a report of the effects of a reactive power compensation at Angus Street network using OpenDSS. For this purpose it has been chosen the centralized power factor correction because of its particularly suitable for installations with various services, which have also discontinuous utilization times, and moreover for its cheapness.

5.2.1 Reactive power calculation for centralised power factor correction

Considering knowing the initial $\cos\varphi$ and choosing the final desired $\cos\varphi'$ of the network, the corrected reactive power rating of the capacitor bank is:

$$Q_c = P \cdot (\tan\varphi - \tan\varphi') \quad (5.1)$$

Where:

P is the maximum total 3-phase real power of the substation

φ is the angle of the average cos φ of the network

φ' is the angle of the average final cos φ' desired for the network

5.2.2 Locations for centralised power factor correction devices

In this section are described the advantages of a reactive power compensation in a LV network and also is shown the worthwhile location to connect the compensator devices. As shown in figure 5.1 and 5.2 a 3-phase shunt capacitor bank has been placed at the feeding supply point of an hypothetical network and also downstream of the main busbar (SUBBUS).

The LV networks generally have an X/R ratios lower than 1, therefore the resistive part of the impedance of each cable/line prevail. For this reason, in order to have a convenient reactive compensation, the capacitor bank should be connect where the X/R ratio is higher. In figure 5.1 and 5.2 can be seen two qualitative diagrams of the effects of worthwhile and not suitable collocation of the reactive compensator devices in order to finalize a centralised power factor correction. Assuming a general LV network, for instance a power factor 0.8 (lagging) and a transformer (TX) 11/0.415 kV in which is flowing an I_{tx} current (at LV side). According to figure 5.1 and 5.2 in which are shown two different LV network configurations, the TX has evidently two buses (both with X/R>1): BUS1 at HV transformer side, where V_1 is the bus voltage magnitude, and BUS2 at the LV transformer side in which V_2 is the relative bus voltage. Downstream the TX there is an another busbar called BUS3 with a X/R<1 and its relative voltage V_3. At this last busbar is connected an hypothetical main load. When a reactive power compensator device, as may be a three-phase capacitor bank, is connected at BUS2 (figure 5.1), the relative capacitive current I_C (angle 90° leading) adjust the magnitude and the angle of the new transformer current I_{tx}' and consequently voltage V_1'. In this scenario there is a substantial reduction of current magnitude and voltage drop at BUS1.
In the other case (figure 5.2) when the reactive compensator devices are connected at BUS3, the relative contributions do not help to reduce the feeder voltage drop but may slightly reduce the current magnitude.

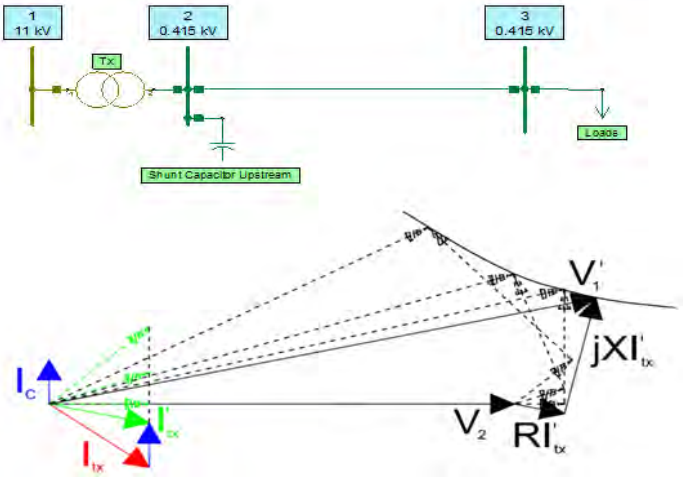

Figure 5.1 Shunt capacitor bank connected at the LV side of the transformer (X/R>1)

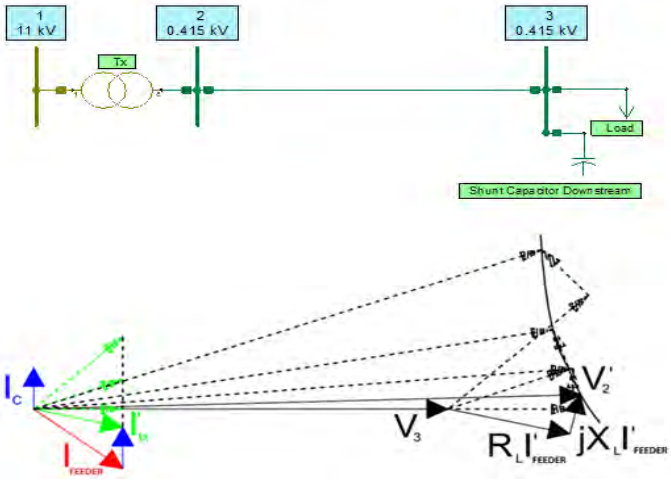

Figure 5.2 Shunt capacitor bank connected downstream the transformer (X/R<1)

To better understand the importance of the X/R ratio and the opportune collocation of the reactive compensator devices, table 18 should be considered because are shown the X/R ratio of the positive and zero sequence of Angus Street network.

Table 18 X/R ratios of each bus at Angus Street network on power flow and fault studies.

Bus	X1/R1 (positive sequence)	X0/R0 (zero sequence)
MT1	4	3
SUBBUS	4.343	4.358
SUBFDR10	4.342	4.358
N1_BJT1	2.344	1.849
N2_SJT2	0.7574	5.474
N3_SJT3	0.6942	5.635
N4_LE4	0.6688	5.7
N5_BJT5	1.002	0.9649
N6_SJT6	0.901	2.133
N7_SJT7	0.8272	2.559
N8_SJT8	0.7263	3.105
N10_BJT10	0.5968	3.748
N11_LE11	0.5703	3.873
N12_LE12	0.5496	3.969
N13_BJT13	0.9129	1.688
N14_LE14	0.5997	4.81
N16_BJT16	0.795	0.8853
N17_SJT17	0.7878	0.8636
N18_LDB18	0.7849	0.8265
N19_BJT19	0.7884	0.8238
N20_CUTOUT20	0.7802	0.8216
N21_SJT21	0.7787	0.9228
N22_LE22	0.7462	0.8016
SUBFDR20	4.342	4.358
N23_SJT23	1.493	1.272
N24_BJT24	0.9801	0.9525
N25_SJT25	0.6052	3.226
N26_BJT26	0.5297	3.725
N27_LE27	0.509	3.853
N28_LDB28	0.5119	3.837
N29_BJT29	0.9445	1.016
N30_BJT30	0.6048	3.217
N31_LE31	0.5718	3.44

Bus	X1/R1 (positive sequence)	X0/R0 (zero sequence)
N33_BJT33	0.9393	0.9267
N34_CUTOUT34	0.3738	1.614
N36_SJT36	0.6089	4.425
N37_SJT37	0.601	4.281
N38_SJT38	0.5669	4.67
N39_SJT39	0.5389	4.971
N40_SJT40	0.5365	4.997
N41_SJT41	0.5306	5.058
N42_SJT42	0.5284	5.082
N43_BJT43	0.5112	4.379
N44_FP44	0.5106	4.336
N45_SJT45	0.511	4.366
N46_SJT46	0.4838	4.446
N47_BJT47	0.481	4.454
N48_LE48	0.4726	4.48
N49_LDB49	0.462	4.512
SUBFDR30	4.343	4.358
N51_BJT51	1.241	1.252
N52_SJT52	0.9375	1.175
N53_SJT53	0.8945	0.9404
N54_BJT54	0.86	0.9168
N55_LE55	0.7084	2.786
N56_BJT56	0.702	1.558
N57_LE57	0.6112	3.223
N58_BJT58	0.6257	1.429
N59_CUTOUT59	0.6765	3.022
N60_SJT60	0.5938	1.028
N61_SJT61	0.5937	0.7169
N62_SJT62	0.5858	0.739
N63_FP63	0.5858	0.7081
N64_SJT64	1.238	1.144
N65_FP65	1.085	3.172
SUBFDR40	4.342	4.358

Bus	X1/R1 (positive sequence)	X0/R0 (zero sequence)
N66_BJT66	1.254	1.123
N67_LE67	0.7295	3.154
N68_BJT68	1.148	1.058
N69_LE69	0.7109	3.016
N70_BJT70	1.075	2.117
N71_SJT71	0.6644	3.963
N72_LE72	0.6435	4.031
N73_SJT73	1.053	1.492
N74_SJT74	1.056	1.008
N75_SJT75	1.055	1.008
SUBFDR50	4.342	4.358
N77_SJT77	1.373	3.378
N78_BJT78	1.224	1.753
N79_CUTOUT79	0.9837	0.9767
N80_BJT80	1.071	2.313
N81_SJT81	1.052	2.196
N82_SJT82	1.015	2.029
N83_LDB83	0.9666	0.9497
N85_SJT85	0.8389	3.739
N86_LDB86	0.8375	3.769
N87_SJT87	0.9508	0.9292
N88_SJT88	0.9061	1.088
N90_SJT90	0.5537	3.311
N91_SJT91	0.5475	3.357
N94_LE94	0.4454	4.071
N95_SJT95	0.9508	0.9292
N96_SJT96	0.9075	1.083
N98_BJT98	0.6387	2.98
N99_LE99	0.604	3.219
N101_SJT101	0.4452	4.191
N103_LE103	0.4177	4.345
N106_BJT106	0.4745	3.739
N107_LE107	0.4674	3.762
N108_CUTOUT108	0.3223	3.252

5.3.1 Reactive power compensation simulation on Angus Street network

The reactive power compensator devices may sensible change the behaviour of the network. For this reason to assess the possible variation of the network load shape, it has been carried out a study, using OpenDSS, at Angus Street network in which a 3-phase shunt capacitor was tied at the main supply busbar (SUBBUS) of the network. Following the equation (5.1) the proper size of this capacitor has been calculated. The shunt capacitor data are shown in table 19. In order to have some benefits on the grid when the power demand is higher, the capacitor bank considered is automatically switch on in the network by a time-controller regulator from 8 a.m. until 18 p.m. This solution reduces the total current flowing at the power supply point and enhance the voltage profile along the feeder, frees additional feeder capacity, and reduces losses.

Table 19 Shunt capacitor data

Rated Voltage [kV]	Size [kVAr]	No. Phases	Type of connection
0.415	285	3	Delta

5.3.2 Simulation results of reactive power compensation at Angus Street network: voltage limits

A comparison of two different simulation cases on Angus Street network is shown in the next graphs. Figure 5.3 shows the voltage (L-N) result simulations of the three phases at the feeding point of Angus Street network (SUBBUS) under nominal load case and power factor 0.9 (Case 2 – see table 17), before the reactive power compensation. As can be seen from the figure there are voltage fluctuations over the day which are more evident from 6 a.m. until 21 p.m., but all of the phases follow almost the same trends. The voltages remain within the range 101.7% − 103.8% of nominal voltage and this is well within statutory limits (-6%/+10% of 230V) [2]. Figure 5.4 shows the simulation resulting voltage (L-N) of the three phases at the feeding point of Angus Street network (SUBBUS), considering the second load scenario: case 2 but when a capacitor bank is tied to the grid. As can be seen from the graph the phase voltage tendencies, from 6 a.m. until 18 p.m., are shift up of an average value of about 3.4 V over this period. The voltages remain within the range 102.6% − 104.5% of nominal voltage and still the statutory limits are not violated. Therefore there is a slightly improvement in the voltage profile along the network, in fact a voltage rise on each phase of the network branches can be detected.

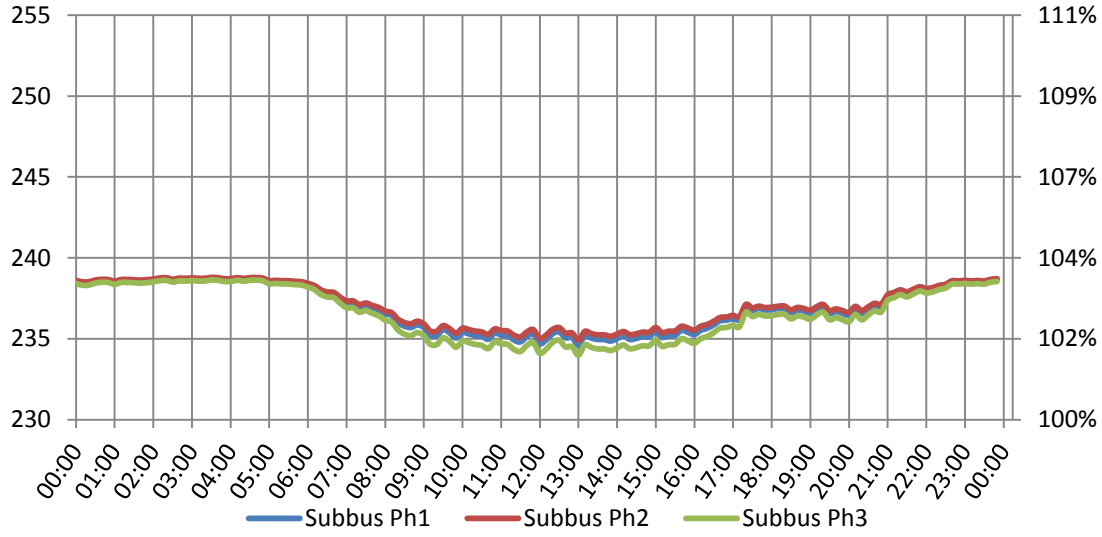

Figure 5.3 Simulation results of phase voltage profiles (L-N) at the feeding point of Angus Street network - case 2 (before reactive compensation)

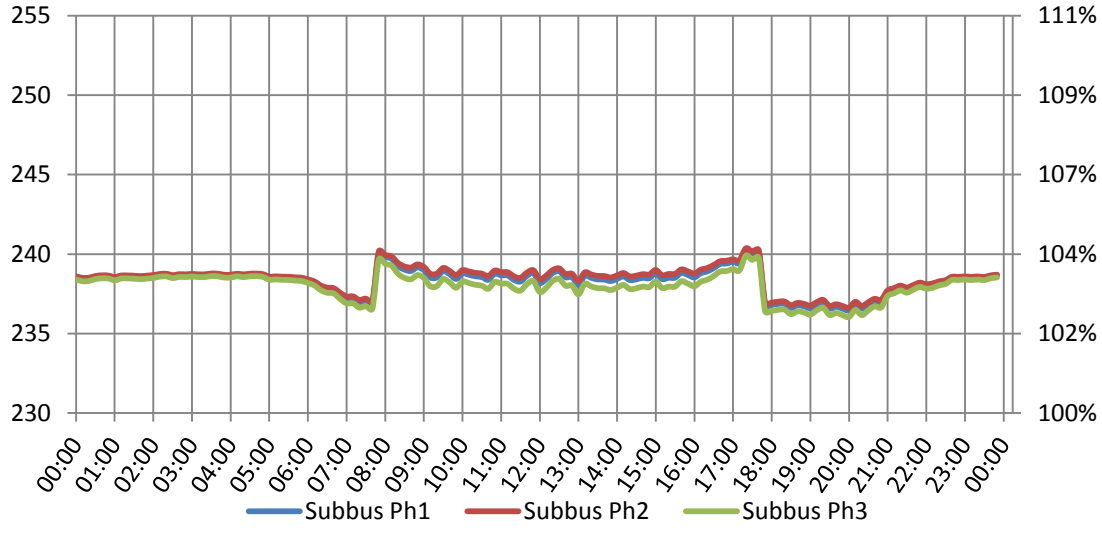

Figure 5.4 Simulation results of phase voltage profiles (L-N) at the feeding point of Angus Street network – case 2 (after reactive compensation)

5.3.3 Simulation results of reactive power compensation at Angus Street network: current limits

Figure 5.5 shows the phase currents simulation results of the three phases at the feeding point of Angus Street network (SUBBUS) under nominal load case and power factor 0.9 (Case 2). From the figure it can be seen that there is a sudden pick up in phase currents in the early morning around 6.00 until 23.00. Concerning the differences between phase currents, the data reveal that there is an important imbalance on the peak of the load shape, also from figure 5.5 can be seen that the third phase is more loaded than the other two. Figure 5.6 shows the phase currents simulation results of the three phases at the feeding point of Angus Street network (SUBBUS) when a capacitor bank is connected on it. The most relevant aspect of the reactive compensation is the current magnitude reduction per phase indeed a comparison between figure 5.5 and figure 5.6 shows that the maximum achieved current reduction on each phase is: I_1=221.8, I_2=208.9 and I_3=283.7. Therefore this economic reactive compensation may be worthwhile to alleviate voltage drop and current loading. A summary of the total current reduction at the SUBBUS is shown in table 20.
Concerning the phase currents flowing on each branch of the network, it has been noted a very slightly current raise on those phases not connected to photovoltaic systems, instead in the other phases the current is sensible reduced.

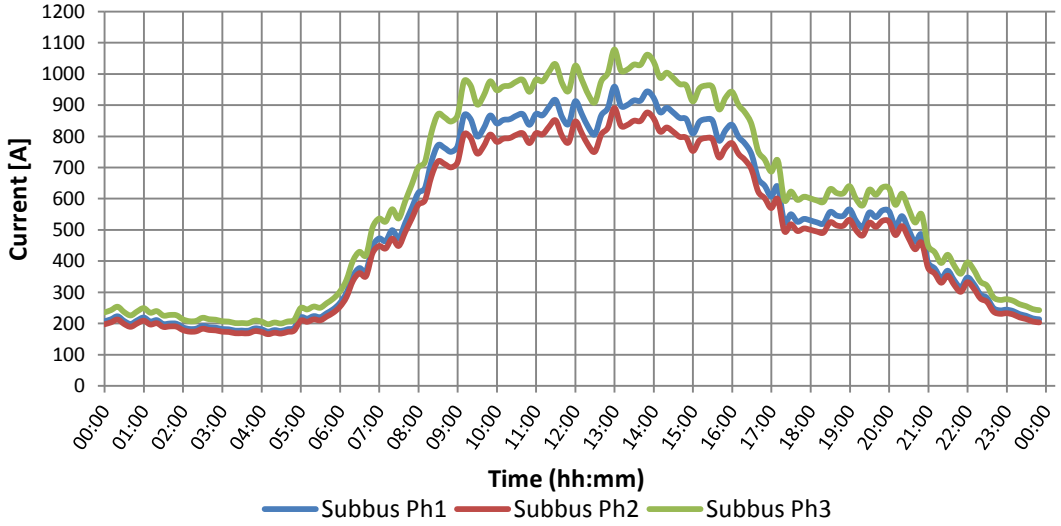

Figure 5.5 Simulation results of phase current profiles at the feeding point of Angus Street network - case 2 (before reactive compensation)

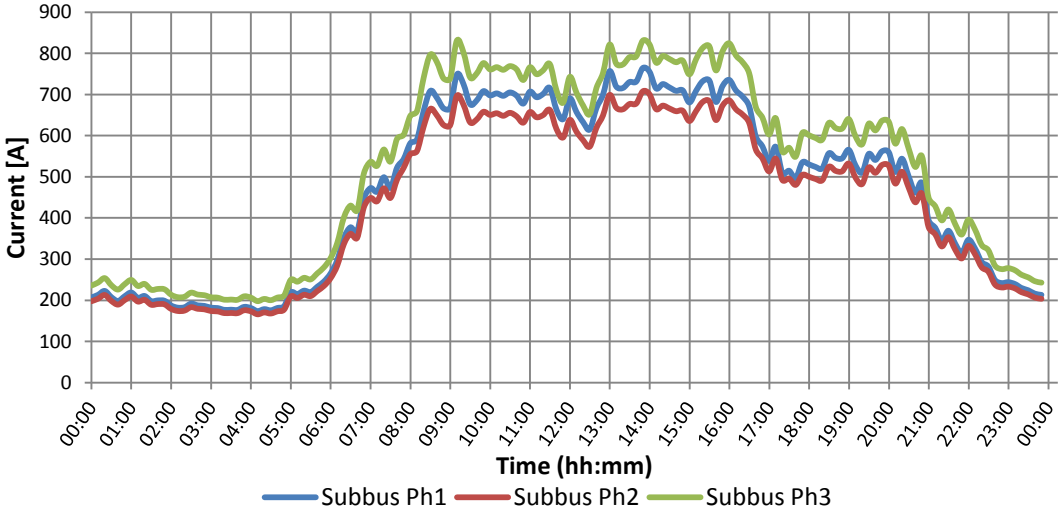

Figure 5.6 Simulation resulting phase current profiles at the feeding point of Angus Street network – case 2 (after reactive compensation)

Table 20 Comparison of phase currents at the feeding point of Angus Street before and after reactive compensation

	Ph 1 [A]	Ph 2 [A]	Ph 3 [A]
Before reactive compensation	959.956	890.619	1078.43
After reactive compensation	764.902	707.542	830.896

5.4 Effects of the reactive compensation on high voltage network

If reactive power compensation devices are tied to low voltage networks is important to understand the relative influences of them at the high voltage grid. In accordance with Western Power Distribution in order to analysed this aspect was decided to carry out a short study on a HV network using NEPLAN. This HV network was already modelled in a previous project developed by David Tuffery (a student of the School of Engineering at the Cardiff University).

The network analysed is called New Lodge Primary of 11kV and is located in South Wales, all its feeders from New Lodge Primary were modelled back to New Lodge or two other primaries 11kV substations: Llanelli and Kidwelly.

However, in our evaluations has been chosen only one feeder, Coastal Park (about 7 km route length), whereas the others were disconnected in order to simulate an extreme operating case. The main feeding point was set at V_{rated}=103%. The X/R ratios of 11kV cables were about 0.2 and the 11kV overhead lines about 1.0.

As the aim of the analyses, two different operating scenarios were carried out just changing the PF of each load. The first case was with PF=0.9 (lag) and the second one was with PF=1 in order to simulate the effects after the 'LV' compensation.

As reported in table 21, in case 2 the node voltage at the feeder-end is not much different in comparison to case 1, therefore the reactive compensation at the low voltage side is not much relevant on the voltage profile at 11 kV. While an important difference between the two cases is in the total reactive power (Q) which is over one thousand and a hundred kVAr, whereas for the total power P the difference is just about 21 kW.

Table 21 Effects of the LV compensation at New Lodge Primary - Coastal park network (11 kV)

Case	Total P (kW)	Total Q (kVAr)	Feeder end node voltage (%)
1) PF=0.9 (lag)	3973	1887	97.6
2) PF=1	3952	750	98.2
Difference	21	1137	0.6

5.5 Voltage control systems

In LV networks the grid impedance is mainly resistive, above all in cable networks, therefore the voltage regulation, if required, is rather difficult with traditional voltage control systems. In fact, due to the low X/R ratio at the LV networks, the reactive power compensation may be not useful in all of the cases, for this reason unconventional ways of voltage control should be used. In figure 5.7 are represented the X/R ratios of some underground cables and an overhead line employed in the Western Power Distribution LV networks. As can be noted, the X/R ratio of each cable/line is less than one due of its intrinsic resistive nature.

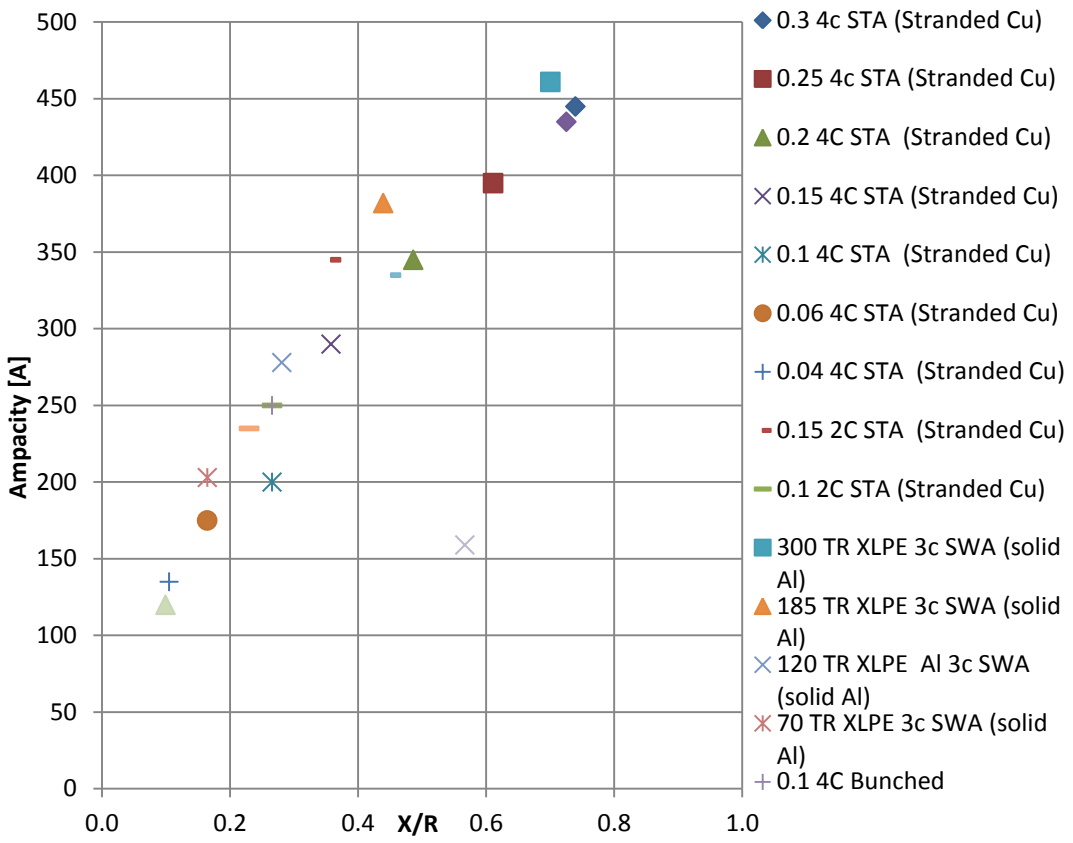

Figure 5.7 X/R ratio graph of some underground cables/overhead lines deployed in Western Power Distribution LV networks

In addition to the shunt capacitor, another possible way to generate or exploit reactive power to mitigate the network voltage profiles is the inverter interfaced DGs.

The Inverter interfaced generation unit is suitable to actuating a sort of reactive compensation in the same time of normal operating active power injection in the network. This kind of technique may be used for local voltage control strategies when DGs are connected on the grid by Inverters. This process is accomplished by adapting the injected current phasor according to the local voltage level requirement or in response of an external signal. [12]

In a normal LV network this types of voltage regulation, especially if are single-phase DG units, might worsening the power quality due to the unbalance and harmonic distortion that may be increased [12]. Consequence of this approach is a reactive power variation through the three-phase system. The current flowing on the LV branches are typically not symmetrical due to the domestic/industrial loads connected and to the uncoordinated regulation action of single-phase inverter interfaced generation units. Thus, at the point of common coupling (PCC) the voltage unbalance get worse. For this reason a mitigation of the voltage profiles can be achieved by the three-phase inverter-connected DGs which recombine the negative and zero sequent currents [12]. Therefore the purpose of this voltage regulator is to generate a current triplet which have a zero and negative sequence components with exactly the same magnitude but in phase opposition, according to the components measured downstream branches [12]. Figure 5.8 depicts a block diagram of the three-phase inverter-interfaced DGs and how it works.

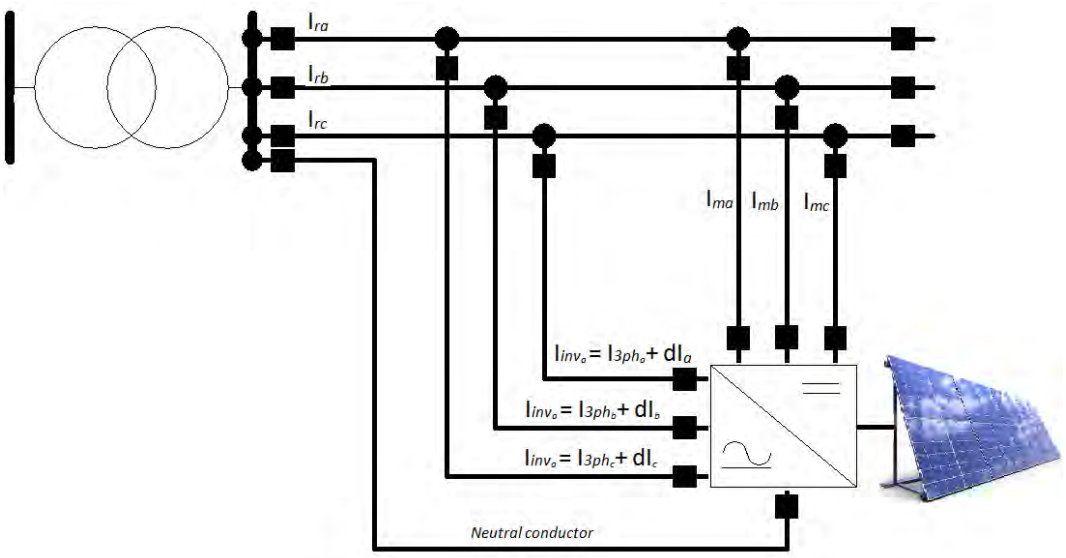

Figure 5.8 Three-phases interfaced DGs diagram [12]

Another interesting possible voltage control system but in HV networks is the controllable series inductance. The aim of this solution is to increase the inductance by using power electronics in HV networks in combination with reactive power control by DG units. Due to the low X/R ratio of the grids the reactive power injected by DGs normally have a limited influence therefore to improve the voltage regulation a variable inductor could be connected in parallel with two anti-parallel thyristor [13].

5.6 Impact of distributed generation units on low voltage network

The X/R ratio is determinant parameter also to assess the impact of DG units on the voltage profile at distribution networks. To express this kind of evaluation the short-circuit impedance Z_{sc} and its X/R ratio shall be considered [13]. In according to [13], the voltage change on the network profile is due to active and reactive power of the DGs.

The voltage variation depends on three main network characteristics:

1. The X_{sc}/R_{sc} ratio of Z_{sc}
2. The ratio between the rated DG unit apparent power and the short-circuit power at the point of connection
3. The active and reactive DG unit power [13]

5.7.1 Hosting capacity of low voltage networks

The Hosting capacity is the capability of a network to accommodate distributed generations (DGs), like photovoltaic and wind systems which are non-dispatchable generation, without any types of integration technology such energy storage devices (for smoothing energy purposes) or other devices to prevent systems instability on the network. [10]
In order to carry out Hosting capacity network studies a procedure should be follow. The network parameters to focus on may be different, that is due to the network type under analyses and to the types of embedded generation (photovoltaic systems, wind electric systems etc.) on the grid. According to [14], which is an approach to carry out studies on the hosting capacity of some Italian

networks, the branch currents and the bus voltages of the selected network are calculated by load flow analysis and afterwards compared with statutory and operating limits. In order to evaluate the extreme network operating case according to the statutory limits and amapacity, the DGs powers injected in the network will increase until the violation of the limits (i.e. thermal and voltage). [14]

For each type of network different limits and parameters may be taken into account. For example in [14], the procedure focus on three limits which are: thermal limits, supply voltage variations (SVV) of each bus and rapid voltage changes (RVC) related to of sudden variations of DGs power output (typical of intermittent renewable energy sources).
Figure 5.9 shows a possible scrupulous procedure to carry out an assessment of the hosting capacity in distribution networks exploiting the features of OpenDSS. [15]

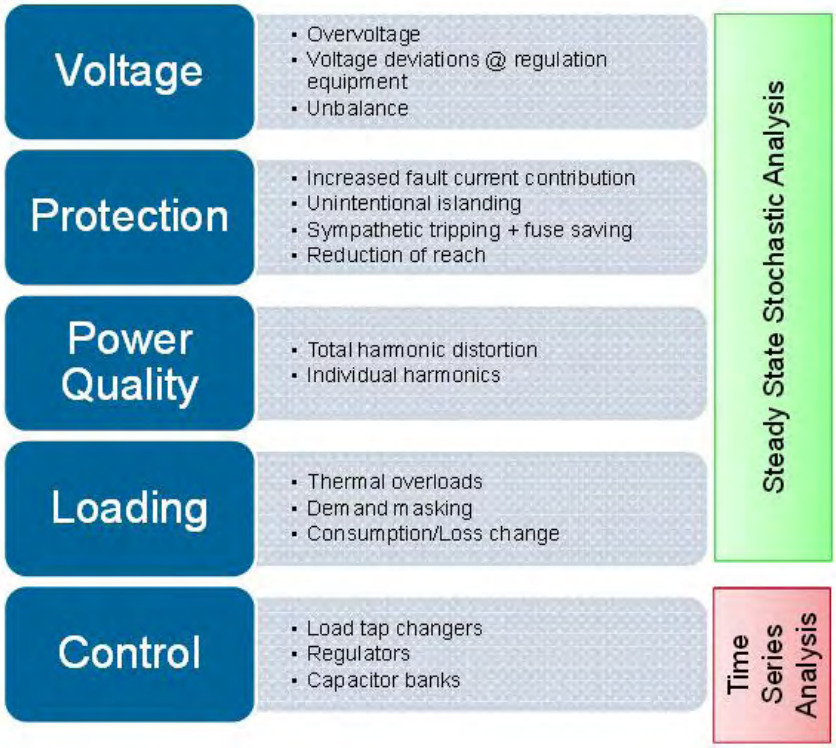

Figure 5.9. DGs Impact analysis [15]

5.7.2 Hosting capacity of Angus Street

In this section has been presented a short study on a possible approach to evaluate the hosting capacity at Angus Street network. A hosting capacity estimation on Angus Street network has been carried out by considering twenty-five photovoltaic (PV) systems, considering unity PF, connected on four customer locations of each network feeder considering different PV penetrations.
It was evaluated an hypothetical PV penetration exploiting a stochastic algorithm function of OpenDSS. As an hosting capacity evaluation some important limits shall be considered, some of them are: voltage and thermal limits and the maximum embedded generation of the LV distribution network, which is according to [6] the 30% of the transformer capacity.
At Angus Street network the transformer size is 1000 kVA therefore 300 kW has been chosen as the maximum PV penetration acceptable. [11]
Figure 5.10 shows the hosting capacity evaluation at Angus Street network considering the maximum feeder voltage (at SUBBUS) in relation to PV penetration. As can be seen in the graph the maximum embedded generation that may be connected on the network is about 300 kW but sometimes to prevent islanding operation at substation level, the DGs penetration is limited to 20% of the substation transformer capacity. [11]

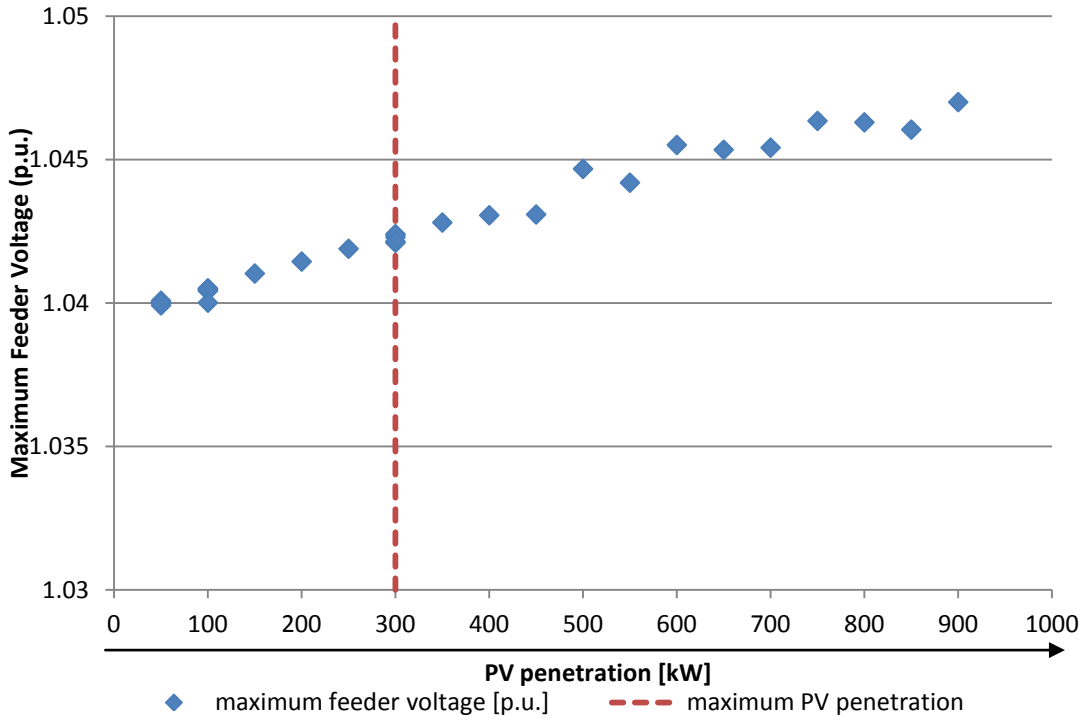

Figure 5.10 Hosting capacity study at Angus Street network

Conclusions

In this project a deep analyses of real data on five real low voltage (LV) networks has been carried out in order to understand the network trends of V, I, P, Q and calculated power factor (PF). These studies reveal that on urban networks the power patterns are quite predictable during the weekdays whereas for rural networks the powers trends are more variable due to the numerous domestic loads connected at the networks.
Through statistical analyses, the voltage and current distributions has been assessed to understand the behaviours of the networks. From the recorded data examined, the voltage has an approximate Gaussian distribution while the current recordings showed a non-normal distribution in fact at rural substations there are approximate Poisson distributions whereas at urban networks there are bi-modal or tri-modal distributions. However, the statutory limits were always not violated.
Significant PF variations were observed over a daily load cycle and the relative patterns were different at each substation analysed. In urban networks at the feeder supply point the PF may vary inversely with load during the day. However, the PF variation is more variable in rural networks than the urban ones analysed.
Concerning the voltage profiles of the LV networks under study, the voltage drop across the supply transformer is more affected by variation in PF than the voltage drop across the feeders, due to its higher X/R.
The study of the reactive power compensation on Angus Street network was developed in order to mitigate the strong unbalance present and to find out the possible voltage regulation advantages. The shunt compensator tied to the supply substation may be useful to limit the voltage drop across the transformer and the current magnitude. On the contrary if the compensator devices are applied downstream the transformer, the contributions of the reactive power compensation is not so effective in reducing feeder voltage drop but may help to reduce network currents and operate within cable ampacity.
The analysis of the simulation results at Angus Street network indicated that standard quantities of DGs can alleviate voltage drops and current loading. At high level of DGs, connected to the LV buses, there is a general substantial improvement on the voltage and current profile but in lighter loaded branches the embedded generation can overload cable conductors.

Possible future work

This project may be considered as a good exploration on the low voltage networks behaviours exploiting real recorded data. For this reason some contents of this thesis might be studied in deep. A first additional study on the project it might be an extended analysis on other unbalanced WPD networks always with the aid of OpenDSS. Further developments should be a comprehensive quantification of embedded generation 'Hosting Capacity' for selected networks, an investigation on the benefits of reactive power compensation at the main LV substation and a possible comparison with other techniques, examine the specific effects of LV reactive compensation on the 11kV networks.
Another very interesting aspect for a research extension might be the assessment of the impact of inverter-interfaced DG units for local voltage control and its relative transient impact on WPD low voltage networks.

Acknowledgements

I would like to acknowledge Huw Griffiths for his strong support and his helpfulness throughout this project.

Special thanks to my family and to the Balords because I would have not been able to do this incredible experience in Cardiff without them.

Appendix A

Technical data of the networks

This section shows the provided data of the five networks that has been analysed in the previous chapters. In table 1, 2, 3, 4 and 5 are shown the networks data provided by Western Power Distribution (WPD) in which are described each line section of the relative networks.

Table A1 shows the technical data of Stuttgarter Strasse (urban network)

Type of cable		"Bus 1" Start point	"Bus 2" End point	X bus1	Y bus1	X bus2	Y bus2	Length [m]
Ug	300 TR	SUB TAIL	LE 1	318480.214	176828.26	318479.798	176827.044	1.726
Ug	300 TR	SUB FDR 10	SJT 2	318480.47	176828.388	318471.99	176824.056	14.524
Ug	0.25 4c STA	BJT3	SJT 2	318462.286	176850.194	318471.99	176824.056	27.881
Ug	185 WCON	BJT 3	CUT OUT 4	318462.286	176850.194	318477.355	176848.092	26.352
Ug	0.25 4c STA	BJT 5	BJT 3	318461.63	176851.957	318462.286	176850.194	1.908
Ug	0.25 4c STA	BJT 5	LE 6	318461.63	176851.957	318462.839	176851.905	4.635
Ug	0.25 4c STA	BJT 7	BJT 5	318456.874	176864.52	318461.63	176851.957	13.466
Ug	0.25 4c	LE 8	BJT 7	318440.078	176860.014	318456.874	176864.52	18.145
Ug	0.25 4c STA	LDB 9	BJT 7	318456.038	176867.211	318456.874	176864.52	2.818
Ug	185 TR	SUB FDR 20	CUT OUT 10	318480.95	176828.516	318499.057	176828.551	18.687
Ug	300 TR	SUB FDR 30	CUT OUT 11	318481.184	176828.603	318498.993	176828.839	18.322

Legend:

X bus , Y bus are the XY bus coordinates
UG is the underground cable type
OH is the overhead line type
SJT (Straight Joint) – joining two different cables together
BJT (Breach Joint)– connecting one cable to two other cables
LE is a Live End, this is the end of a cable
LDB is a link box which is used for maintenances and fault restoration
CUTOUT is the electricity delivery point for customers premises
DUMMY is a fictitious node of the network
FP is a feeder pillar, this is the equivalent of a link box that is installed above ground

Table A2 shows the technical data of Nettlefold Road (urban network)

Type of cable		"Bus 1" Start point	"Bus 2" End point	X bus1	Y bus1	X bus2	Y bus2	Length [m]
Ug	300 TR	SUB FDR 10	SJT 1	319867.2	175578.46	319865.66	175577.06	2.626
Ug	300 TR	SJT 1	BJT 2	319865.66	175577.06	319863.6	175577.39	2.274
Ug	300 TR	BJT 2	CUT OUT 3	319863.6	175577.39	319840.38	175588.37	32.318
Ug	300 WCON	BJT 2	SJT 4	319863.6	175577.39	319859.88	175574.72	5.669
Ug	300 TR	SJT 4	BJT 5	319859.88	175574.72	319827.99	175559.23	35.458
Ug	185 WCON	BJT 5	CUT OUT 6	319827.99	175559.23	319803.63	175601.14	53.651
Ug	300 TR	BJT 5	SJT 7	319827.99	175559.23	319812.11	175551.68	17.573
Ug	300 TR	SJT 7	SJT 8	319812.11	175551.68	319811.57	175551.43	0.6
Ug	300 TR	SJT 8	BJT 9	319811.57	175551.43	319788.85	175540.68	25.138
Ug	185 TR	BJT 9	BJT 10	319788.85	175540.68	319792.69	175528.54	13.778
Ug	185 TR	BJT 10	SJT 11	319792.69	175528.54	319806.65	175523.6	15.13
Ug	185 TR	SJT 11	CUT OUT 12	319806.65	175523.6	319814.23	175513.88	20.836
Ug	185 WCON	BJT 10	LE 13	319792.73	175528.36	319762.2	175516.73	35.199
Ug	185 TR	BJT 9	SJT 14	319788.85	175540.68	319759.25	175553.87	37.948
Ug	185 WCON	SJT 14	CUT OUT 15	319759.25	175553.87	319745.58	175576.84	38.517

Table A2 shows the technical data of Nettlefold Road (urban network)

Type of cable		"Bus 1" Start point	"Bus 2" End point	X bus1	Y bus1	X bus2	Y bus2	Length [m]
Ug	185 WCON	SUB FDR 20	BJT 16	319867.52	175578.62	319870.18	175578.02	3.267
Ug	300 TR	BJT 16	DUMMY 17	319870.18	175578.02	319886.51	175560.25	30.549
Ug	300 TR	DUMMY 17	BJT 18	319886.51	175560.25	319901.57	175529.78	33.989
Ug	300 TR	BJT 18	BJT 19	319901.57	175529.78	319935.64	175557.94	50.922
Ug	300 TR	BJT 19	DUMMY 20	319935.64	175557.94	320000	175586.68	70.491
Ug	300 TR	DUMMY 20	BJT 21	320000	175586.68	320010.5	175591.28	11.468
Ug	300 TR	BJT 21	LE 22	320010.5	175591.28	320016.75	175594.11	6.85
Ug	185 WCON	BJT 21	CUT OUT 23	320010.5	175591.28	320036.21	175571.79	36.794
Ug	185 TR	BJT 19	CUT OUT 24	319935.64	175557.94	319955.08	175536.52	29.539
Ug	300 TR	BJT 18	BJT 25	319901.57	175529.78	319905.75	175522.58	8.328
Ug	120 TR	BJT 25	CUT OUT 26	319905.75	175522.58	319894.12	175516.76	13.28
Ug	300 TR	BJT 25	BJT 27	319905.75	175522.58	319922.63	175495.55	31.868
Ug	300 TR	BJT 27	LE 28	319922.63	175495.55	319923.7	175494.69	1.407
Ug	300 TR	BJT 27	BJT 29	319922.63	175495.55	319932.51	175480.5	18.335
Ug	300 TR	BJT 29	LE 30	319932.51	175480.5	319932.28	175481.58	1.142
Ug	300 TR	BJT 29	SJT 31	319932.51	175480.5	319944.93	175453.23	33.97
Ug	70 TR	SJT 31	SJT 32	319944.93	175453.23	319865.84	175412.76	90.628
Ug	70 TR	SJT 32	SJT 33	319865.84	175412.76	319863.89	175413.07	2.033
Ug	300 TR	SJT 33	LE 34	319863.89	175413.07	319847.32	175438.15	30.229
Ug	300 TR	BJT 16	SJT 35	319870.18	175578.02	319884.45	175609.12	46.535
Ug	300 TR	SJT 35	LDB 36	319884.45	175609.12	319886.75	175632.48	23.988
Ug	300 TR	SUB FDR 30	SJT 36	319867.87	175578.77	319869.73	175602.56	32.351
Ug	300 TR	SJT 36	SJT 37	319869.73	175602.56	319864.13	175679.62	86.935
Ug	300 TR	SJT 37	SJT 38	319864.03	175679.68	319831.6	175730.79	62.542
Ug	300 TR	SJT 38	DUMMY 39	319831.6	175730.79	319851.24	175750	30.719
Ug	300 TR	DUMMY 39	BJT 40	319851.24	175750	319859.83	175754	9.477
Ug	185 TR	BJT 40	LE 41	319859.83	175754	319937.55	175734.12	97.729
Ug	300 TR	BJT 40	SJT 42	319859.83	175754	319896.59	175751.91	45.733
Ug	300 TR	SJT 42	LE 43	319896.59	175751.91	319942.27	175741.45	149.156
Ug	300 TR	SUB FDR 40	BJT 44	319868.26	175578.93	319869.71	175578.7	1.811
Ug	300 TR	BJT 44	SJT 45	319869.71	175578.7	319865.79	175576.7	5.075
Ug	300 TR	SJT 45	BJT 46	319865.79	175576.7	319863.65	175576.33	2.216
Ug	300 TR	BJT 46	LE 47	319863.65	175576.33	319861.69	175575.57	2.103
Ug	185 WCON	BJT 46	SJT 48	319863.65	175576.33	319921.78	175505.46	103.138
Ug	185 WCON	SJT 48	SJT 49	319921.78	175505.46	319908.72	175451.88	84.22
Ug	185 WCON	SJT 49	BJT 50	319908.72	175451.88	319897.92	175465.39	19.275
Ug	185 WCON	BJT 50	LE 51	319897.92	175465.39	319852.04	175441.68	52.909
Ug	185 WCON	BJT 50	LE 52	319897.92	175465.39	319860.27	175472.35	49.468
Ug	185 WCON	BJT 44	LE 53	319869.71	175578.7	319870.41	175579	0.763

Table A3 (1/2) shows the technical data of Angus Street (urban network)

Type of cable		"Bus 1" Start point	"Bus 2" End point	X bus1	Y bus1	X bus2	Y bus2	Length [m]
Ug	0.2 4c	SUB FDR 10	BJT 1	319099.01	177899.25	319087.14	177895.38	12.487
Ug	0.15 2c	BJT 1	SJT 2	319087.14	177895.38	319072.53	177940.04	46.966
Ug	0.15 2c	SJT 2	SJT 3	319072.53	177940.04	319068.35	177952.01	12.672
Ug	0.15 2c	SJT 3	LE 4	319068.35	177952.01	319066.2	177958.38	6.725
Ug	0.2 4c	BJT 1	BJT 5	319087.14	177895.38	319055.71	177955.55	77.615
Ug	0.1 2c	BJT 5	SJT 6	319055.71	177955.55	319065.6	177959.74	11.236
Ug	0.1 2c	SJT 6	SJT 7	319065.6	177959.74	319063.3	177966.75	7.377
Ug	0.1 2c	SJT 7	SJT 8	319063.3	177966.75	319058.91	177980.05	14
Ug	0.1 2c	SJT 8	BJT 10	319058.91	177980.05	319049.25	178009.33	30.834
Ug	0.1 2c	BJT 10	LE 11	319049.25	178009.33	319040.1	178006.26	9.654
Ug	0.1 2c	BJT 10	LE 12	319049.25	178009.33	319037.06	178014.86	18.478
Ug	0.2 4c	BJT 5	BJT 13	319055.71	177955.55	319047.74	177979.89	25.607
Ug	0.15 2c	BJT 13	LE 14	319047.74	177979.89	319076.59	177893.09	91.704
Ug	0.15 4c	BJT 13	BJT 16	319047.74	177979.89	319035.71	178017.3	39.316
Ug	0.15 4c	BJT 16	SJT 17	319035.71	178017.3	319035.36	178014.55	3.243
Ug	0.15 4c	SJT 17	LDB 18	319035.36	178014.55	319033.96	178013.89	1.559
Ug	0.15 4c	BJT 16	BJT 19	319035.71	178017.3	319033.92	178020.03	3.302
Ug	0.15 4c	BJT 19	CUT OUT 20	319033.92	178020.03	319030.43	178019.63	3.787
Ug	0.15 4c	BJT 19	SJT 21	319033.92	178020.03	319032.64	178023.62	3.807
Ug	0.15 4c	SJT 21	LE 22	319032.64	178023.62	319027.17	178041.55	18.769

Table A3 (2/2) shows the technical data of Angus Street (urban network)

Type of cable		"Bus 1" Start point	"Bus 2" End point	X bus1	Y bus1	X bus2	Y bus2	Length [m]
Ug	0.2 4c	SUB FDR 20	SJT 23	319080.22	177880.88	319099.1	177898.86	34.363
Ug	0.2 4c	SJT 23	BJT 24	319080.22	177880.88	319045.73	177848.91	61.51
Ug	0.1 2c	BJT 24	SJT 25	319045.73	177848.91	319030.46	177895.33	48.895
Ug	0.1 2c	SJT 25	BJT 26	319030.46	177895.33	319014.24	177944.32	51.776
Ug	0.1 2c	BJT 26	LE 27	319014.24	177944.32	319004.48	177941.06	10.256
Ug	0.1 2c	BJT 26	LDB 28	319014.24	177944.32	319000	177987.46	45.429
Ug	0.2 4c	BJT 24	BJT 29	319045.73	177848.91	319035.46	177845.52	10.922
Ug	0.1 2c	BJT 29	BJT 30	319035.46	177845.52	319019.87	177891.86	48.942
Ug	0.1 2c	BJT 30	LE 31	319019.87	177891.87	319029.66	177894.99	10.277
Ug	0.1 2c	BJT 30	LDB 28	319019.87	177891.86	318998.46	177991.81	112.015
Ug	0.2 4c	BJT 29	BJT 33	319035.46	177845.52	319033.63	177844.48	2.144
Ug	70 TR	BJT 33	CUT OUT 34	319033.63	177844.48	319018.72	177873.49	40.665
Ug	0.15 2c	BJT 33	STJ 36	319033.63	177844.48	318980.03	177877.05	88.283
Ug	95 WCON	STJ 36	STJ 37	318980.03	177877.05	318979.27	177879.33	2.401
Ug	0.15 2c	SJT 37	SJT 38	318979.27	177879.33	318968.94	177910.21	32.564
Ug	0.15 2c	SJT 38	SJT 39	318968.94	177910.21	318957.3	177946.01	37.641
Ug	0.15 2c	SJT 39	SJT 40	318957.3	177946.01	318956.15	177949.84	4
Ug	0.15 2c	SJT 40	SJT 41	318956.15	177949.84	318946.75	177947.9	10.156
Ug	0.15 2c	SJT 41	SJT 42	318946.75	177947.9	318944.92	177951.24	4.107
Ug	0.15 4c BUNCHED	SJT 42	BJT 43	318944.92	177951.24	318934.13	177983.05	33.756
Ug	185 WCON	BJT 43	FP 44	318934.13	177983.05	318932.17	177984	2.77
Ug	185 WCON	BJT 43	SJT 45	318934.13	177983.05	318934.68	177982.43	0.833
Ug	0.1 2c	SJT 45	SJT 46	318934.68	177982.43	318959.42	177990.43	26.078
Ug	0.1 2c	SJT 46	BJT 47	318959.42	177990.43	318962.3	177991.38	3.031
Ug	0.1 2c	BJT 47	LE 48	318962.3	177991.38	318965.34	177982.11	9.753
Ug	0.1 2c	BJT 47	LDB 49	318962.3	177991.38	318984.48	177998.83	23.396
Ug	0.3 4c	SUB FDR 30	BJT 51	319099.23	177898.5	318985.66	177826.72	160.091
Ug	0.1 4c	BJT 51	SJT 52	318985.66	177826.72	318978.24	177848.76	23.259
Ug	95 WCON	SJT 52	SJT 53	318978.24	177848.76	318976.53	177853.89	5.4
Ug	0.1 4c	SJT 53	BJT 54	318976.53	177853.89	318974.86	177858.91	5.298
Ug	0.15 2c	BJT 54	LE 55	318974.86	177858.91	318965.82	177888.04	31.37
Ug	0.1 4c	BJT 54	BJT 56	318974.86	177858.91	318964.79	177888.79	31.527
Ug	0.15 2c	BJT 56	LE 57	318964.79	177888.79	318955.45	177919.68	33.68
Ug	0.1 4c	BJT 56	BJT 58	318964.79	177888.79	318954.41	177920.5	33.37
Ug	0.15 2c	BJT 58	CUT OUT 59	318954.41	177920.5	318942.61	177943.89	31.073
Ug	0.1 4c	BJT 58	SJT 60	318954.41	177920.5	318945.74	177946.5	27.408
Ug	0.15 4c	SJT 60	SJT 61	318945.74	177946.5	318940.35	177962.59	16.967
Ug	0.15 4c	SJT 61	SJT 62	318940.35	177962.59	318933.86	177982.97	21.452

Table A4 shows the technical data of Rhos Wenallt (rural network)

Type of cable		"Bus 1" Start point	"Bus 2" End point	X bus1	Y bus1	X bus2	Y bus2	Length [m]
Ug	120 TR	SUB FDR 10	SJT 1	301418.649	203632.357	301433.526	203608.258	31.108
Ug	120 TR	SJT 1	SJT 2	301433.531	203608.256	301436.111	203606.726	3
Ug	120 TR	SJT 2	SJT 3	301436.114	203606.725	301444.065	203603.559	9.176
Ug	120 TR	SJT 3	BJT 4	301444.065	203603.559	301463.033	203612.217	20.916
Ug	120 TR	BJT 4	SJT 5	301463.033	203612.217	301463.261	203613.294	2.148
Ug	120 TR	SJT 5	LE 6	301463.261	203613.294	301463.133	203614.142	0.858
Ug	120 TR	BJT 4	BJT 7	301463.033	203612.217	301483.181	203603.635	24.457
Ug	300 TR	BJT 7	LE 8	301483.181	203603.635	301606.883	203604.778	154.555
Ug	120 TR	BJT 7	SJT 9	301483.181	203603.635	301483.826	203602.856	1.011
Ug	120 TR	SJT 9	SJT 10	301483.826	203602.856	301484.685	203600.841	2.196
Ug	70 TR	SJT 10	SJT 11	301484.686	203600.837	301485.36	203592.358	8.519
Ug	70 TR	SJT 11	SJT 12	301485.36	203592.358	301507.285	203560.807	39.286
Ug	70 TR	SJT 12	SJT 13	301507.285	203560.807	301533.166	203523.303	48.987
Ug	70 TR	SJT 13	LE 14	301533.166	203523.303	301547.529	203530.062	19.285

TableA5 shows the technical data of Fforchneol Farm Godreaman (rural network)

Type of cable/line		"Bus 1" Start point	"Bus 2" End point	X bus1	Y bus1	X bus2	Y bus2	Length [m]
Ug	300 TR	SUB FDR 10	BJT 1	300983.054	200474.015	300968.066	200486.764	21.782
Ug	70 TR	BJT 1	BJT 2	300983.054	200474.015	300960.375	200459.986	27.93
Ug	70 TR	BJT 2	LE 3	300960.375	200459.986	300931.09	200444.27	40.577
Ug	70 TR	BJT 2	BJT 4	300960.375	200459.986	300949.418	200450.148	14.733
Ug	70 TR	BJT 4	LE 5	300949.418	200450.148	300946.948	200447.992	3.28
Ug	70 TR	BJT 4	LE 6	300949.418	200450.148	300925.226	200418.58	44.375
Ug	300 TR	BJT 1	BJT 7	300983.054	200474.015	300988.296	200469.522	7.025
Ug	300 TR	BJT 7	SJT 9	300988.296	200469.522	301001.091	200467.631	13.543
Ug	300 TR	SJT 9	SJT 10	301001.091	200467.631	301021.063	200470.492	25.612
Ug	70 TR	SJT 10	BJT 11	301021.063	200470.492	301045.578	200492.303	32.815
Ug	70 TR	BJT 11	LE 13	301045.578	200492.303	301029.536	200545.696	60.274
Ug	70 TR	BJT 11	BJT 14	301045.578	200492.303	301051.624	200497.487	7.964
Ug	70 TR	BJT 14	LE 15	301051.624	200497.487	301052.763	200498.693	1.659
Ug	70 TR	BJT 14	LE 17	301051.624	200497.487	301058.65	200515.798	25.739
Ug	300 TR	BJT 7	SJT 19	300988.296	200469.522	301020.015	200432.336	48.895
Ug	300 TR	SJT 19	SJT 20	301020.015	200432.336	301027.488	200433.612	8.156
Ug	70 TR	SJT 20	POLE 552149-1 21	301027.488	200433.612	301054.486	200427.675	29.312
Oh	ABC 0.05 XLPE	POLE 552149-1 21	POLE 552149-2 22	301054.486	200427.675	301080.714	200438.43	28.347
Oh	4w 0.05	POLE 552149-2 22	POLE 552149-3 23	301080.714	200438.43	301070.743	200470.306	33.399
Oh	ABC 0.05 XLPE	POLE 552149-1 21	POLE 552148-31 24	301054.486	200427.675	301017.071	200398.874	47.216

Appendix B

Underground cables and Overhead lines data base

Table B1 shows the underground cables/overhead lines database of some WPD networks that has been made exploiting handbook, cable catalogues and standards.

		Resistance [Ω/km]					Reactance [Ω/km]				Capacitance [μF/Km]	Cable parameters			Diameter overall [mm]	Ampacity [Amps]
		WPD data		Other sources			WPD data		Other sources	Calculated	Manifacturer data	Calculated				
Cables and overhead lines		R_{DC} at 20°C Phase [Ω/km]	R_{DC} at 20°C Neutral [Ω/km]	R_{DC} at 20°C Phase [Ω/km]	Maximum R_{ac} at 80°C Phase [Ω/km]	Maximum R_{ac} at 90°C Phase [Ω/km]	Reactance at 50 Hz Phase [Ω/km]	Reactance at 50 Hz Neutral [Ω/km]	Reactance at 50 Hz Phase [Ω/km]	Reactance at 50 Hz Phase [Ω/Km]	Capacitance (core to core) [μF/Km]	GMD calculated [m]	GMR calculated [m]	Radius of each equivalent circular conductor [m]		
WPD cable description	Metric size or equivalent [mm²]															
PILC 0.3 4c STA (Stranded Cu)	195	0.092	0.092	0.092	0.124	-	0.0678	0.0678	0.068	-	1.21	-	-	-	55.5 < D < 61.8	445
PILC 0.25 4c STA (Stranded Cu)	160	0.113	0.113	0.113	0.155	-	0.0689	0.0689	0.069	-	1.09	-	-	-	51.5 < D < 55.5	395
PILC 0.2 4C STA (Stranded Cu)	125	0.142	0.142	0.142	0.190	-	0.0689	0.0689	0.069	-	1.20	-	-	-	45.9 < D < 51.5	345
PILC 0.15 4C STA (Stranded Cu)	95	0.188	0.193	0.193	0.239	-	0.0700	0.0700	0.069	-	1.06	-	-	-	33.5	290
PILC 0.1 4C STA (Stranded Cu)	65	0.276	0.275	0.275	0.479	-	0.0733	0.0733	0.073	-	0.79	-	-	-	34.6 <D < 38.4	200
PILC 0.06 4C STA (Stranded Cu)	40	0.464	0.463	0.463	0.648	-	0.0755	0.0755	0.076	-	0.69	-	-	-	31.9 < D < 34.6	175
PILC 0.04 4C STA (Stranded Cu)	25	0.702	0.726	0.726	0.898	-	0.0787	0.0787	0.076	-	0.62	-	-	-	29.4	135
PILC 0.15 2C STA (Stranded Cu)	95	-	-	0.193	0.239	-	-	-	0.069	-	1.06	-	-	-	34.3	345
PILC 0.1 2C STA (Stranded Cu)	65	-	-	0.275	0.479	-	-	-	0.073	-	0.79	-	-	-	28.6 < D < 31.4	250
PILC 0.15 4C Bunched	95	-	-	0.193	0.239	-	-	-	0.069	-	1.06	-	-	-	-	290
PILC 0.1 4C Bunched	65	-	-	0.275	0.479	-	-	-	0.073	-	0.79	-	-	-	-	250
300 TR XLPE Al 3c SWA (solid aluminium)	300	0.100	0.100	0.100	-	0.130	0.0725	0.0108	0.07	0.069	0.528	0.023144	0.007612	0.009772	53.9	461
185 TR XLPE Al 3c SWA (solid aluminium)	185	0.164	0.164	0.164	-	0.211	0.074	0.0140	0.072	0.07106	0.478	0.018548	0.005978	0.007674	45.1	382
120 TR XLPE Al 3c SWA (solid aluminium)	120	0.253	0.253	0.253	-	0.325	0.073	0.0153	0.071	0.07032	0.493	0.01476	0.004814	0.00618	36.4	278
70 TR XLPE Al 3c SWA (solid aluminium)	70	0.443	0.443	0.444	-	0.568	0.0755	0.0152	0.073	0.0723	0.426	0.01164	0.003677	0.00472	29.4	203
300 Wavcon Al 3c (CNE: solid aluminium + copper neutral wires)	300	0.100	0.164	0.100	0.126	-	0.0725	0.0108	0.0725	0.0698	0.528	0.023144	0.007612	0.009772	53.4	435
185 Wavcon Al 3c (CNE: solid aluminium + copper neutral wires)	185	0.164	0.164	0.164	0.205	-	0.0740	0.0140	0.074	0.07106	0.478	0.018548	0.005978	0.007674	45.3	335
95 Wavcon Al 3c (CNE: solid aluminium + copper neutral wires)	95	0.320	0.320	0.320	0.398	-	0.0735	0.0155	0.0735	-	0.471	-	-	-	33.5	235
35 HYB Al	35	0.868	0.760	0.868	-	-	0.075	0.075	0.041	-	-	-	-	-	-	140
ABC 4x35 Al XLPE (overhead line)	35	-	-	0.868	-	-	-	-	0.086	-	-	-	0.002425	0.00334	24	120
4w 0.05 Cu (Open Wire)	32	0.541	0.541	0.5243	-	-	0.325	0.325	0.297	0.297	-	-	-	-	3.192	190

Reference exploited to made the data base are:

[1] Western Power Distribution (WPD) data provided, 2013.

[2] Table 46 - BICC cable design and construction catalogue, date unknown.

[3] BICCCables, "Electric Cables handbook Third Edition", p. 945 (table A12.16), UK Blackwell Science, 1997

[4] Pirelli Cables Limited, "Energy Cable: Building Wires and Cables, Cable catalogue 300V- 33000V: Power Cables", England, 1996.

[5] Prysmian group, low voltage cable 600/1000V BS7870 - 3.40,2011, UK.

[6] E-on Central Networks, "Network Design Manual", 2006.

Appendix C

Calculation of electrical parameters

Resistance calculation

The resistance of the cable varies largely with frequency because of skin effect and proximity effect of conductors, also the temperature is an important parameter that could change significantly the relative magnitude.

In cable manufactures data sheet is common to find the DC resistance of the conductor at the room temperature of the surrounding area or of the relative country, whereas the AC resistance most of the times must be calculated.

- DC resistance of conductor

The DC resistance per unit length of the conductor at its maximum operating temperature θ is given by:

$R' = R_0 [1 + \alpha_{20}(\theta - 20)]$ [Ω/m]

Where:

R_0 is the DC resistance of the conductor at 20 °C [Ω/m]

α_{20} is the constant mass temperature coefficient at 20°C per Kelvin

θ is the maximum operating temperature in °C which will be determined by the material of the insulation of the cable [16]

- AC resistance of conductor

The AC resistance per unit length of the conductor at its maximum operating temperature is given by (except in the case of pipe-type cables):

$R = R' (1 + y_s + y_p)$ [Ω/m]

Where:

R' is the DC resistance at the conductor operating temperature (3.1) [Ω/m]

y_s is the skin effect factor

y_p is the proximity effect factor.

For skin effect factor y_s and y_p refer to [16]

Cable inductance calculation

The cable inductance depends on geometrical structure and permeability of conductor and insulation material.

Below are shown two calculation methods of cable inductance which give always similar results:

- In a 3-core cable or of 3 single-core cables, the core inductance L comprises the self-inductance of the conductor and the mutual inductance with other cores.

$$L = K + 0.2 \log_e \frac{2S}{d} \qquad \text{[mH/km]} \qquad \text{c.1}$$

Where:

K = constant regarding the conductor formation (see table C1)
S = axial spacing between conductors within the cable [mm]
= axial spacing between conductors of a trefoil group of a single-core cables [mm]
= 1.26 x phase spacing for a flat formation of three single-core cables [mm]
d = conductor diameter or in case of solid shaped conductors it is the diameter of an equivalent circular conductor [mm] [17]

Note: For 2-core, 3-core and 4-core cables, the inductance value obtained from (c.1) should be multiplied by 1.02 in case of circular or sector-shaped conductor, and by 0.97 if the cable is composed by 3-core oval conductors [17].

Table C1 Typical values for constant K for stranded conductor at 50 Hz [17]

Number of wires in a conductor	**K**
3	0.078
7	0.064
19	0.055
37	0.053
61 and over	0.051
1 (Solid)	0.05

- Another formula to calculate the operating inductance is given by:

$$L_o = 0.46 \cdot \log_{10} \frac{GMD}{GMR} \cdot 10^{-3} \qquad \text{[mH/km]}$$

Where:

L_o = Operating inductance at 50 Hz [mH/km]
GMD = geometric mean distance [m]
GMR= geometrical mean radius [m**]** [18]

GMR calculation

The Geometrical Mean Radius (GMR) is given by:

$GMR = r_{eq} \cdot k''$ [m]

Where:

r_{eq} is the equivalent radius of the shaped conductors (assumed circular) or the outside radius of the stranded conductor [m]

k'' is a constant that depends of the type of conductor: solid or stranded (see the table C2)

Table C2 shows the k'' constants of solid or stranded conductor [18]

Type of conductor	**k"**
Solid round conductor	0.779·R
7 Strands	0.726·R
19 Strands	0.758·R
37 Strands	0.768·R
61 Strands	0.772·R
91 Strands	0.774·R
127 Strands	0.766·R

Capacitance calculation

The capacitance of cable depends on geometrical structure and dielectric constant of the insulation material. It should be noted that the dielectric constant varies with frequency and temperature.

- Operating capacitance

  In order to have robust studies on the networks provided by Western Power Distribution, it is necessary also to focus on the approximate capacitance per unit length between phases and among phase-neutral as well known as operating capacitance:

  $C_1=C_0+3C$

  Where:

  C_0 is capacitance between each core and sheath

  3C is capacitance between cores

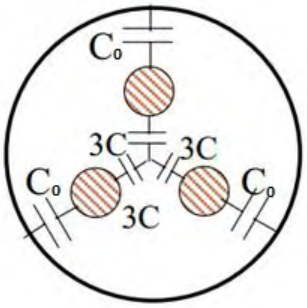

Figure 3.15 Theoretical capacitance template of three-core belted cable

- Operating capacitance calculation

The Operating capacitance calculation of the underground cable may carry out using two different formulas:

i. Simons's equation (Empirical formula) of three-core belted type cables:

$$C_1 = \frac{0.03\ \varepsilon_r}{\log_{10}\left[\left(0.52\cdot\left(\frac{t}{T}\right)^2 - 1.7\cdot\left(\frac{t}{T}\right) + 3.84\right)\cdot\left(\frac{T+t}{d}\right) + 1\right]} \qquad [\mu F/km]$$

Where:

t is the thickness of belt insulation
T is the thickness of conductor insulator
d is the diameter of conductor
ε_r is the dielectric constant [19]

ii. Theoretical capacitance equation of three-core belted type cables:

$$C_1 = \frac{\epsilon_r}{18\log_e\left(\frac{D}{d}\right)} \qquad [\mu F/km]$$

Where:

D = diameter of one conductor plus the thickness of insulation between conductors plus the thickness of insulation between any conductor and the metal sheath, screen or armour.

d= diameter of the conductor [m]

ϵ_r = relative permittivity (i.e. XLPE=2.5) [18]

Capacitive reactive power calculation

In low voltage networks is common to negligible the operating capacitance of the cables because in major cases the relative values (X_C) are very low if compared with the other cable parameters (R and X_L).

In our network studies to make sure if what has been said is true, the capacitive reactive power contribution of the cables have been calculated by the following formula:

$$Q_C = \omega l C V^2 \qquad [Var/km]$$

Where:

ω= 2πf is the angular frequency (operating frequency= 50 Hz)

l is the length of the cable [m]

C is the operating capacitance [µF/km]

V is the rating voltage of the cable [V]

Capacitive reactive power calculations were carried out for some cables network and it was discovered that these capacitive contributions on the total reactive power were negligible, in fact the relative values were not exceeding 0.5 − 1 VAr/m.

Appendix D

Basic steps to carrying out network simulations using OpenDSS

In this project Western Power Distribution (WPD) provided to our researcher group some technical data about 5 low voltage networks (urban and rural).

This data are essentially:

- General information about LV cables: size, resistance, reactance, length, start/end coordinates of the cables and overhead lines.

- Electrical data from energy meters at the feeding point of each network. The relative data recorded by these equipment are: voltages, currents, THD (V) of each phase and Real Power Imported, Real Power Exported, Reactive Power Imported, Reactive Power Exported.

The basic steps that have been followed to run simulations on five modelled networks using OpenDSS are:

1. Make a robust database of the most important technical parameters of underground cables and overhead lines which is called WIREDATA.

2. OpenDSS has several approaches to model the cables or the overhead lines. The most important parameters needed for each approach are:

   a) Wire/Line geometry Approach: it will calculate line constants, including sequence impedances like: R1,X1,R0,X0,C1 and C0.

   Rac/Rdc = AC or DC Resistance [Ω/km]

   GMRac = geometric mean radius [m]

   Radius = Radius of each conductor [m]

   Normamps = the ampacity of the cable/line [Amps]

   Nconds = numbers of conductors of the cable/line (including the neutral conductor)

   Nphases = numbers of phases of the cable/line

   Wire = code from WireData (must be previously defined)

   X = x coordinate [m]

   H = height of conductor (it must be >0) [m]

   Reduce = yes/no. It is used to reduce out the neutral. Reduce to Nphases (Kron reduction)

b) LineCode approach:

Nphases = numbers of phases of the cable/line

R1 = Positive-Sequence resistance [Ω/km]

X1 = Positive-Sequence reactance [Ω/km]

R0 = Zero-Sequence resistance [Ω/km]

X0 = Zero-Sequence reactance [Ω/km]

C1 = Positive-Sequence capacitance [Ω/km]

C0 = Zero-Sequence capacitance [Ω/km]

Units = km

c) Matrix approach:

Rmatrix = Series resistance matrix [Ω/km]

Xmatrix = Series reactance matrix [Ω/km]

Cmatrix = Shunt nodal capacitance matrix [nF/km]

BaseFreq= Base Frequency at which the impedance values are specified [Hz]

Normamps= Normal ampacity [amps]

Note: OpenDSS converts all the impedance definitions to a matrix. So to be absolutely confident in what OpenDSS is using should be better to specify Rmatrix, Xmatrix, and Cmatrix directly (if is it possible). (i.e. For a 1-phase line, these would be 1x1 matrices).

3. Find out the easiest and most accurate way to model the different types of cables or overhead lines for the OpenDSS scripts. This point is crucial because some assumptions and approximations shall be taken.

4. Make a network template of each one analysed with the aid of the provided technical data.

5. Define: the magnitude of main source, transformer data, loads and type of solution desired (power flow, fault studies, harmonic flow analysis, dynamics, load parametric variation, geometrically induced current analysis).

6. Create the OpenDSS master scripts of each modelled network.

Appendix E

OpenDSS solution algorithms

The OpenDSS software is a comprehensive electrical power system simulation tool intended primarily for the analysis of electric utility power distribution systems. This software enables to perform power flow analysis, harmonic studies, neutral-earth voltage studies, volt-var control studies and other special applications.

OpenDSS is evolved from programs designed for harmonic flow analysis [20]. The main reason of that is because it is easier for a harmonic flow analysis program to perform a power follow solution compared to the contrary. OpenDSS has two different solution algorithms that can be used. The first one which is called "Normal" is based on a "fixed-point iteration" method which can solve non-linear equations. The system model is build by the primitive admittance (Y_{prim}) matrix approach in which every current-carrying circuit element in the network modelled is either represented entirely by its Y_{prim} matrix or just some aspect ,as may be the linear part, of the model is represented by a Y_{prim} [20]. Figure E1 shows the default solution algorithm of OpenDSS. In order to build the system nodal admittance matrix (Y) all of the Y_{prim} matrix of the circuit elements are sums directly in a location part of Y. Afterwards an equation is formed by populating the injection current vector with the compensation current from the Power Conversion or PC element which are load devices, generators, Vsource, Isource and storage. [20]

The strength of this algorithm is the speed in sequential time solutions and is adequate for most radial distribution circuits. The "Normal" algorithm has for radial circuits similar characteristics to most forward-backward sweep methods moreover the number of iterations are not so many. During the solution process the system Y matrix does not change very often, in this way the efficiency of the solution on the yearly simulations is increased. Good convergence characteristics for distribution systems are achieve if the starting voltage guess is close to the final solution. The initial solution is performed by a non-iterative solution of the system Y matrix where the compensation current is not present, except for Vsource and Isource. In sequential-time power flow analysis the initial solution is used as the starting point. Also to reach a well convergence the power delivery elements series impedance must be less than the equivalent shunt impedance of load devices. [20] To avoid the failures during for example an annual simulation, even if the voltage of the system is close to collapse, the power conversion models revert to a linear model when the voltage is overrunning the band ±5% or ±10% of rated voltage [20]. The other algorithm that could used in OpenDSS is called "Newton" method which is not the classic decoupled Newton-Raphson power flow method. The Newton power flow is a multi-phase and it couples the real and the imaginary parts. This algorithm is more robust for circuits that are difficult to solve but is very seldom required for solving distribution systems.

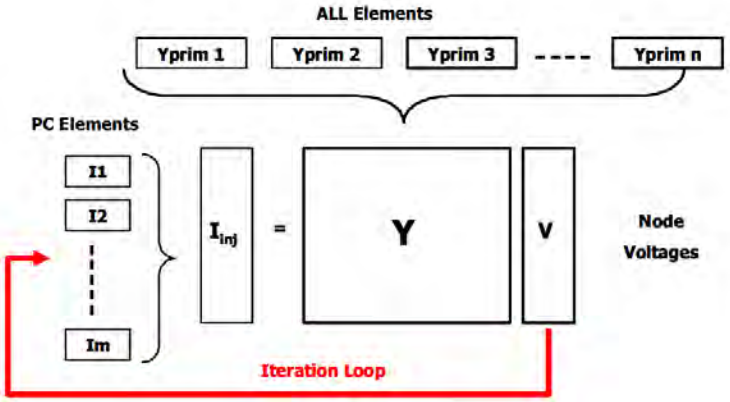

Figure E1 The default solution algorithm [20]

References

[1] *Network design manual*, Version 7.7., E-on Central Networks,UK, Dec. 2006, pp. 55-60.

[2] Western Power Distribution, "Standard technique: SD5A/1: Design of Low Voltage Domestic Connections", UK, 20 April 2012.

[3] R. Singh, Bikash C. Pal and Rabith A. Jabr, " Statistical representation of distribution system loads using Gaussian mixture model", *IEEE Trans. Power Syst.,* vol. 25, no. 1, p. 29, Feb. 2010.

[4] *BICC cable design and construction catalogue,* BICC cables Ltd, Table 46, Date unknown.

[5] Pirelli Cables Limited, "Energy Cable: Building Wires and Cables, Cable catalogue 300V- 33000V: Power Cables", England, 1996.

[6] BICC Cable power division, "Waveform cables for use in PME systems", UK, 1989.

[7] Prysmian group, "Prysmian cables and systems catalogue: Low Voltage aerial bundled cable systems", UK, 2007.

[8] ENA (energy networks association), "35-1 Distribution Transformers (from 16kVA to 2000kVA)," London, June 2007.

[9] EPRI (2013, Sep. 20), Smart Grid Resouce Centre - Resources [Online]. Available: http://www.smartgrid.epri.com/SimulationTool.aspx

[10] Worawit Tayati and Hai Bui, "PV generation hosting capacity of remote area power supply systems", presented at 50th Annual Conference: Australia Solar Energy Society (Austalian Solar Council), Melbourne, Australia, Dec. 2012.

[11] Western Power, "Western Australian Distribution Connection Manual," 4th ed., Australia, 2013, p. 283.

[12] R. Caldon, M. Coppo, R. Turri, "Voltage unbalance compensation in LV networks with inverter interfaced distributed energy resources", presented at *IEEE International Energy Conference and Exhibition (ENERGYCON),* pp. 527-532, Florence, Italy, 9-12 Sep. 2012.

[13] J. Morren, Sjoerd W. H. de Haan, J. A. Ferreira, "Contribution of DG units to voltage control: active and reactive power limitations", presented at *IEEE Power Tech*, pages 1-5, Russia, 27-30 June 2005.

[14] V. Olivieri, M. Delfanti, L. Lo Schiavo, "The Italian regulatory framework for developing smart distribution grids," *International Journal of Emerging Electric Power Systems,* vol. vol. 13, no. 4, Dec. 2012.

[15] Jeff Smith, Matt Rylander, Chris Trueblood, "PV Hosting Capacity in Electric Distribution,

Monitoring and Feeder Analysis Results from the US", presented at *5th International Conference on Integration of Renewable and Distributed Energy Resources,* Berlin, Germany, Dec. 2012.

[16] BS IEC 60287-1-1:2006, "Electric cables. Calculation of the current rating Current rating equations (100% load factor) and calculation of losses", British Standard Istitution, pp. 11-12, 31 Jan. 2007.

[17] *Electric Cables handbook*, 3rd ed., BICC Cables, UK, 1997, pp. 11-12.

[18] R. Benato, L. Fellin, *Impianti elettrici*," Utet Scienze Tecniche, Italy, 2011, pp. 33-39.

[19] C. L. Wadhwa, *Electrical Power Systems,* New Age International, 4th ed., 2005.

[20] Roger C. Dugan and Thomas E. McDermott, "An open source platform for collaborating on smart grid research," presented at *IEEE PES General Meeting*, Detroit, USA, 28 July 2011.